SHEAR STRENGTH OF ROCK JOINTS BASED ON QUANTIFIED SURFACE DESCRIPTION

THESE N°2404 (2001)

PRESENTEE AU DEPARTEMENT DE GENIE CIVIL

ECOLE POLYTECHNIQUE FEDERALE DE LAUSANNE

POUR L'OBTENTION DU GRADE DE DOCTEUR ES SCIENCES TECHNIQUES

PAR

Giovanni GRASSELLI

Laurea in Ingegneria Civile, Univeristá di Parma, Italie
de nationalité italienne

acceptee sur proposition du jury :

Prof. François Descoeudres, directeur de thèse
Prof. Peter Egger, rapporteur
Dr. George Darbre, rapporteur
Dr. Deborah Hopkins, rapporteur
Dr. Frédéric Pellet, rapporteur
Prof. Ian Smith, rapporteur

Lausanne, EPFL
2001

Acknowledgments

I am deeply grateful and I would like to express my thanks to:

Prof. F. Descoeudres for accepting me into his group at the EPFL and for his interest in the project.

Prof. P. Egger for his skillful supervision of the research, for his useful criticism in the development of the project, for his constant patience and great assistance.

Dr. D. Hopkins for her highly motivating enthusiasm, her continuous scientific and moral support and for the excellent supervision during my stage at the LBNL.

Dr. J. Wirth for making available to me his expertise in the field of software engineering and for helping me with his interdisciplinary and open mind approach to the rock mechanical problems.

F. Huot, F. Mayoraz, and R. Garber for their fruitful suggestions and their precious help in the different phases of the research.

F. Mottier, J. F. Mathier, G. Lombardi and B. Marguerat for their excellent technical assistance.

Everybody in the Rock and Soil Mechanic Laboratory at the EPF of Lausanne and everybody in the Engineering Group at the LBNL of Berkeley for the wonderful working atmosphere and the continuous fruitful collaboration.

My dearest friends Elena, Francesco, Marco, Matteo, Luigi, Eric, Erika, Stefano, Madhu, Anna and Elisa for always supporting me as much as they could in the dark moments of the thesis.

To all the friends I met at the “Castello” that made easy to me the choices I did.

This study was performed between May 1998 and May 2001 at the Swiss Federal Institute of Technology of Lausanne in the frame of a research project funded by the Swiss Federal Institute for Water and Geology.

Abstract

One of the primary objectives of this work is to better understand the frictional behavior of joints under shear loads, including the creation of damage zones. Discontinuities have an important influence on the deformational behavior of rock systems. The choice of a general criterion to determine the shear strength of rough rock joints is a general problem that has been investigated for many years. Numerous shear models have been proposed in the last decades to relate shear-strength to measurable joint parameters, but their limitations have to be recognized. The problem is how to measure and then to express the roughness with a number (e.g. JRC) or a mathematical expression in order to introduce the morphology of the joint into a shear strength criterion.

In the frame of this work it has been pointed out that the geometry of roughness influences the size and distribution of contact areas during shearing. In order to locate and estimate the contact area during the shearing, it was argued that only the zones of the surface faced to the shear direction, and steeper than a threshold inclination are involved in the shearing. An empirical relation between the potential contact area and the minimal apparent dip inclination of the surface is proposed. The close agreement between this empirical description of the potential contact area, and experimental points permits to predict the real contact area involved in the phenomena.

A new constitutive law, relating stress and displacements, is proposed to model the shear resistance of joints under constant normal load conditions. It is based on the empirical surface description, and on the results from more than fifty constant-normal-load direct-shear tests performed on both replicas of tensile joints, and induced tensile fractures for seven rock types. It is shown that this constitutive model is able to describe experimental shear tests realized in laboratory. Moreover, the parameters required in the model can be easily obtained through standard laboratory tests. The proposed model was also used to estimate the JRC value. The expression obtained to evaluate the joint roughness coefficient is capable of predicting the JRC. It was successfully compared with JRC values obtained by back analysis of shear tests.

In the current research no attention was paid to investigate the influence of the scale on the shearing. The results have been validated only in the range of the samples tested in laboratory. Further studies are needed to explore the applicability of the proposed model in field conditions.

Résumé

Un des premiers objectifs de ce travail est de mieux comprendre le comportement sous l’effet du cisaillement des joints rugueux, y compris la création des zones endommagées. Le choix d'un critère général pour déterminer la résistance au cisaillement des joints rugueux est un problème qui est étudié depuis plusieurs années. De nombreux modèles de comportement au cisaillement ont été proposés afin d’associer l’effort de cisaillement aux paramètres morphologiques de la surface, mais leur validité est discutable. Le problème est de mesurer, puis d’exprimer la rugosité par une valeur (par exemple le JRC) ou une expression mathématique afin de considérer la morphologie du joint dans un critère de résistance au cisaillement. En effet, la géométrie de joint rugueux influence la taille et la distribution des zones de contact pendant le cisaillement.

Dans le cadre de ce travail, afin de localiser et d’estimer la zone de contact pendant le cisaillement, on a considéré que seules les zones de la surface qui font face à la direction de cisaillement, et plus raides qu'une inclinaison de seuil, sont impliquées dans le cisaillement. On propose une relation empirique entre la zone de contact et l’angle apparent minimal de pendage de la surface. La relation entre cette description empirique de la zone de contact potentielle et les données expérimentales permet d’évaluer la zone de contact impliquée dans le phénomène.

On propose une nouvelle loi constitutive, effort-déplacement, pour modéliser des joints cisaillés dans des conditions de charge normales constantes. Elle est basée sur la description empirique de la surface, et sur les résultats de plus de cinquante essais de cisaillement réalisés sur des répliques ainsi que sur des joints en roche. On a vérifié que ce modèle constitutif peut décrire les essais expérimentaux de cisaillement réalisés en laboratoire.

Par ailleurs, les paramètres utilisés dans le modèle peuvent être facilement obtenus par des essais standards en laboratoire. Le modèle proposé a été également employé pour estimer la valeur du JRC. L'expression obtenue pour évaluer le coefficient de rugosité du joint permet d’estimer le JRC. Elle a été comparée avec succès aux valeurs du JRC obtenues par analyse inverse des essais de cisaillement. Dans cette recherche aucune attention n'a été prêtée à l'influence de l'échelle sur le cisaillement. Les résultats ont été validés seulement pour la taille des échantillons testés en le laboratoire. D'autres études sont nécessaires pour explorer l'applicabilité in-situ du modèle proposé.

Riassunto

Uno degli obiettivi principali di questo lavoro è la ricerca di una migliore comprensione del fenomeno della resistenza al taglio dei giunti in roccia. Le discontinuità hanno un'importante influenza sul comportamento degli ammassi rocciosi. La scelta di un criterio generale per determinare la resistenza al taglio dei giunti scabri, è un problema generale, studiato da lungo tempo. Negli ultimi decenni sono stati proposti numerosi modelli di comportamento che cercano di legare lo sforzo di taglio a parametri morfologici della superficie della frattura, tuttavia la loro validità resta da provare. Il vero problema risulta essere la misura ed, in seguito, l'espressione della scabrezza per mezzo di un valore (ad esempio il JCR) o attraverso un'espressione matematica. L'obiettivo é di introdurre, in un criterio di resistenza meccanica, un fattore che consideri la morfologia del giunto. La geometria della superficie influenza, infatti, la dimensione e la distribuzione delle zone a contatto durante il taglio.

Nel corso di questo lavoro, considerando le sole zone del giunto inclinate nella direzione di taglio, è stata proposta, allo scopo di localizzare e stimare le aree di contatto, una relazione empirica che lega la percentuale della superficie in contatto durante il taglio, con l'angolo minimo d'immersione apparente. La stretta concordanza tra l'espressione empirica e i risultati sperimentali, permette di stimare la zona di contatto implicata nel fenomeno.

In seguito è stata proposta una nuova legge costitutiva, sforzi-deformazioni, per modellizzare le fratture soggette a sforzo di taglio in condizioni di carico normale costante. La sua formulazione è basata sulla descrizione empirica della superficie e sull'analisi dei risultati di più di cinquanta prove di taglio diretto eseguite sia su repliche che su giunti in roccia. Questo modello costitutivo risulta capace, utilizzando parametri facilmente misurabili tramite prove standard, di descrivere i risultati dei test di laboratorio realizzati. Il criterio di resistenza di picco proposto è poi utilizzato per stimare obbiettivamente il valore di JRC. I valori ottenuti con tale procedura sono stati confrontati con successo con i corrispondenti JRC ricavati tramite "back analysis" delle prove di taglio. I risultati presentati sono stati validati solo nell'intervallo di scala testato in laboratorio. Successivi studi sono necessari per esplorare l'applicabilità in-situ del modello proposto.

Table of contents

Symbols and abbreviations

a	*horizontal displacement necessary to mate the joint [mm]*
A_0	*ratio between the part of the joint surface, which is oriented towards the chosen shear direction, and the total area [-]*
a_0	*surface best fitting coefficient [-]*
A_c	*potential contact area ratio [-]*
a_s	*area where shearing through the asperities takes place (Ladanyi & Archambault 1970)* $[m^2]$
B	*roughness parameter [-]*
b_0	*surface best fitting coefficient [deg]*
C	*roughness parameter, calculated using the best-fit function [-]*
c_j	*apparent joint cohesion [MPa]*
c_r	*residual cohesion after triaxial test [MPa]*
d	*true dip vector*
E	*Young's modulus [GPa]*
i	*inclination angle of the teeth asperity (Patton 1966) [deg]*
JCS	*Joint Compressive Strength (Barton 1977) [MPa]*
JMC	*Joint Matching Coefficient (Zhao 1997) [-]*
JRC	*Joint Roughness Coefficient (Barton 1977) [-]*
k_s	*shear stiffness* $[mm^{-1}]$
l_x	*dimension of the sample in the direction normal to the shear direction [mm]*
l_x	*dimension of the sample in the direction of shearing [mm]*
N	*normal force [kN]*
n	*ratio between the compressive and tensile strength* ($n=\sigma_c/\sigma_t$)
n	*normal vector to the joint surface*
P	*best fitting coefficient [-]*
p_n	*median angle pressure (Maksimovic 1996) [MPa]*
S_F	*shear force required for sliding over the asperities (Ladanyi & Archambault 1970) [kN]*
S_r	*force required to shear through the asperities (Ladanyi & Archambault 1970) [kN]*
t	*shear vector*
T_p	*the peak shear force [kN]*
T_r	*residual shear resistance [kN]*
u_p	*horizontal displacement at the peak, measured in the shear direction [mm]*
v_p	*vertical displacement of the average joint plane at the peak [mm]*
w	*true dip vector projection on the shear plane*
x_0	*surface best fitting coefficient [deg]*
Δu_p	*horizontal deformation of the joint before the peak [mm]*

Δu_r	*horizontal displacement that the joint needs, to fall from the peak to the residual state [mm]*
$\Delta\phi$	*inclination of the steepest asperities (Maksimovic 1996) [deg]*
α	*angle between the schistose plane and the plane normal to the joint [deg]*
α	*Azimuth (angle between* **w** *and* **t**, *measured clockwise from* **t***) [deg]*
β	*contribution of the roughness to the residual friction angle [deg]*
ϕ'_r	*residual friction angle after standard displacement of 5 mm [deg]*
ϕ_b	*basic friction angle [deg]*
ϕ_p	*peak friction angle [deg]*
ϕ_r	*residual friction angle [deg]*
μ	*coefficient of friction [-]*
θ_p	*dilatancy angle [deg]*
θ	*dip angle (between the shear plane and the joint surface) [deg]*
θ^*	*apparent dip angle [deg]*
θ^*_{cr}	*threshold inclination [deg]*
θ^*_{max}	*maximum apparent dip angle of the surface [deg]*
ρ	*density [t/m^3]*
σ_c	*uniaxial compressive strength of the rock [MPa]*
σ_n	*normal load [MPa]*
σ_t	*tensile strength of the rock [MPa]*
τ_p	*peak shear strength of the joint [MPa]*
τ_r	*residual shear strength of the joint [MPa]*
τ_{rock}	*shear strength of the intact rock [MPa]*

Introduction

"The function of Rock mechanics engineers is not to compute accurately but to judge soundly."
Hoek & Londe

One of the earliest definitions of engineering occurs in the 1828 charter of the British Institution of Civil Engineers: engineering is “the art of directing the great sources of power in nature for the use and convenience of man” (Ferguson 1997). Although civil engineers have been designing and constructing structures that interact with the natural environment for centuries, it was only in the sixties that rock mechanics came to be recognized as an independent engineering discipline. Rock mechanics deals with the properties of rock and the special methodology required for design of construction in rock. Rock, like soil, is sufficiently distinct from other engineering materials that the process of “design” in rock is its own discipline. In contrast to concrete structures, the applied loads in rock are often less significant in evaluating performance than the forces arising from the redistribution of initial in-situ stresses. Since rock structures can fail in many different modes, the determination of material “strength” relies on judgment as much as measurement.

In fact, rock is a material quite apart from what a mathematician would choose for tractable analysis. The engineer’s rock is heterogeneous and quite often discontinuous; i.e. rock masses are typically fractured. The mechanical behavior is often dominated by the joints and faults that run through the rock mass. For example, it was sliding on the downstream joints that undermined the Malpasset Arch Dam in 1959. With respect to mechanical behavior, one of the most significant effects of a single fracture in a rock mass is decrease shear strength in the direction parallel to the fracture plane. The shape, size, number, distribution and strength of contacts between the walls of the joint control its mechanical properties (ignoring infilling). Therefore, the choice of an appropriate shear-strength criterion for rock joints, that can be used to engineer structures in rock, depends on a sound understanding of the basic mechanics of shear failure. This requires an understanding of the factors that influence the shear-strength characteristics of a rock mass. It is the aim of this work to contribute to this understanding, and to encourage readers to further explore the subject of joint shear strength.

1. Rock joint shear-strength criteria: state of the art

"No one wants to learn from mistakes, but we cannot learn enough from successes to go beyond the state of the art."
Henry Petroski

Joints, bedding plane, faults, and other recurrent planar fractures radically alter the behavior of rock. As joints are generally not randomly distributed, their effect is to create pronounced anisotropy in the properties of the rock mass, in particular, anisotropy of strength. For example, the strength of a foundation loaded obliquely to the orientation of bedding-planes may be less than one half of the strength when the load is applied perpendicular or parallel to the bedding planes. Moreover, anisotropy commonly exists in many rocks that have continuous structure, because of preferred orientations of mineral grains or directional stress history. Thus, rock masses are generally anisotropic in the properties that affect mechanical behavior. In particular, discontinuities and planar weaknesses make the rock mass weaker, more deformable, and highly anisotropic in strength because they reduce shear strength. Joints also affect hydraulic behavior; for example, they result in higher permeability in directions parallel to discontinuities. These factors combine to create a variety of potential problems. Foundations resting on jointed rocks may settle significantly as the joints close under load even if the rock itself is very stiff. Dams underlain by discontinuous rock are subjected to damage if rock blocks slip along one or more weak surfaces (Figure 1.1). More than one dam failure has been attributed to this failure mechanism. Movement of rock blocks along single or multiple planes of weakness also causes failure of rock slopes (Figure 1.2).

Figure 1.1 A picture of the abutment of the Malpasset arch dam after its failure in 1959. The movement of a wedge delimited by discontinuities in the rock caused the rupture of the concrete arch.

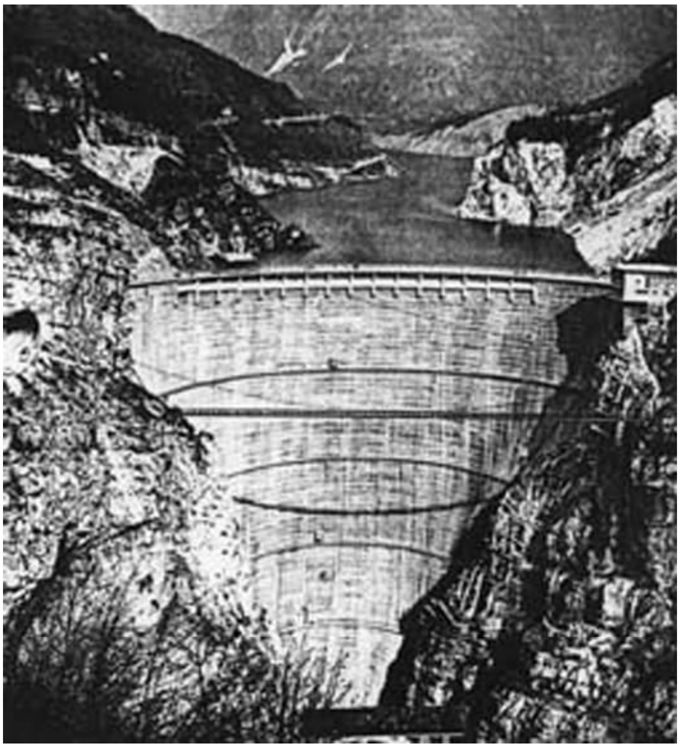

Figure 1.2 Vajont dam in Italy. In 1963, heavy rains and intermittent load-induced earthquakes dislodged the piece of mountainside marked by the scar in the right of the photo. Falling into the reservoir, it created a huge wave, which swept over the dam drowning 2,600 people in the valley below.

Movements along rock discontinuities in foundations, dams, tunnels, and slopes can occur in any direction, depending on kinematic constraints and the external forces (including water pressures, and forces induced by earthquakes) acting on the structure. Therefore, it is imperative to understand the variation of shear strength of rock discontinuities in all directions. It is also important to note that even for a specified orientation, the shear strength of a natural joint can be substantially different for load applied in different directions.

In studying the shear strength of rock joints, it is important to distinguish between filled and unfilled joints (Figure 1.3). Filled joints, ranging from those that contain soft plastic materials such as clay at a microscopic level, to faults that contain gouge or breccia at a macroscopic level, constitute a rather special set of problems and their shear strength principally depends on the physical and mineralogical properties of the material separating the joint walls. In contrast, the shear-strength behavior of unfilled joints depends on, apart from the level of effective normal stress acting on the plane of sliding, the properties of the rock walls including rock type, degree of roughness, size of the joint (scale effect), degree of weathering, presence of moisture, and water pressure. The effect of roughness on shear strength is more pronounced at low levels of effective normal stress (up to 20% of the unconfined compressive strength) and tends to be more important than the other factors. As explained more fully in Chapter 5, direct shear tests are advantageous for studying friction in rock mechanics because normal and shear displacements can both be measured easily during shearing (Figure 1.4). These tests make it possible to identify several basic mechanisms governing shear behavior. Initially, when a shear load is applied to a sample, the joint closes:

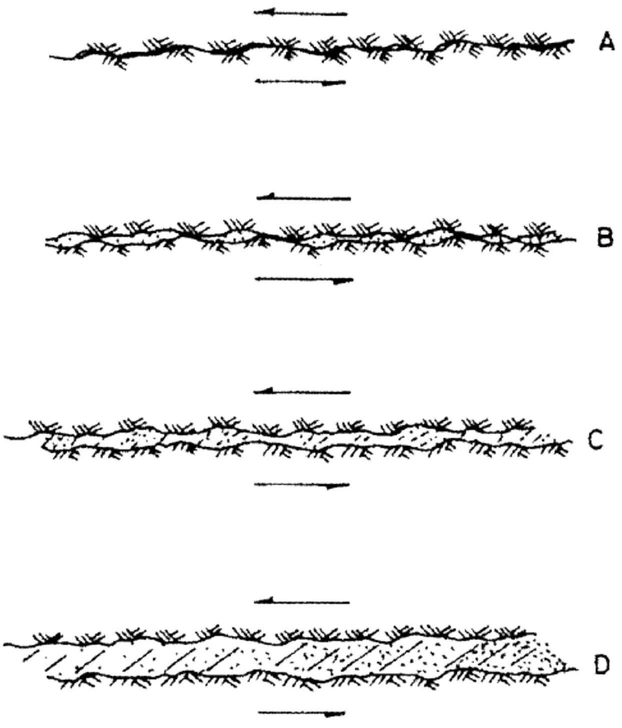

Figure 1.3 Filled and unfilled joints.

following closure, the asperities in contact deform elastically up to the yield point. If the joint is rough, it will tend to open “dilate” during shearing. Dilatancy is defined as the normal displacement of the upper block with respect to the lower block measured during shearing. The yield point marks the initiation of local micro cracks grow until failure (peak shear stress). Contacting asperities may deform elastically or be sheared or crushed, depending on the effective normal load and local geometry. Post peak, the shear load decreases tending toward a constant value that corresponds to what is termed the ultimate or residual strength of the joint.

A series of direct-shear tests conducted at different confining pressures generates a series of peak-stress points through which a joint shear-strength curve can be drawn. During shearing, as the shear stress builds, a period of adjustment with slight dilatancy is followed by a rapid increase in the rate of dilatancy, which is greatest as the peak-shear stress (“shear strength”) is attained. Thereafter, the shear stress falls continuously; the joint also dilates continuously until the residual displacement is reached. Residual displacement corresponds to the distance the joint displaces after peak-shear stress before reaching residual-shear strength. Residual displacement can be as much as several millimeters or even centimeters after the peak. In the field, with very rough joint surfaces, residual displacement may not be reached for as much as a meter of displacement.

Figure 1.4 Typical curve for direct-shear tests conducted under constant normal load conditions.

Significant contributions to the development of peak-shear-strength criteria for unfilled rock joints under low-effective-normal stresses have been made by Patton (1966), Ladanyi and Archambault (1970), and Barton (1977), whose approaches are discussed below. However, none of the strength criteria proposed take into account the fact that joint peak-shear strength is anisotropic depending on the variation in roughness with respect to the shearing direction. This anisotropy is routinely observed during direct-shear tests performed on laboratory samples (e.g. Huang & Doong 1990; Jing et al. 1992).

Development of a shear-strength criterion that takes account of surface roughness is the subject of Chapter 7.

1.1 COULOMB MODEL

The first known shear-strength criterion was proposed by Coulomb in the eighteenth century. Studying friction between two flat surfaces, he concluded that the relationship between normal and shear loads may be expressed as:

$$\tau = \mu \cdot \sigma_n \qquad 1.1$$

where μ is termed the coefficient of friction, which is a material property. Observing a block on an inclined plane, Coulomb noticed that it would remain at rest on the planar surface if the resultant of all forces acting on the block was at an angle with respect to the normal to the surface of less than ϕ_b, which he termed the basic friction angle. The coefficient of friction is related to ϕ_b by:

$$\mu = \tan \phi_b \, . \qquad 1.2$$

It is common for engineers to envision the concept of frictional resistance in terms of friction angles rather than the frictional coefficient. For example, in order to quantify the residual resistance of a joint, engineers often refer to the residual-friction angle (ϕ_r).

1.2 DILATANCY MODELS

Patton (1966) was the first researcher in rock mechanics to relate the shear behavior of joints to normal load and roughness. His work is based on an idealized model of a joint in which roughness is represented by a series of constant-angle triangles or saw-teeth. For these profiles, the dilatancy angle (arc tangent of the ratio between vertical and shear displacement of the sample during the shearing) is constant, assuming that the rock is rigid. Patton observed that at low normal loads, when there was practically no shearing of asperities, the shear strength of the joints was

$$\tau = \sigma_{\mathrm{n}} \cdot \tan(\phi_b + \mathrm{i}) \qquad 1.3$$

where σ_n is the normal load, ϕ_b is the basic friction angle, and i is the inclination angle of the teeth.

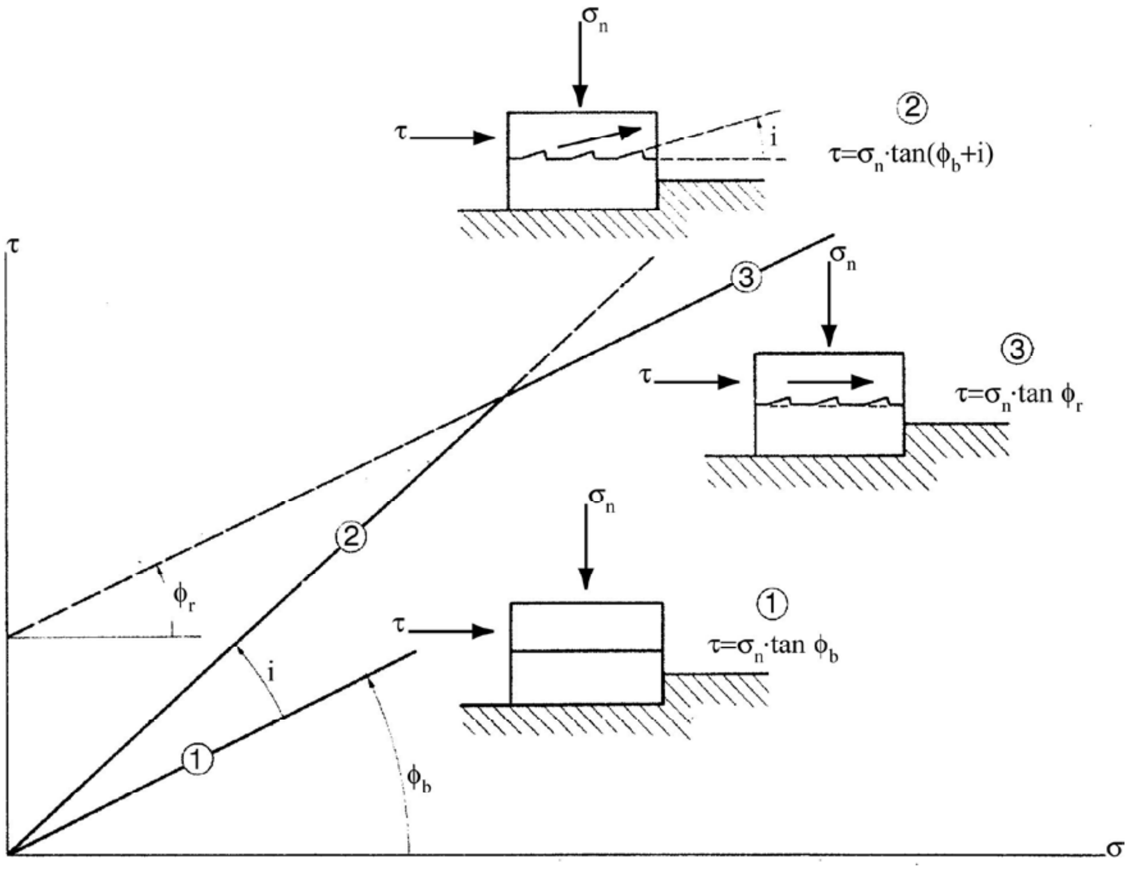

Figure 1.5 Bilinear failure envelope for multiple inclined surfaces after ((Patton 1966)).

At high normal loads, when the tips of most asperities were sheared off, he found reasonable agreement with experimental results using a different failure criterion:

$$\tau = c_j + \sigma_n \cdot \tan\phi_r \qquad 1.4$$

where c_j is the apparent joint cohesion and ϕ_r is the residual friction angle.

Combining the two failure criteria together, Patton obtained a bilinear envelope that describes fairly well the shear strength of plane surfaces containing a number of regularly spaced teeth of equal dimensions (Figure 1.5). However, these criteria are not satisfactory for describing the shear behavior of irregular rock surfaces, for which continuous failure envelopes are normally obtained. Patton correctly describes the discrepancy with real joints by explaining that unlike saw-tooth surfaces, where the failure envelope reflects a simple change in the mode of failure, the failure envelope for rock surfaces reflects changes in the intensities of different modes of failure occurring simultaneously.

Another extremely important aspect of shearing on asperities, which are inclined with respect to the direction of the applied shear stress τ, is that any shear displacement is

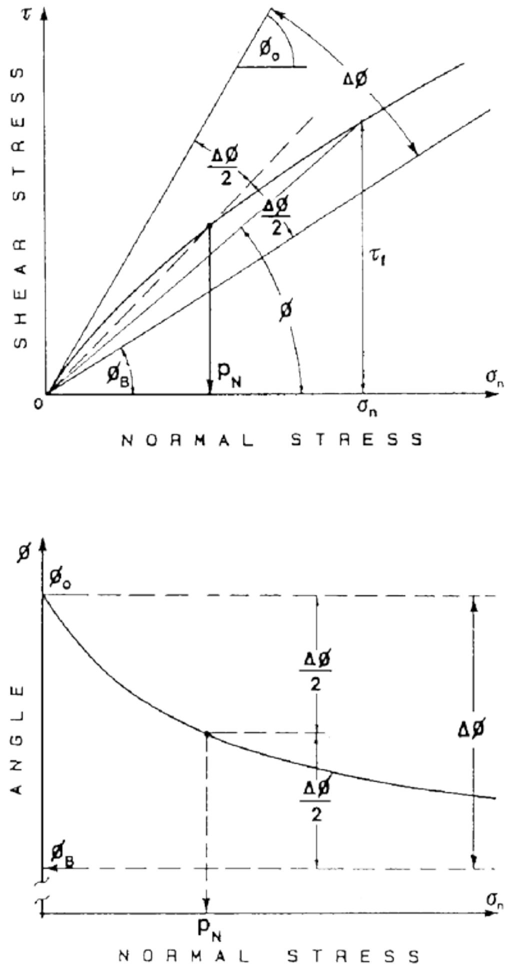

Figure 1.6 Definition of parameters used to derive nonlinear failure envelope ((Maksimovic 1992)).

accompanied by a normal displacement. In the case of a specimen with several projections, such as that tested by Patton, this means that the specimen dilates. This dilatancy plays a very important role in the shearing behavior of actual rock surfaces.

Patton's model was extended to natural profiles by Maksimovic (1996) to take into account dilatation. To describe the variation of dilatation of rough joints as a function of normal load he proposed the following equation to estimate the peak-shear strength of a joint:

$$\tau=\sigma_{\mathrm{n}}\cdot\tan\left(\phi_b+\frac{\Delta\phi}{1+\dfrac{\sigma_{\mathrm{n}}}{p_{\mathrm{n}}}}\right) \qquad 1.5$$

where: $\Delta\phi$ is the inclination of the steepest asperities; p_n is the median angle pressure, "equal to the value of the normal stress at which the contribution of dilatation and breakage of asperities is equal to one half of the angle of dilatancy for zero normal stress ($\Delta\phi/2$) ." The initial angle of the failure envelope at the origin is simply the sum of the basic frictional angle and the inclination of the surface asperities (Figure 1.6). A technical problem in trying to use this criterion is that it is necessary to perform at least three shear tests on the same surface to calculate the parameter p_n (Maksimovic 1992). Moreover, it is not clear from the paper how to obtaining these parameters in laboratory.

Again looking at two-dimensional saw-tooth profiles, the transition from dilatancy to shearing was studied theoretically and experimentally by (Ladanyi & Archambault 1970) who approached the problem of joint-shear strength by identifying the areas on the joint surface where sliding and breaking of asperities are most likely to occur. They define a_s to be the area where shearing through the asperities takes place. Over the rest of the surface, 1-a_s, the asperities are assumed slide over each other without damage. The proposed expression for the total resisting force is given as:

$$T_p = S_F\left(1-a_s\right)+S_r\cdot a_s \tag{1.6}$$

where T_p is the peak shear force; S_F is the shear force required for sliding over the asperities, and S_r is the force required to shear through the asperities. Based on these assumptions, and dividing Equation 1.6 by the total joint area, the proposed equation for peak-shear strength is:

$$\tau_p = \frac{\sigma_n\cdot\left(1-a_s\right)\cdot\left(\tan\theta_p+\tan\phi_b\right)+a_s\cdot\tau_{rock}}{1-\left(1-a_s\right)\cdot\tan\theta_p\cdot\tan\phi_b} \tag{1.7}$$

where τ_{rock} is the shear strength of the intact rock; $\theta_p = \arctan\left(v_p/u_p\right)$ is the dilatancy angle at the peak; v_p is the vertical displacement of the average joint plane at the peak, and u_p is the horizontal displacement at the peak, measured in the shear direction.

At very low normal stress levels when there is almost no shearing of asperities, $a_s\to 0$ and $\theta_p\to i$ (where i is the inclination of the teeth), and the equation reduces to Patton's law. At very high normal stresses, when $a_s\to 1$ and $\tau_p\to\tau_{rock}$, Ladanyi and Archambault suggested that τ_{rock}, the shear strength of the material adjacent to the joint surfaces, can be represented by the equation of a parabola in accordance with a proposal by Fairhurst (1964):

$$\tau_{rock} = \sigma_c\cdot\frac{\sqrt{1+n}-1}{n}\cdot\sqrt{1+n\cdot\frac{\sigma_n}{\sigma_c}} \tag{1.8}$$

where σ_c is the uniaxial compressive strength of the rock; σ_t is its tensile strength, and n is the ratio between the compressive and tensile strength ($n=\sigma_c/\sigma_t$).

It is important to note that in using Ladanyi and Archambault's equation, it is not necessary to adopt the definition of τ_{rock} suggested. Any other appropriate intact-rock shear-strength criterion can be used.

Unfortunately, the parameter a_s is not easy to measure, even under laboratory conditions. In contrast, the dilatancy rate is easily measured during a shear test, but it is difficult to estimate under in-situ conditions. To overcome these problems, and to make their equation more generally useful, Ladanyi and Archambault carried out a large number of shear tests on concrete saw-tooth surfaces and, on the basis of these tests, proposed the following empirical relationships:

$$\tan \vartheta_p = \left(1-\frac{\sigma_n}{\sigma_c}\right)^K \cdot \tan i \qquad 1.9$$

$$a_s = 1-\left(1-\frac{\sigma_n}{\sigma_c}\right)^L \qquad 1.10$$

where, for rough-rock surfaces, $K = 4$, $L = 1.5$, and i is the inclination angle of the teeth on the profile.

Ladanyi and Archambault's shear-strength model was later reviewed by (Saeb 1990) in light of the stress-dilatancy theory of sand, and he suggested the following simplified expression:

$$\tau_p = \sigma_n \cdot (1-a_s) \cdot \tan(\phi_b + i) + a_s \cdot \tau_{rock} . \qquad 1.11$$

To better represent rock surfaces, Haberfield and Johnston (1994) extended the triangular-asperity concept and considered a series of irregular triangular profiles. In this model, the asperities have variable inclination and base length in an attempt to predict the variation of dilatancy angle with shear displacement (Figure 1.7), and the different basic mechanisms controlling joint movement (Figure 1.8). While the Haberfield and Johnston models are an improvement over the regular triangular-asperitiy idealization, they are still difficult to apply

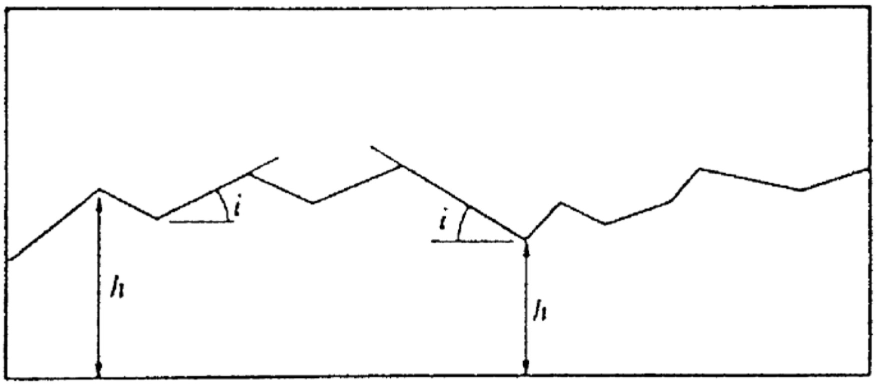

Figure 1.7 Idealized rock joint showing definition of roughness parameters ((Haberfield & Johnston 1994)).

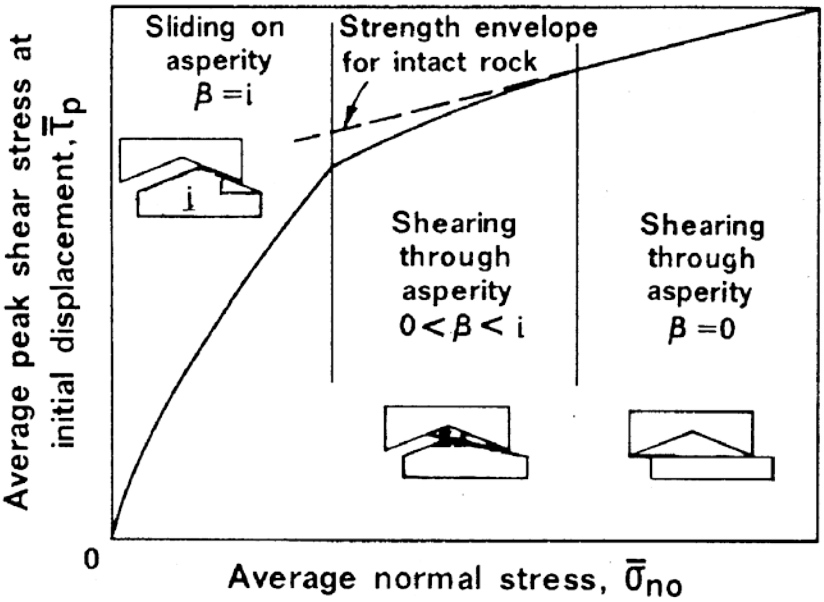

Figure 1.8 Peak-shear response of a triangular concrete joint under constant load conditions. Analyzing the mechanical behavior of the rock joints, (Johnston & Lam 1989) observed several basic mechanisms controlling joint movement. These mechanisms include initial deformation, sliding at individual asperities (including the smoothing of micro-asperities, which subsequently results in a sudden loss of apparent cohesion), asperity shearing, and asperity crushing.

to natural joints. For example, the choice of an appropriate base length is rather arbitrary, and the process for approximating a rough surface as triangulated profiles is not well defined. Furthermore, for more realistic profiles, the dilatancy angle will vary with shear displacement, and difficulty arises in predicting the variation in dilatancy angle, and hence in shear strength, with shear displacement.

1.3 JRC MODELS

An alternative approach to the problem of predicting the shear strength of rough joints was proposed by Barton (1977). Based on tests carried out on natural rough joints, Barton derived the following empirical equation

$$\tau_p = \sigma_n \cdot \tan\left(\phi_b + \mathrm{JRC} \cdot \mathrm{Log}_{10}\left(\frac{JCS}{\sigma_n} \right) \right) \qquad 1.12$$

where JRC (Joint Roughness Coefficient) is a parameter that represents the roughness of the joint and JCS (Joint Compressive Strength) is the compressive strength of the rock on the joint surface, taking into account possible reductions in resistance resulting from fatigue, chemical alteration, or other processes that weaken the rock at the interface. When the joint is “fresh,” JCS is equal to the compressive strength of the rock (i.e. JCS=σ_c). JCS is determined using a Schmidt hammer as outlined by Barton (1977).

Comparing Equation 1.12 to that proposed by Patton (Equation 1.3), it is evident that the difference between the two expressions is that the roughness angle i of Patton's equation has been replaced by a term dependent on normal stress that contains JRC.

Barton's original experiments were carried out at extremely low normal stress levels, and his equation is probably most applicable for stresses in the range $0.01 < \sigma_n/\mathrm{JCS} < 0.3$.

Moreover, it is important to note that as $\sigma_n \rightarrow 0$, the logarithmic term in Barton's equation tends to infinity and the equation ceases to be valid. Barton suggested that the maximum value for the total friction angle (argument in the tangent term) should be 70º.

Barton proposed estimating JRC either by back-analyzing shear tests that have been performed, or by visual comparison of roughness to ten standard profiles given in Figure 1.9. For these standard profiles, JRC values between 0 and 20 were assigned in steps of two, with zero corresponding to the smoothest profile and 20 to the roughest. The International Society for Rock Mechanics later adopted these standard profiles in their suggested procedure for measuring the roughness of discontinuities (ISRM 1978).

This visual-comparison method for estimating JRC has been judged to be subjective and unreliable by several investigators (e.g. Hsiung et al. 1993, Maerz et al. 1990). Therefore, many researchers have studied alternative ways to calculate JRC, and consequently, many parameters have been proposed in the literature. Many researchers have investigated the correlation between statistical parameters (Tse & Cruden 1979, Reeves 1985) (see Chapter 4) or fractal dimensions (Lee et al. 1990) of the profiles and the JRC values. However, the JRC values themselves include a few problems. For example, while the shear strength of a joint depends on the direction of shearing (Huang & Doong 1990, Jing et al. 1992), the statistical parameters and fractal dimensions give no directional information. At present, there is not general agreement on a methodology for quantifying JRC.

The problem of mismatched joints is addressed by (Zhao 1997a, Zhao 1997b) by modifying Barton's criterion:

$$\tau_p = \sigma_\mathrm{n} \cdot \tan\left(\phi_b + \mathrm{JCM} \cdot \mathrm{JRC} \cdot \mathrm{Log}_{10}\left(\frac{JCS}{\sigma_\mathrm{n}}\right)\right) \qquad 1.13$$

where JMC is defined as the joint-matching coefficient. JMC is obtained by estimating, primarily through visual inspection, the approximate percentage area in contact between the upper and lower walls of the joint. Thus, JMC has a value between 0 and 1. This is the first approach for estimating shear-strength that introduces a parameter to explicitly account for the matching of the joint surfaces. However, its usefulness is limited because it is very difficult to estimate JMC.

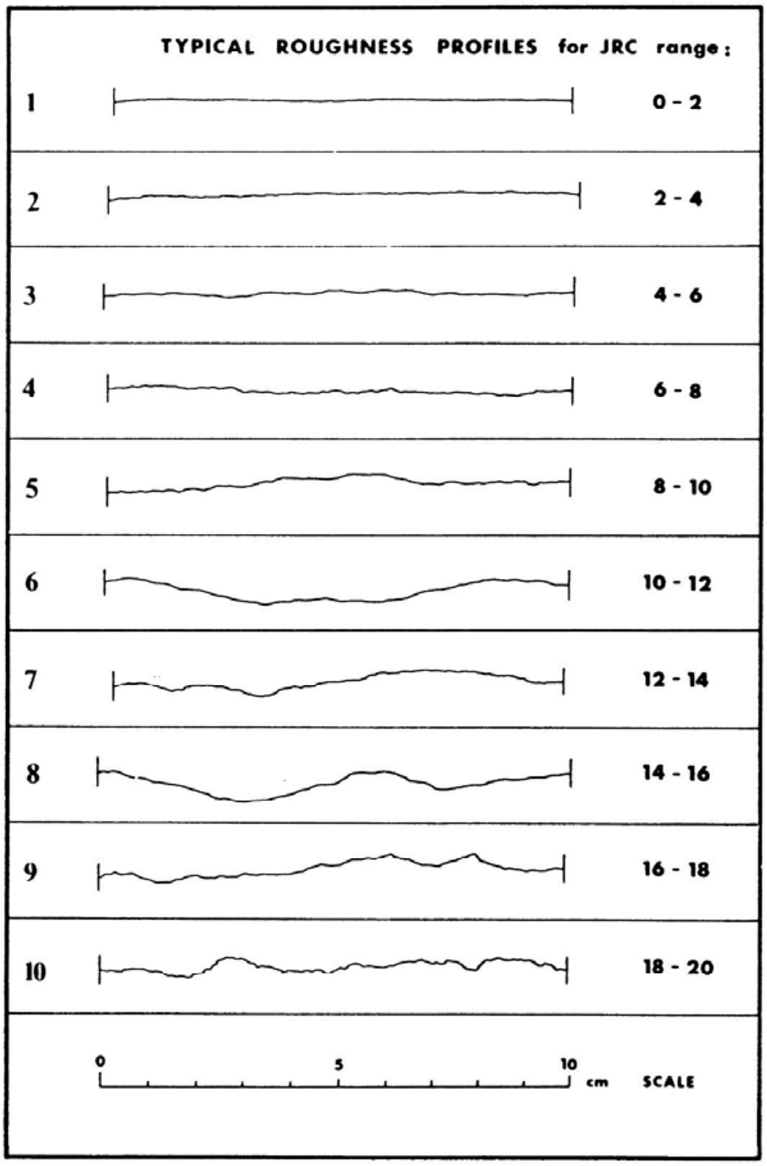

Figure 1.9 Standard profiles used for visual estimation of JRC (Barton & Choubey 1977).

1.4 SUMMARY

The choice of a general criterion to determine the shear strength of rough rock joints is a general problem that has been investigated for many years. Numerous shear models have been proposed in the last decades to relate shear-strength to measurable joint parameters. While these models have improved our understanding of rock joint behavior, their limitations have to be recognized. The models available in the literature are questionable when applied in practice either because they are too simplistic (Patton), or rely too heavily on empiricism (JRC models), or require estimation of complex input parameters that is beyond the capabilities of normal site investigation practice or laboratory procedures (Ladanyi & Archambault). Moreover the shear behavior of rock joints has been studied mainly on artificial joints having regular surfaces such as saw-tooth and stepwise shapes (Xu & De Freitas 1990, Qui et al. 1993, Fishman 1990, Dong & Pan 1996, Dight & Chiu 1981, Yang & Huang 1995). In this case, two modes of failure, sliding and shearing, are clearly distinguishable, and it may be valid that all asperities are sheared through at the same time, as assumed by (Huang et al. 1993). However, since the surface of a natural rock joint has asperities with various base lengths (projected lengths) and inclinations, the failure envelope for the natural joint would not reflect a simple change in the mode of failure. For these reasons, it would appear that existing models are not capable of capturing the complex shear behavior of rough rock joints with sufficient accuracy. Thus, to go beyond state of the art, a new peak-shear-strength criterion is necessary.

Today many of the technical limitations that have prevented quantifying surface parameters have been overcome. For example, high performance computers make it possible to map entire surfaces easily, and new algorithms are opening the way to new approaches for studying friction in rock that go beyond the use of two-dimensional profiles to those that use data describing the entire surface (Chapter 3). Shear-test data can now be recorded in real time at infinitesimal intervals of time. Tests that once were only possible to realize under laboratory conditions, are now available for use in-situ. Therefore, many more pieces are now available to solve the puzzle. The challenge today is incorporating new parameters into expressions of shear strength. To be useful, these expressions must provide accurate estimates of peak-shear strength, based on parameters easily measured under both laboratory and in-situ conditions.

2. Surface measurement of joint

"When you can measure what you are speaking about, and express it in numbers, you know something about it, but when you cannot measure it, when you cannot express it in numbers, your knowledge is of a meager and unsatisfactory kind; it may be the beginning of knowledge, but you have scarcely, in your thoughts, advanced to the stage of science."
Lord Kelvin

For scientists and engineers, measurement and measurement devices are the only way to analyze, explore, probe, study and discover the truth about details not readily obvious. Measurement is the way we gain substantive knowledge about things. We get numbers. This is more than the philosophical "knowing" of something to gain knowledge. The type of knowledge needed by scientists and engineers in order to understand things and how they interact with each other is called quantitative knowledge, or, knowledge that is expressed in terms of numerical values and units. You know things better when you know about something quantitative about them. Using Kelvin's words, being able to describe and to quantify attributes allows us to move beyond "meager" knowledge. Measurement devices are moving toward critical link in obtaining quantitative knowledge. So, too, are the ways in which one uses them. You have to use not only the appropriate measuring device, one that measures the parameter you need, but also the appropriate version, one that is capable of resolving the least significant magnitude of the quantity desired and also one which has sufficient range to cover the largest expected value. Once a system has been chosen, a measurement device must be carefully calibrated and work with a known measuring error under the conditions prevailing when the measurement is made (Peacock 1998). Learning the correct way to measure, to select the appropriate device with the needed range, resolution and other important properties are part of the job of gaining more than "non-meager" knowledge.

In the late sixties and early seventies, (Rengers 1970, Patton 1966, Ladanyi & Archambault 1970), researchers in rock-mechanics, confirmed that the shear strength of rock joints is strongly related to the roughness of the joint surfaces, as well as to the nature of the rock material. Therefore, it was recognised that a precise measurement of the rough surface topography was necessary to study the shearing mechanism and predict both the peak and residual strength of rock joints, as well as the amount of dilatation a discontinuity undergoes during shearing. Roughness is difficult to quantify and, even when measured, the result strongly depends on the method of measurement. The accuracy of measurements and the spatial-resolution necessary to make useful measurements depend on application. Furthermore, for many applications, the data of interest is the contact-areas between the joint faces and/or the joint aperture. In these cases it is necessary to determine the matching between the joint–surfaces.

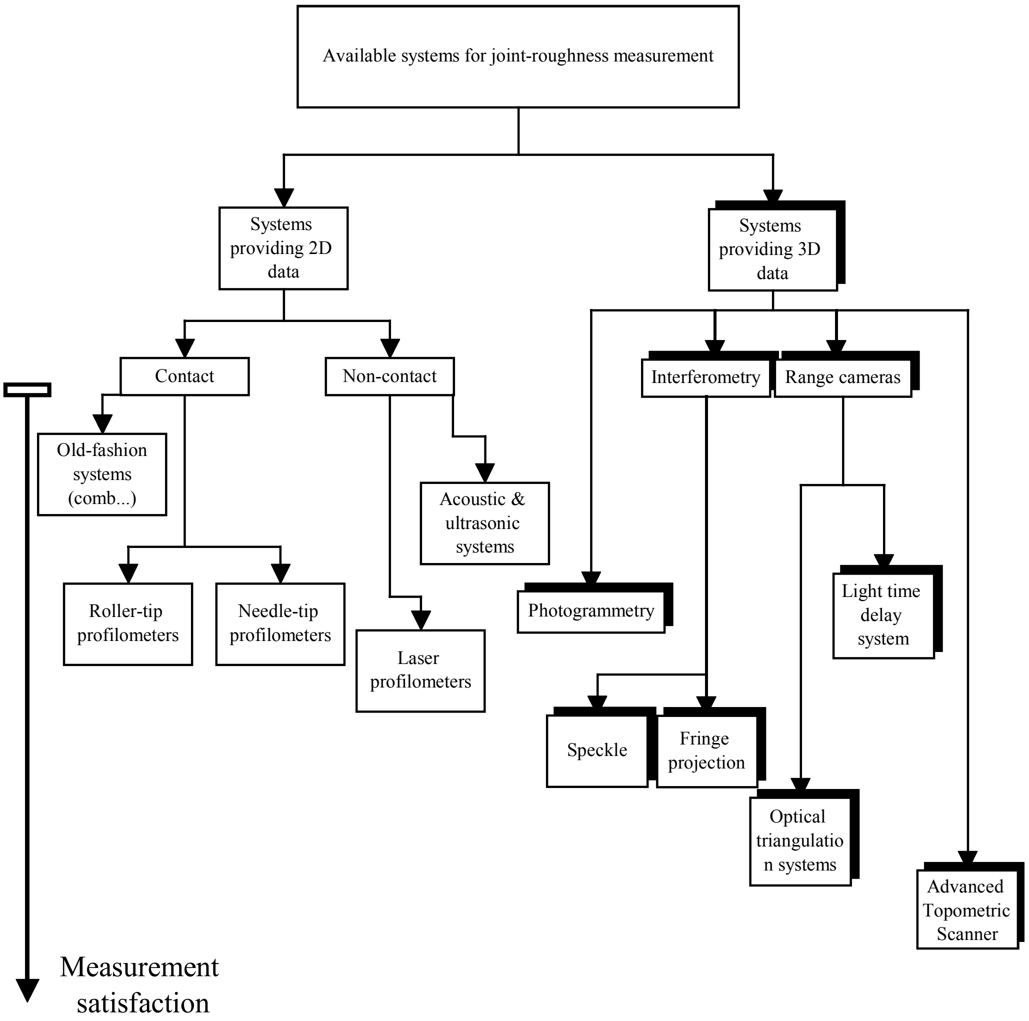

Figure 2.1 Methods available today can be classified into two categories depending on whether they provide two- or three-dimensional data. The different systems are classified on a general measurement-satisfaction scale. It is based on criteria which: speed; accuracy of the system; precision of the measurement; measurement resolution; measurement time; data-analysis time; in-situ use

2.1 STATE OF THE ART

A natural way to gain a feel for the roughness of a surface is to run a finger across it. Mechanical profilometers work in the same way: a contacting-probe moves across the surface measuring the height of the surface along a line. The principle is to measure the vertical displacement of the stylus as it moves across the surface. Based on this principle, a number of devices to establish the surface profile of rocks have been developed, ranging from a simple contour gauge (Stimpson 1982) to today's highly sophisticated and accurate profilometers. The first profilometer developed recorded on paper the profile measured mechanically (Rengers 1970). During the eighties computer advances made it possible to develop faster and more accurate systems.

Methods available today can be classified into two categories depending on whether they provide two- or three-dimensional data (Figure 2.1). Mechanical and laser profilometers, and ultrasonic methods, are the most common 2D measurement techniques, providing data along profiles. These measurement systems can be further classified as either contact or non-contact. Among the contacting methods, mechanical or electronic stylus profilometers give precise measurements along a traverse (Swan 1983). It is possible to identify two different subgroups of mechanical devices: the group using a stylus with a roller tip that slides along the joint-surfaces, and the group uses a needle-like stylus that measures at discrete points the surface. For both, the lowering of the stylus is recorded as a function of its position on the joint-surface. Whit this systems, resolution depends in part on the dimension of the stylus (0.5-2.0mm radius). The profile recorded by the stylus is the locus of the center of stylus itself (ISO3274 1996). If the contacting point is assumed to be spherical, the effective profile error is related to the stylus radius (Figure 2.2). The curvature of a peak may be exaggerated, while a valley may be represented as a cusp. A profile containing many peaks and valleys with radius of curvature 10 µm or less, or with many slopes steeper than 45°, is not well-suited measurement by a stylus instrument (Thomas 1999b). Another source of error, with contact systems, is the load on the area of contact. Caused by the probe even a small pressure, as small as 0.75 mN (ISO3274 1996), may be sufficient to cause local downward deformation or

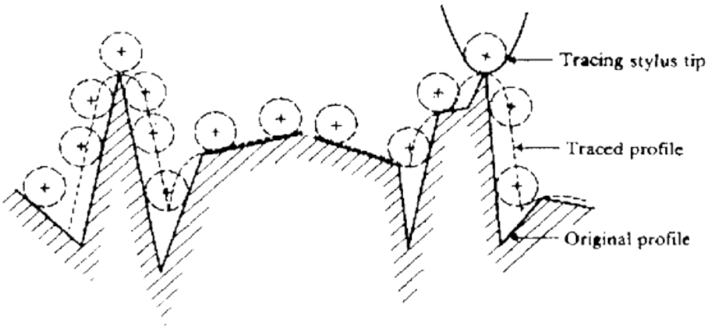

Figure 2.2 Distortion of measured profile due to finite dimensions if stylus tip (exaggerated) (Thomas 1999b)

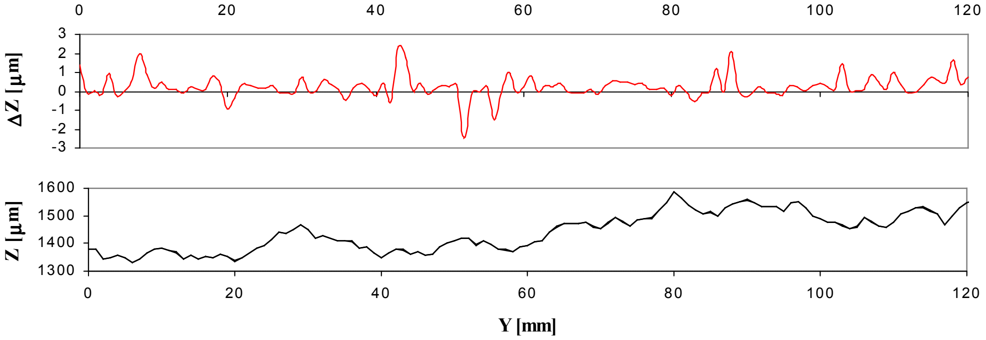

Figure 2.3 Forward and backward profiles measured with the LMR-profilometer (lower curb). In the upper graphic it has been plotted the difference between forward and backward profile. It results smaller than the precision of the instrument.

brittle cracks on the surface being measured. Asperities on the surface also cause a lateral displacement of the stylus on which explaining why profiles measured in one direction do not agree exactly with measurements made in the opposite direction (Figure 2.3). Abrasion of the stylus (usually made of steel) during measurement is not usually sufficient to affect the precision of the instrument.

Subsequently, the need to do not touch nor to damage the surface features, the need of increasing the measurement speed and the new possibilities opened by hardware development, permitted the adoption of laser profilometers, instead of mechanicals, that utilize reflected light beams. Surface-measurements and data acquisition are generally carried out automatically with a personal computer. A laser-displacement sensor is used to measure scan-lines across the surface profile (Jeremy 1995, Lee & Juang 1991, Haberfield & Johnston 1994). The light is reflected off the surface being measured, and recorded by a position-sensing diode. The voltage output of the diode is directly related to the distance measured. An important source of measurement error is related to surface refraction, which depends on presence of quartz crystals. Thus rocks that contain quartz crystals or other refracting features may be difficult to accurately measure with a laser-based system. The resolution of the measurement is also limited by the laser-spot-diameter, normally in the range of 0.3-2.0 mm.

A rather ingenious two-dimensional method is the shadow-profilometer. It analyzes the image, recorded on a VHS tape, of the edge of the shadow produced by the rough joint illuminated by a 45° light source (Maerz et al. 1990).

Figure 2.4 Kreon KLS 51 3D laser scanner used by (Lanaro et al. 1998) (http://www.kreon3d.com)

Although the results obtained analysing surface profiles have provided useful data on properties of joint surfaces, several authors have shown that jont morphology must be handled, more rigorously, in a three-dimensional manner, considering both anisotropy and volumetric features (Lanaro et al. 1998, Xie et al. 1999). For exemple, many authors have begun to develop systems that allow measurement of the entire surface to obtain 3D data directly in one reading.

One of the first approaches was based on stereoscopic images of the surface (terrestrial-photogrammetry) used to calculated the elevation of the surface on a regular grid. This procedure is time consuming and generally not accurate enough to provide useful data. Another approach to the whole surface measurement is interferometry. Interferometry and speckle interferometry use the interference fringes produced when monochromatic and laser light are reflected off a rough surface and a flat reference surface. The fringes correspond to contours of roughness at a contour interval of about one-half the wavelength of the light used (Bergmann et al. 1997). By analyzing the digital images of the fringe patterns it is possible to calculate the roughness. It is, however, necessary to accurately calibrate the system and to use a flat reference surface.

The development of CCD (charge coupled device) cameras made possible to study and analyse the images of the surface directly using a personal computer, without any manual procedures. CCD-based instruments exploit the ability of cameras to measure the angle subtended by a scanned spot of light come in many shapes and sizes in the late nineties. Three-dimensional measuring cameras, also known as range cameras, are as diverse as their intended applications. They are differentiated by the optical principles they are based upon.

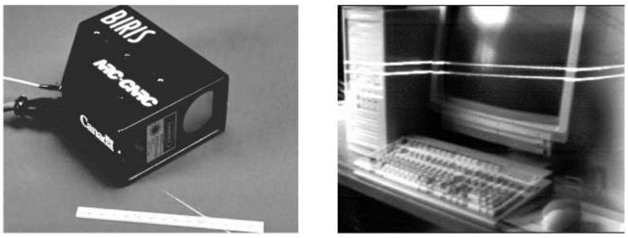

Biris camera Video image of laser line

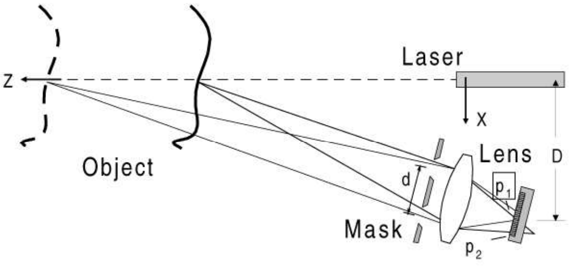

Biris range camera principle

Figure 2.5 Biris camera principle (Beraldin et al. 1998)

The majority of instruments either exploit optical triangulation or time delays generated by light traveling in a medium.

For example, the Kreon 3D-laser scanner (Lanaro et al. 1998) projects a thin laser strip on the rough surface, which is filmed by two CCD cameras in a stereographic fashion (Figure 2.4). The laser strip moves automatically over the sample, and the data collected are processed by a personal computer. The result is a three-dimensional topographic image of the rough sample with an accuracy of ±50 μm. The interest of this system is that for the first time it has been improved, for measuring rock-rough-surfaces, a system able to take advantage by different techniques: the precision both of the coherent light and the optical triangulation (terrestrial-photogrammetry algorithm).

Among the many non-contact techniques that exist for the extraction of 3-D information, it is important to cite the Biris laser-range camera (Beraldin et al. 1998) because it is a system developed to work especially under in-situ conditions. A laser line, produced by a solid-state laser diode and a cylindrical lens, is projected on the object to be measured. A double image of the laser line is measured by a CCD camera. The separation between the two imaged lines and their relative position of the camera are proportional to the distance between the object and the camera (Figure 2.5).

Other techniques, such as ultrasonics, are fast but are unable to provide sufficient spatial resolution or enough accurate measurements. Time-of-flight light techniques are not accurate enough at close range and are not sufficiently fast (Bell 1998).

2.2 CHOICE OF MEASUREMENT SYSTEM

A review of the literature clearly shows that there is not “The perfect measurement system,” but rather that many approaches exist, and that each one has its advantages and disadvantages. Choosing a method for a particular application means finding the best compromise among criteria that include the:

- Size of the sample that can be evaluated
- Measurement speed
- Precision
- Repeatability
- Spatial resolution
- Ease of measurement
- Ease of analyzing the data
- Suitability for use in-situ

The idea of identifying the “best-system” was a clear vision, but the conversion of this idea into a choice was a long and complex process. For this study several rock samples were analyzed so that the time required for measurement and post-processing of the data were important criteria in choosing a method. Only by testing different systems in the laboratory it was possible to make a decision.

This research of “The perfect measurement system” began with two-dimensional profilometers, moving later toward systems allowing three-dimensional measurements. The experience using profilometers, both mechanical (described in detail in the section 3.3) and laser, shows that they provide data with precision in the range between 10 and 70µm. However, data is collected along lines (profiles). As rock joint-parameters must be obtained in three dimensions, complete surface data can only be obtained by interpolating between profiles, using a statistical or geo-statistical algorithm to calculate the values around the measured point. This process is extremely time consuming, requiring several hours to obtain the profile data, and days to complete the interpolation. Furthermore, interpolation affects the precision of the final result.

After making many measurements with profilometers, it was decided that it was necessary to develop a methodology that would allow direct measurement of the third dimension. The first purely three-dimensional-method tested was based on interferometry, trough collaboration with IMAC-DGC-EPFL laboratory. Interferometric methods can provide very accurate results since individual measurements can be made smaller or of the same size as the laser speckle occurring in the interferogram plane. By means of the selection of the wavelengths of the laser light used, the region can be established within which the spacing of the measuring points in question from a reference surface can be clearly measured. The operating principle is relatively simple: the projections of the same laser-fringe-pattern on both a flat surface and a rough joint are captured by a CCD camera (Figure 2.6). The difference between these two images is used to determine the third dimension (Figure 2.7). However, many practical problems occurred during laboratory tests. For example, any

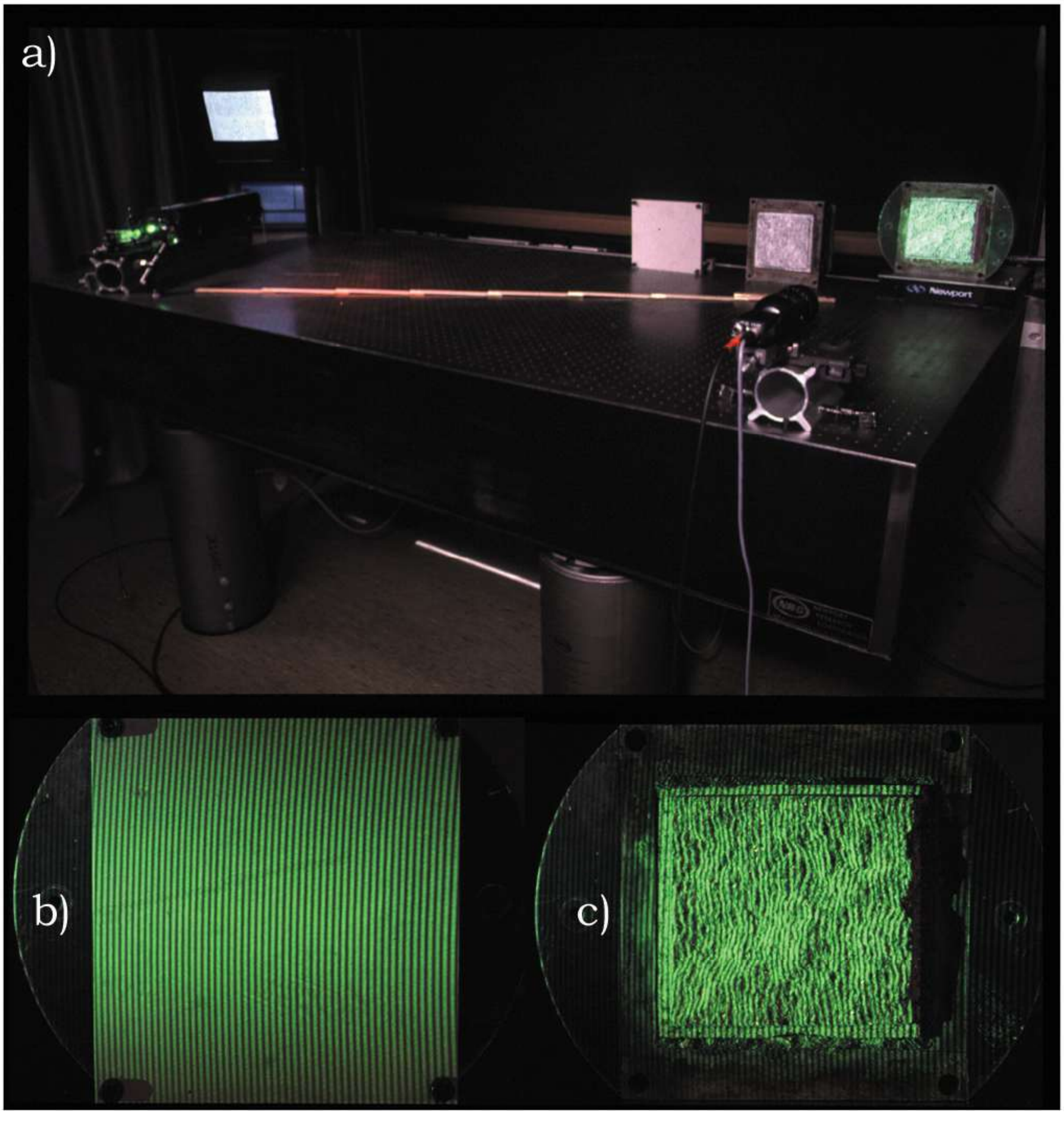

Figure 2.6 IMAC interferometry set-up (a). The fringe-pattern has been projected before on a reference-plane (b) and after on the rough-joint (c). The difference between these two images provides the third dimension.

reflecting areas on the rough surface (e.g., quartz crystals) introduced noise into the measurements, and the reflected laser-light made the system unsafe because the danger to the eyes. Moreover, the laser-projection set-up was time-consuming to calibrate (on the order of one day) and the raw data were difficult to interpret. Furthermore, the IMAC software used was not well suited for our purposes because, at that time, it was on the first stage of development. However, the final results, obtained after substantial data processing, were excellent, with a precision of ±35 μm and spatial resolution of 0.5 mm (Figure 2.8). Even though the precision, and resolution were sufficient, time required to process the data was judged to be long for our need. In addition, the system would be difficult to use in situ.

Although interferometry is a good approach for many applications, it was not the solution to our problem.

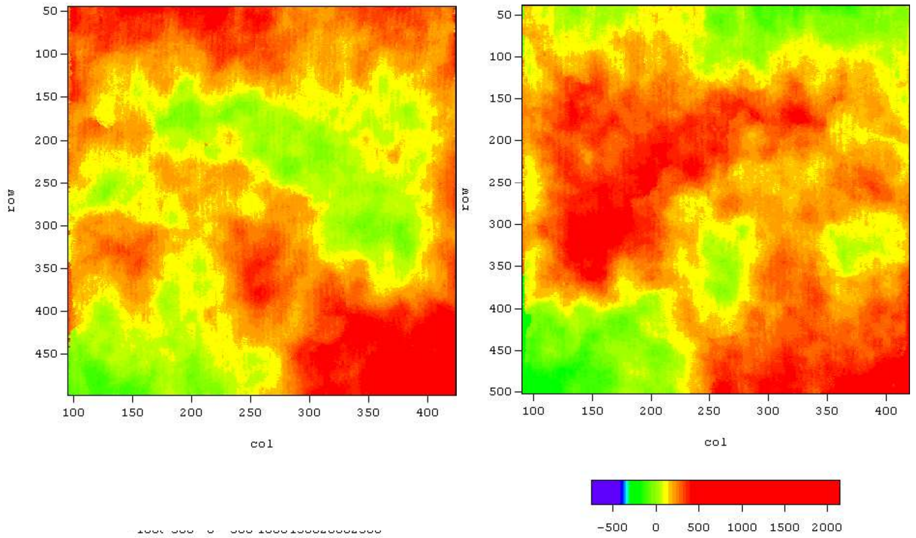

Figure 2.7 Color-scale representation of both sides of a gneiss joint sample measured at IMAC laboratory. The spatial resolution of the measurement has been evaluated in 0.5 mm with a precision of ±35 μm in the vertical direction.

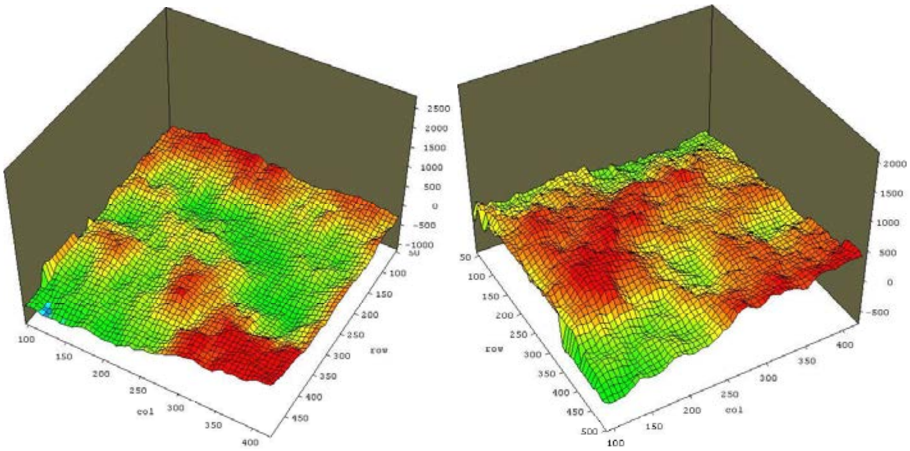

Figure 2.8 Three-dimensional representation of both sides of a gneiss joint sample measured at IMAC laboratory.

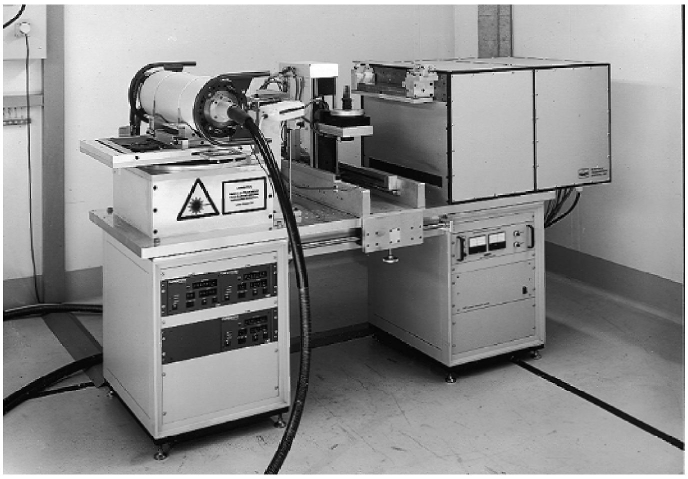

Scanner:	Model CITA 101B+, Scientific Measurement Systems SMS	
X-Ray Source:	450 kV Philips MG 451, Focus Size 1 mm at 2 mA	
Detector System:	125 CdWO4 Scintillators, Tungsten Collimator	
Spatial Resolution:	approx. 0.5 - 1‰ of object diameter (best resolution 50 µm)	
Object:	Diameter:	up to 500 mm
	High:	up to 600 mm
	Weight:	up to 25 kg
Penetration:	Steel:	60 mm
	Ceramic:	100 - 200 mm

Figure 2.9 Industrial computer tomography scanner of EMPA (Swiss Federal Laboratories for Materials Testing and Research).

Another approach considered was terrestrial-photogrammetry, but it was immediately ruled out because it is extremely time consuming, requiring several days to obtain a three-dimensional map of the joint surface on a 1mm grid.

Photogrammetry and interferometry both failed two points of our evaluation-criteria: time required for calibration and in analysis of the raw data.

The last system tested and later adopted for measuring joint roughness is a combination of photogrammetry and interferometry. Specifically, the measurement principle is based on optical triangulation (photogrammetry) combined with white-light fringe projection and phase shifting (interferometry) to obtain a fast and robust calculation of dense 3D-point clouds. The measurement principle and features of the system are explained in detail in section 3.4.

Among the other methods tested, also if not suitable for surface measurements, has to be quoted the computer-tomography (Figure 2.9). One close marble-joint sample has been scanned and the data analyzed. The hardest problem was to handle the measurement noise that occurred because of the density of the rock. The resulting map of the joint-void-space had a spatial resolution of 20 µm but the error was on the same scale. Moreover the measurement of the sample took two full days of continuous scanning and two more days of CPU-time to analyze the raw-data. Tomography was therefore judged too time consuming since we planned to study many sample.

2.3 LMR PROFILOMETER

The first measurement system tested and extensively used was an automatized mechanical profilometer developed during the nineties at the Rock Mechanic Laboratory (LMR) of the Swiss Federal Institute of Technology of Lausanne. The LMR contact profilometer (Figure 2.10) measures the joint-surface profiles by recording the vertical position of a stylus (sphere of 0.5 mm radius) as a function of its x-y position. The measurement is completely automated. A personal computer controls the movement of both the stylus and the rock sample and it records the data in text format. The vertical position of the stylus is measured using optical stylus-transducer (Compac-1030) with a precision of ±20 μm. Up to five stylus transducers are fixed on a rigid frame that can move only in the y direction (Figure 2.11). The rock sample is fixed to a carriage (Amsler-Sok20-130) controlled by a stepper motor (Amsler-DKC041B) moving in the x direction. The minimum step is 0.01 mm and the maximum stroke is 200 mm.

The vertical movement of the styluses is controlled by modulating the air-pressure inside the transducers. To reduce shocks corresponding to the periodical upper motion, each stylus is

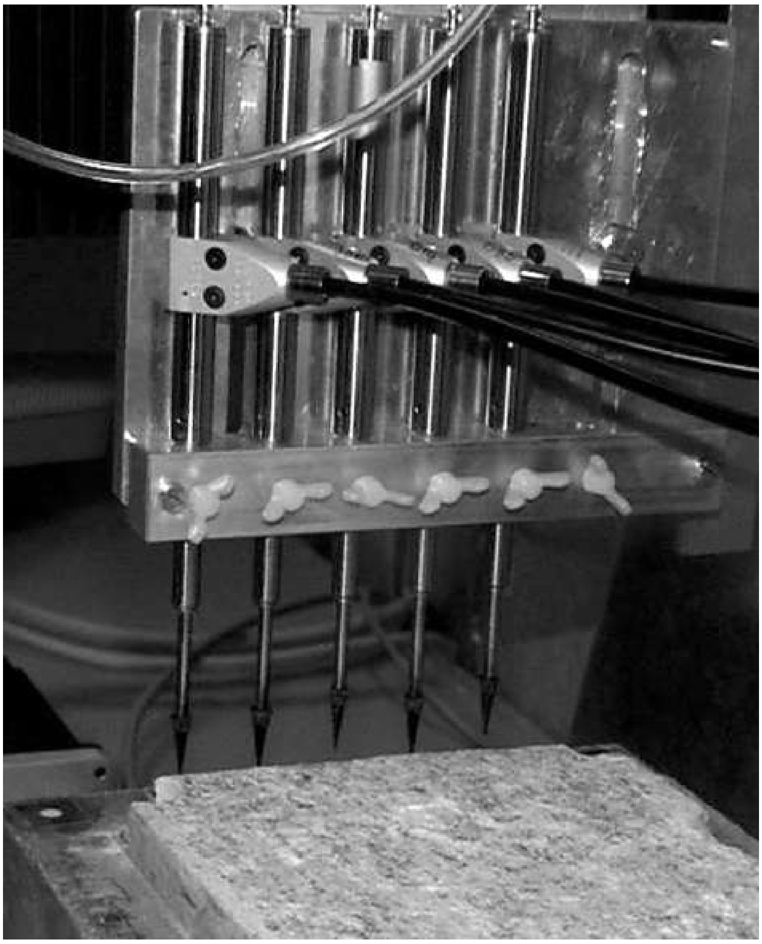

Figure 2.10 The LMR contact profilometer measures the joint-surface profiles by recording the vertical position of a stylus (sphere of 0.5 mm radius) as a function of its x-y position.

equipped with a soft ring. To prevent damage to the stylus-transducer, the motor-control algorithm permits movement only when all the styluses are in the upper position. Even with all these precautions, many errors were introduced because of damage to the transducers that occurred during the measurements. The system measures up to 5 points on the surface (one per stylus) every 5 seconds.

The LMR profilometer was used to collect profiles from a large number of different rock samples. Its primary limitations are the time required to measure the complete surface (many hours), and is extremely difficult to repeat a measurements and obtain the same profile. In fact, we found it nearly impossible to reposition the samples in exactly the same place for repeat measurement. Although the LMR profilometer is adequate for studying general features that may characterize joints in a particular rock type, it is not sufficient for studying three-dimensional joint features or for measuring the evolution of damage during a shear-test.

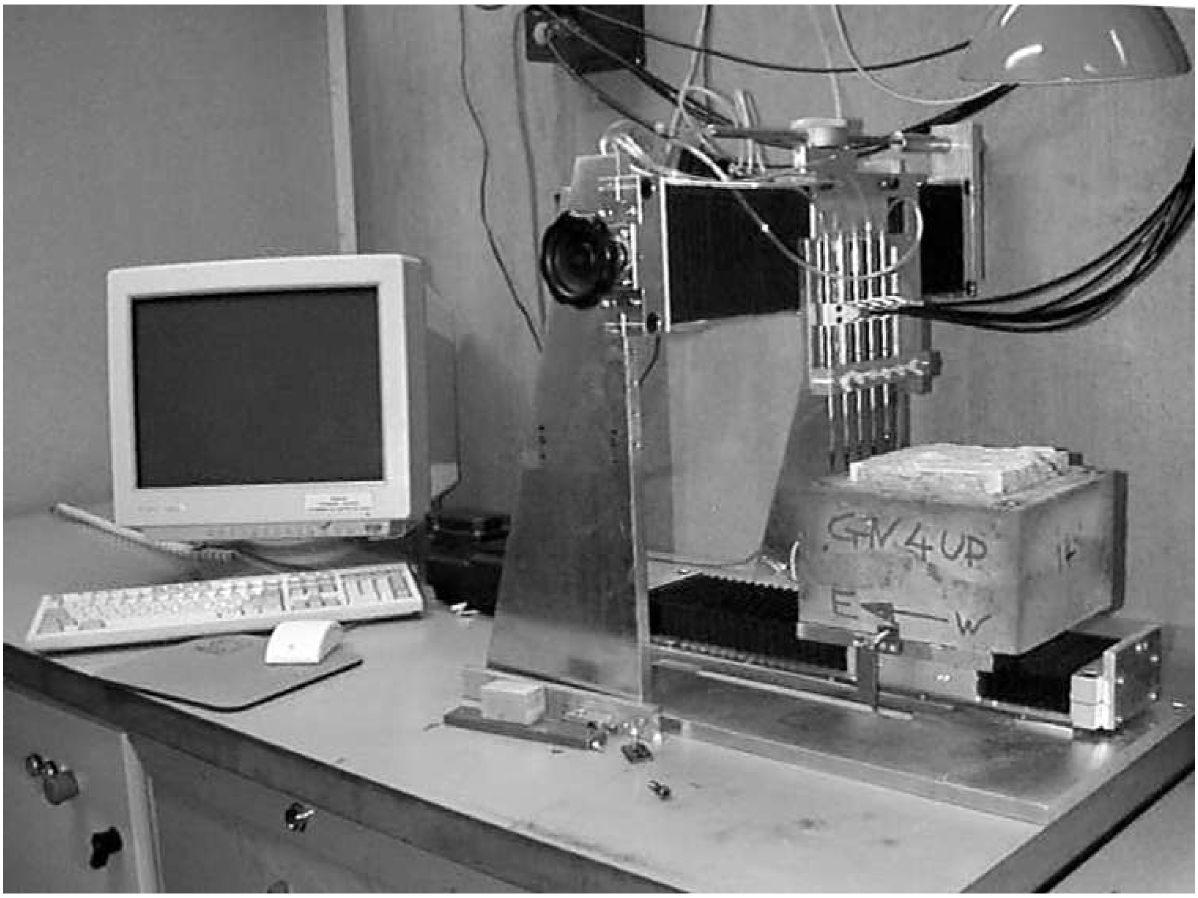

Figure 2.11 The LMR contact profilometer measures rock sample that are fixed to a mobile carriage controlled by a stepper motor moving in the x direction. The minimum step is 0.01 mm and the maximum stroke is 200 mm. .

2.4 ADVANCED TOPOMETRIC SENSOR (ATS)

After evaluation of several measurement techniques, a system based on advanced topometric sensor (ATS) was judged best for. ATS is an optical measurement system developed especially for the automotive industry where 3d-measurement of objects plays an integral role in reverse engineering and quality control. In the last years fringe projection-systems have gained increasing usage in this field. They provide an optical method based on a combination of white light fringe projection, triangulation and phase shifting for a fast and robust calculation of high dense 3d-point clouds. ATS offers both the advantages of high precision and good repeatability with a fast and easy way of utilization. More, the weight and the dimensions of the transport cases make possible its utilization in situ, assuring the same accuracy as the laboratory measurements (Grasselli & Egger 2000a).

2.4.1 *Principle*

The Advanced Topometric Sensor (ATS) measures objects at a high data density (approx. 400,000 object pixels per image) and makes them available as point clouds for reprocessing or visual inspection. The measurement process is based on the principle of optical triangulation and profits from the precision of light.

The system consists of a measuring head (Figure 2.12), a tripod, a controlling-box and a PC. The measuring head, which is screwed on the tripod, is placed about 50cm above the surface. The ATS topometric system works on new principle compared to one-camera fringe projection sensors. During the measurement various white-light fringe patterns are projected onto the object surface and grabbed by two digital cameras, which are integrated into the measurement head, from two different angles. For the computation of the absolute phase function different graycode and phaseshift pattern (Figure 2.13) are projected onto the object and recorded with both cameras. For the photogrammetric calibration of the arrangement a calibration panel with target points must be placed in different positions in the measurement

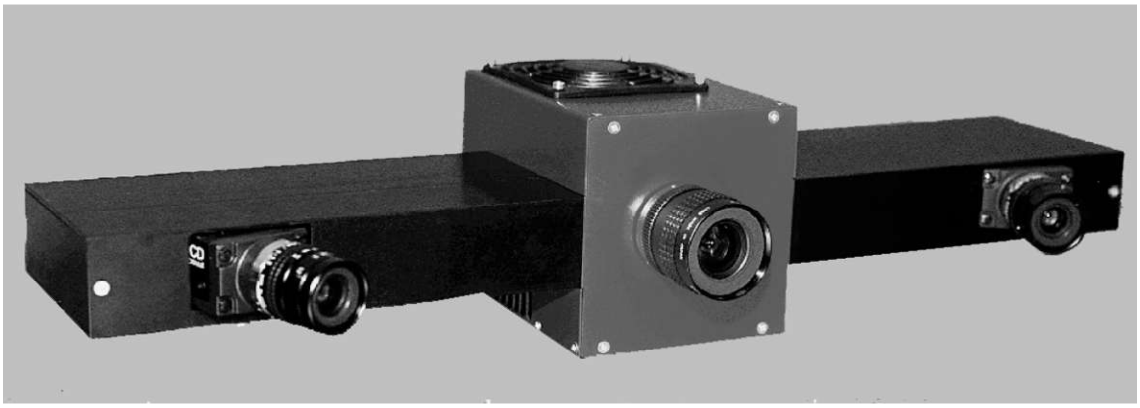

Figure 2.12 Measuring head of the advanced topometric sensor (http://www.gom.com)

space. The positions of the panel and the coordinates of the target points must not be known a priori. After the calibration the interior and exterior orientation of the sensor is determined.

From the graycode and phaseshift images the absolute phase function for each camera is computed. With the known calibration of the sensor the accurate and high resoluted object coordinates can be computed by applying a new correlation algorithm. 3D-coordinates are computed independently with high accuracy for each of the CCD camera pixels using triangulation methods and digital image processing (fringe projection and image shifting). The image characteristics are calibrated simultaneously during each measurement so that possible changes of projection do not affect the result. In fact, the sensor orientation is automatically calculated during each measurement. The consistent exploitation of redundant information covers the results statistically.

Without direct contact to the objects and materially independent, the 3D-digitizing of arbitrary surfaces can be carried out for a variety of applications and situations.

Due to the high data density resulting from the optical measurement process, even details of the rough surface can be depicted precisely as point data. The accuracy of the point cloud has been computed to be ±50µm for the measurement set-up chosen. It is comparable to that of accurate contact measuring machines (LMR profilometer) and single range camera systems (Lanaro et al. 1998).

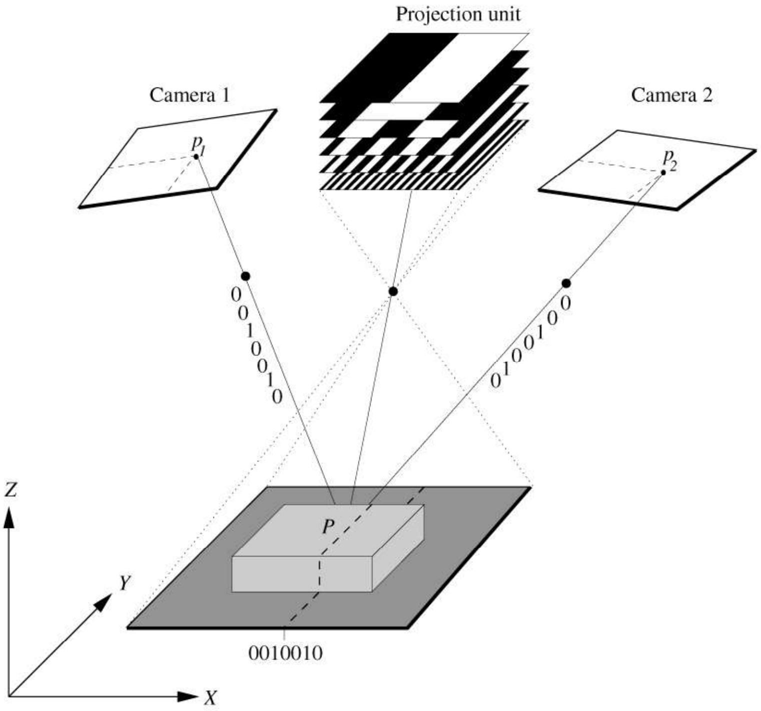

Figure 2.13 Principle of the advanced topometric sensor system (Bergmann et al. 1997)

2.4.2 *Calibration & measurement*

A calibration of the system is required for any scanned method. The calibration procedure relies on the fact that the parameters of a mathematical model describing the camera operation can be extracted from known target locations. This model includes internal (lens focal length, distortion parameters, scanning parameters, etc...) and external (head orientation, room light, etc...) camera parameters.

The base of the surface point triangulation is the interior and exterior orientations of the sensor elements. They must be determined by a special calibration procedure. Because the sensor accuracy depends mainly on the calibration quality, it is very important to compute the orientations as precisely as possible. Good results can be achieved by using a photogrammetric calibration based on the model of a central projection. The relationship between the object and image coordinates can be described mathematically with the collinear assumption. In this context the exact determination of the lens distortion is significant (Bergmann et al. 1997).

The used calibration object consists of a plate with circular targets (Figure 2.14) whose coordinates have not to be known exactly. They are simultaneously calculated by a bundle adjustment with an accuracy better than 1:30000 of the expansion of the calibration object. Only the distance between two points of the calibration object must be known a priori to determine the scale of the coordinates. Beside this 3D coordinates, the parameters of the searched interior and exterior orientation of the sensor elements are determined simultaneously.

After the delicate calibration procedure, basing on the measurement of the target point, the sensor needs no exact positioning but navigates itself autonomically by automatic registration of targets during the measuring process.

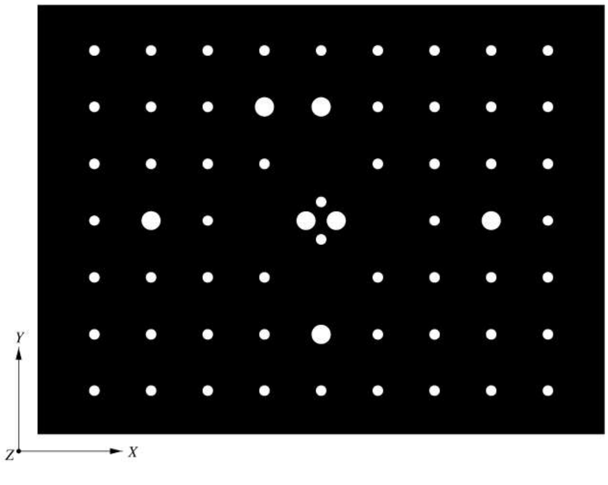

Figure 2.14 Calibration object.

The targets are extracted in each image and an ellipse is fitted to the range data yielding the location of the target center. After the extraction, each coordinate of the centers must be transformed with a rigid body transformation, into a common coordinate system, using the matrices obtained from the registration process originating at the reference point creation level. This process yields the location of the targets in the chosen model coordinate system. Thus, detection, identification, coordinate measurement of the target points and computation of the transformation is completely automated in the ATS system, that means, independently of the actual physical position, the sensor measures the object in the target coordinate system.

The 3D-coordinate measurement system is operated via the program that allows digitizing objects, visualizing the gained measurement data and preparing the digitized point clouds for exporting in plain text format (ASCII) files.

Specific software has been developed in order to manage numerous individual measurements and their computed point clouds into a common coordinate system that is usually required both when digitizing large surfaces and when monitoring the evolution of the morphology due to the shear tests. Starting an individual measurement, the program grabs object and reference points and transforms the new measurement automatically into the target coordinate system. Finally, it generates a point cloud and adds it to the program's preview window (3D-view).

2.4.3 *Measurement results*

The primary goal of a measurement survey is to have an as complete dimensional description of the rough surface and of its evolution as possible. In order to achieve this task, multiple scans are taken at different times (before and after the shearing). An original frame (Figure 2.15) was developed to make possible the survey of both sides of the rock joint in the same co-ordinate system. The use of this frame makes possible and eases the measurement of the same joint before and after the shear test on the same single predefined reference points, with a measured repeatability on the order of the measurement device precision. The relocation is

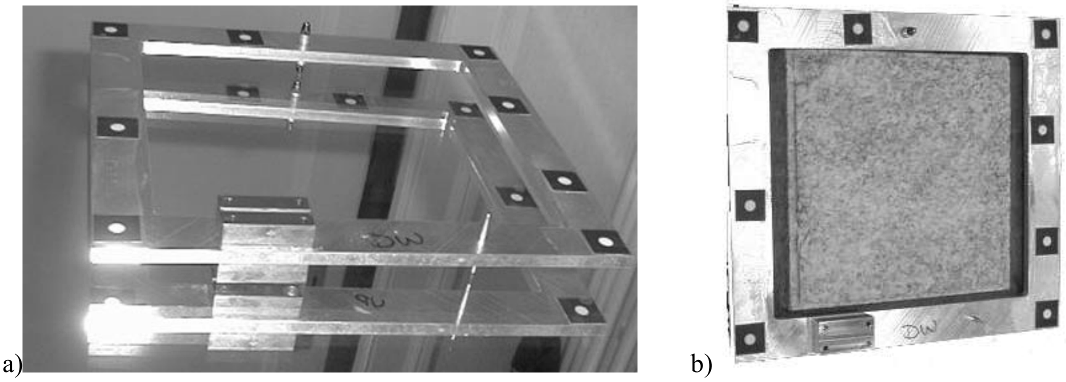

Figure 2.15 An original frame has been developed in order to measure both side of the joint in the same co-ordinate system. Several targets (white circles into black square) have been fixed on both sides of the frame ((a) shows the frame lying on a mirror) and their relative position has been previously measured using a unique co-ordinate system. In figure (b) it is shown the frame placed on the sample for measuring its surface..

very important. A 99% match in x and y implies a mismatching of 2% in area, quite enough to interfere with extreme-value calculations. A linear relocation within 0.1% is necessary to avoid significant error in scare volume (Thomas 1999a). The adoption of the target common coordinate system makes easy to align and to merge different views. By the simply subtraction of the surface data measured before and after the shear test it is possible to determine the areas damaged by the laboratory experiments (Figure 2.16). Thus, it is possible to follow the evolution of the rough surface during the shear test, detecting and measuring the damaged areas. Moreover, the mobile target frame makes possible the overlap of both sides of the same joint, recreating the void network existing inside the fracture and giving the possibility to easily determine the void space in between.

Triangulated surfaces have been chosen for the purpose of handling the “fractal” structures of joint surfaces (Figure 2.17). Specific software has been developed in order to measure and visualize the morphological data of the joint (Figure 2.18). Although the number of points (439.296 pixels) for each digital image may appear high, the complexity of the roughness and the presence of reflecting crystals are such that there could be still some gap remaining. These

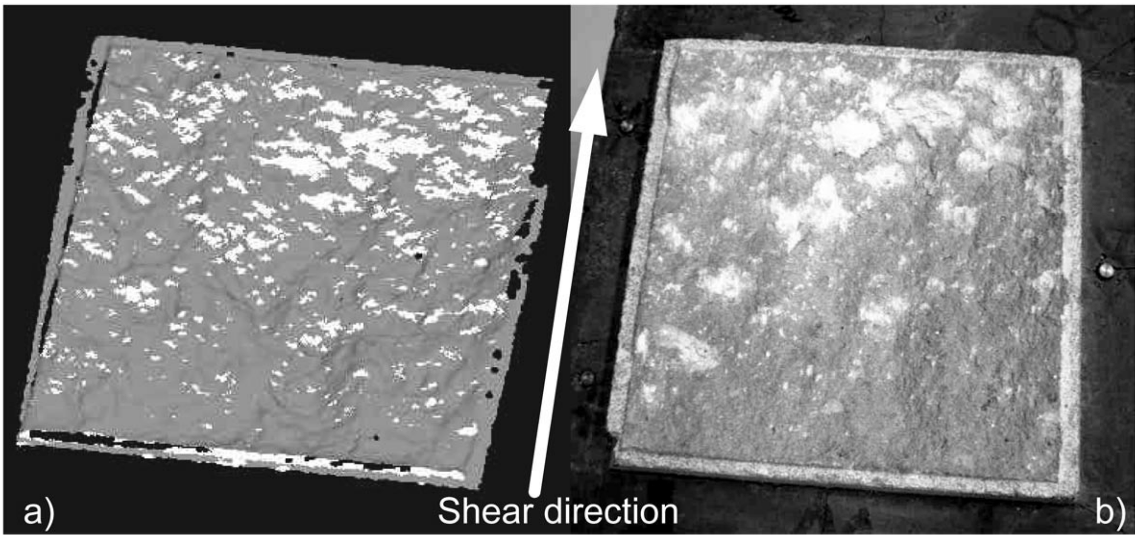

Figure 2.16 Identification of the areas damaged during the shear test.

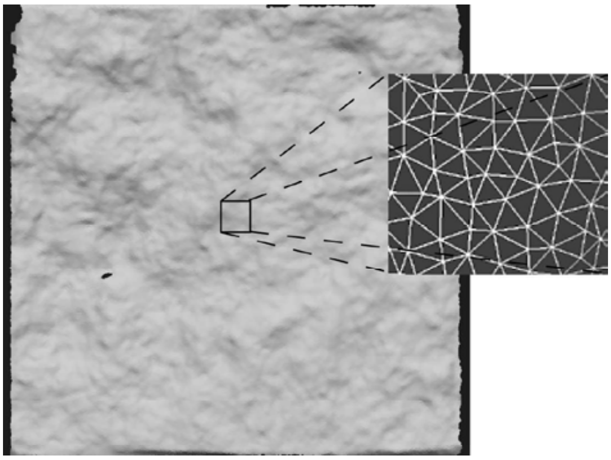

Figure 2.17 Reconstruction of the joint surface by triangulation of the experimental data.

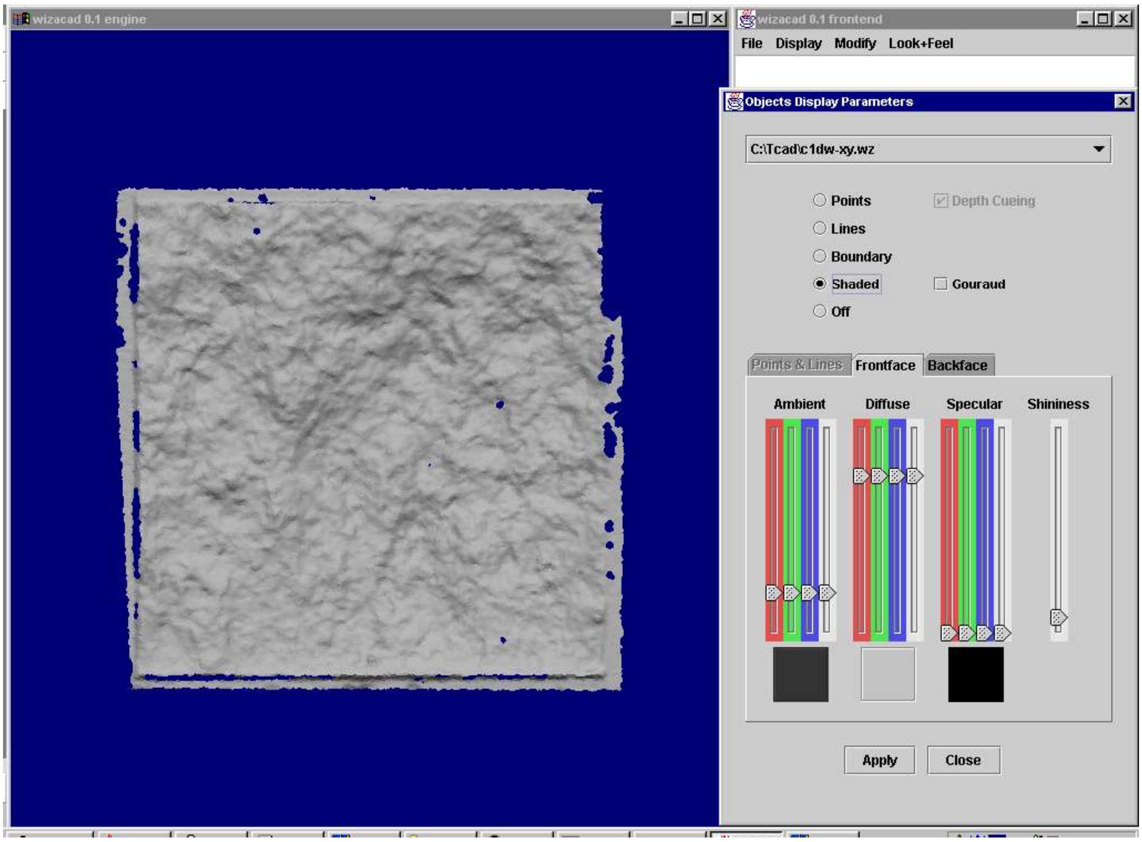

C:\Tcad\c1dw-xy.wz

○ Points ☑ Depth Cueing
○ Lines
○ Boundary
● Shaded ☐ Gouraud
○ Off

Figure 2.18 T-Cad. It is a specific and efficient software developed at the ETHZ in order to visualize the three dimensional data measured with the ATS system.

gaps correspond to holes in the model. But they could be filled by rescanning these areas or by closing the surface with artificial polygons.

2.4.4 *In-situ applications*

One of the big advantages of the chosen optical method is that its utilization is possible in in-situ conditions contrarily to most of the other approaches described in literature. The ATS system can be transported in two flight cases. Shock or changes of temperature during the journey do not influence the system's accuracy due to the easy re-calibration process and to the monitoring of the actual calibration quality during each measurement. The system supervises its calibration and the influence of ambient light itself, so that under rough conditions measurements can be taken with high speed, accuracy and reliability.

One test has been carried out in realistic conditions. Since the optical system profits from the precision of the light, the measure has been done during the night to derive advantage from the dark. Three rough surfaces have been measured in in-situ conditions obtaining a result with the accuracy of laboratory tests (Figure 2.19). It is essential for the future to confirm this first result in order to verify the in-situ use of this proposed measurement system.

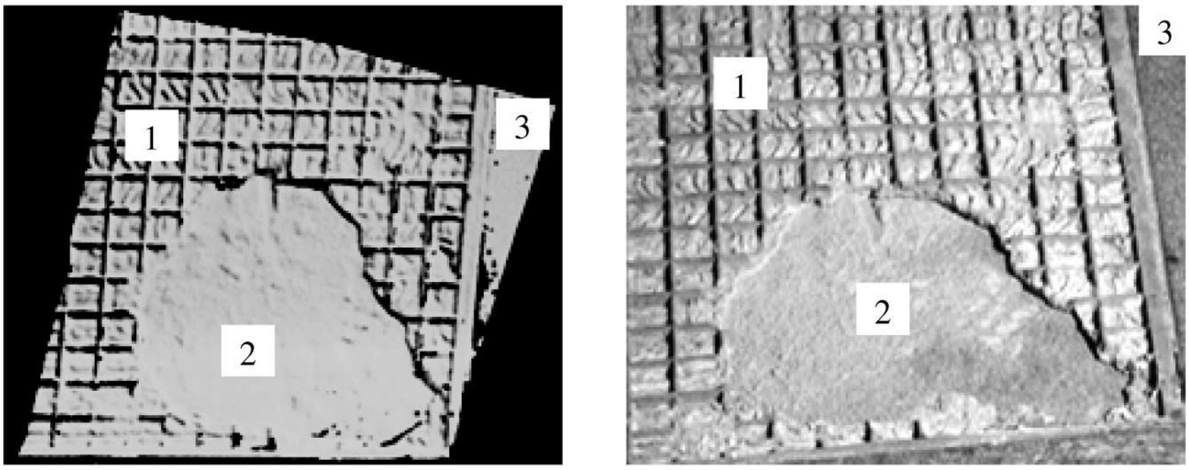

Figure 2.19 Comparison between the rendering of the measured surface in in-situ conditions (left) and the real one (right). Three different types of roughness have been measured at the same time: geometrically square regular one (1), typical sandstone roughness (2) and polished marble (3).

2.5 CONCLUSION

The development of measurement devices is, indeed, the story of civilization's rise from the stone age to the modern age. The measurement devices just kept getting better and better. Along with it our knowledge of our world expands even faster. Moreover, the choice of the measure system is important because the data recorded are the starting point for any empirical study. Although “the perfect” measurement-system does not exist, it is possible to choose the most appropriate solution focused to each special problem at that time. The technique improves each day; the personal-computer-computation-capacity grows up exponentially on the time. The analysis of the images, grabbed by digital-cameras, opened the way to new technologies unbelievable until five years ago. The precision, the spatial resolution and the stability of the measure achieved by many of actual systems, are sufficient for studying the rough surfaces. Today the distinguish parameter to compare different systems is the time consumed to measure the totality of the surface with a given resolution and precision. A detailed researched has been done and several different methods have been tried.

Among all the systems tested for measuring rough-joint-surfaces, the ATS has been chosen because it satisfied at that time all the criteria required: good precision, easy and fast measure, automatically reposition of the object using targets and its possible use on in-situ condition.

Tomorrow we will see...

3. Quantifying surface roughness

"As far as the laws of mathematics refer to reality, they are not certain,
and as far as they are certain, they do not refer to reality"
Albert Einstein

As discussed in Chapter 2, the strength of joints depends on several factors including surface alteration, roughness, thickness of infillings or gouge material, and moisture content. For joints that are well matched and have not undergone shear displacement, wall roughness is a very important factor in determining shear strength; the influence of roughness declines as aperture and filling thickness increase. When a fully matching rock joint is sheared, the roughness of the interface causes dilation, resulting in an increase in the apparent sliding-friction angle. To better quantify shear strength, it is necessary to understand the effect of joint roughness on dilation and shear resistance during displacement.

At present, only one morphological parameter has been commonly adopted in expression for joint strength; i.e., Barton's expression (Barton & Choubey 1977) for shear strength considers the effect of surface roughness on shear resistance. As discussed in Chapter 2, Barton was the first to take into account the influence of natural roughness on joint strength introducing the joint roughness coefficient (JRC) to quantify roughness in one dimension. The method for estimating the JRC value for a measured profile is subjective in that the user must judge where his profile fits within the range of 10 standard profiles (Figure 3.1).

Much of the work to date in developing models for shear strength has been focused on quantifying JRC. Statistical and fractal approaches are discussed in the following sections.

3.1 STATISTICAL MODELS

Several researchers have attempted to quantify joint roughness using statistical parameters for derived from analysis of two-dimensional profiles. For example, roughness has been characterized based on centerline average, mean square, root-mean square (RMS), mean square of the first derivative, RMS of the first derivative (Z_2), RMS of the second derivative (Z_3), auto-correlation function, spectral density function, structure function (*SF*), roughness-profile index (R_p) and micro-average angle (A_t). Many of these parameters are based on the same measurements and, thus, are closely related; for example, centerline average, mean square and root mean square (Table 3.1). Similarly, the mean square of the first derivative, RMS of the first derivative, roughness profile index, micro-average angle, and the structure function are closely related.

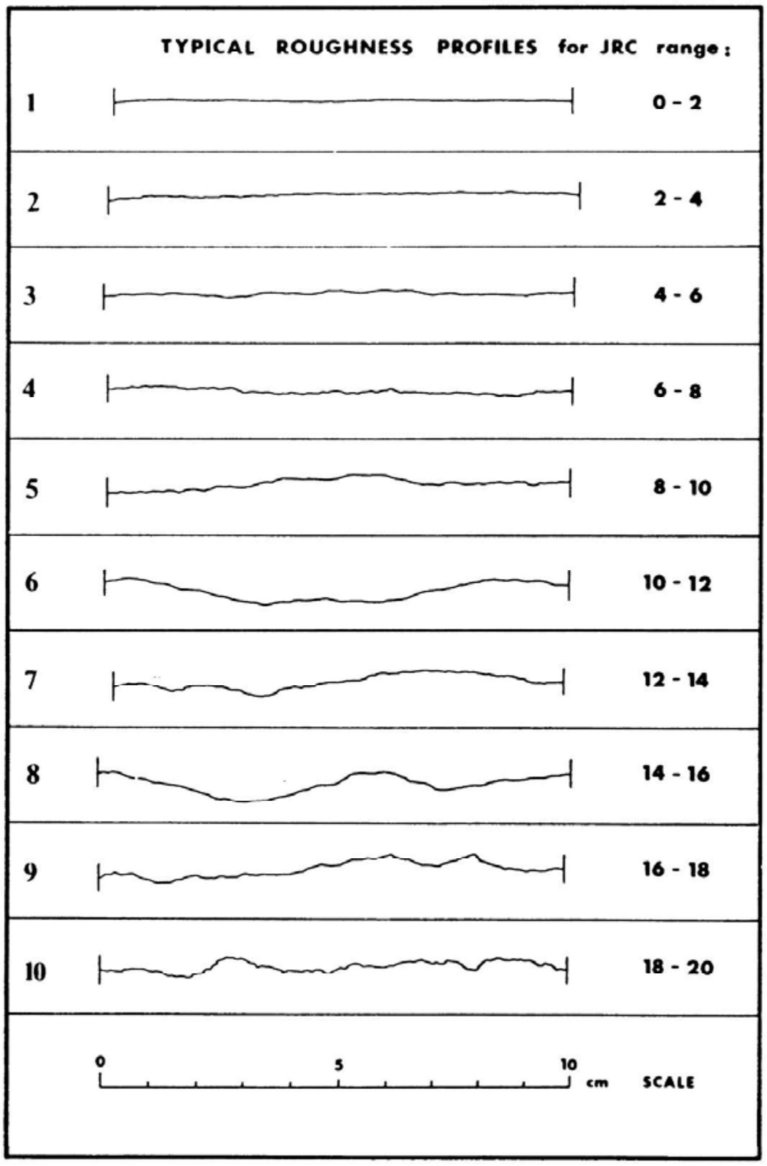

Figure 3.1 Barton's profiles.

By analyzing the digitization of Barton's roughness profiles, Tze and Cruden (1979) found correlations between the RMS of the first derivative of the profile (Z_2) and JRC:

$$JRC = 32.2 + 32.47 \log Z_2 \qquad 3.1$$

and between the structure function (SF), which measures the variation of the profile, and JRC:

$$JRC = 37.28 + 16.58 \log SF \qquad 3.2$$

It is important to note that Z_2 is unitless and scale dependent. Even though Z_2 is a useful parameter when roughness is stationary, it is not an appropriate measure for non-stationaryroughness. Moreover, it is highly questionable whether a single statistical parameter is adequate for capturing the roughness arising from profiles composed of both stationary and

Root-mean square (RMS)	$RMS=\sqrt{\frac{1}{L}\int_0^L z^2\left(x\right)dx}$
Mean square of the first derivative	$R_{m2}=\frac{1}{L}\int_0^L\left(\frac{dz(x)}{dx}\right)^2 dx$
RMS of the first derivative (Z_2)	$Z_2=\sqrt{\frac{1}{L}\int_0^L\left(\frac{dz(x)}{dx}\right)^2 dx}$
RMS of the second derivative (Z_3)	$Z_3=\sqrt{\frac{1}{L}\int_0^L\left(\frac{d^2z(x)}{dx^2}\right)^2 dx}$
Auto-correlation function	$ACF=\frac{1}{L}\int_0^L f(x)\cdot f(x+Dx)dx$
Structure function (SF)	$SF=\int_0^L\left(f(x)-f(x+Dx)\right)^2 dx$
Variance	$\sigma^2=\int_{-\infty}^{\infty} z^2 p\left(z\right)dz$
Standard deviation	$\sigma=\sqrt{\int_{-\infty}^{\infty} z^2 p\left(z\right)dz}$
Normal probability density function (Gauss)	$p\left(z\right)=\frac{\sigma}{\sqrt{2\pi}}\exp\left[-\frac{z^2}{2\sigma^2}\right]$
Semivariogram	$\gamma\left(h\right)=\frac{1}{2\left(N-h\right)}\sum_{i=1}^{N-h}\left(Z_{i+h}-Z_i\right)^2$

Table 3.1 Statistical parameters used to characterize joint rough profiles and roughness distribution.

non-stationary parts of a profile. Using the statistical tools it is only possible to describe the average variation of the profile, but nothing has been said about how the relief varies in the plane of the surface, and, consequently, about the profile slope. Counting the number of peaks per unit of length of a profile results too much dependent by the definition of the peak and by the resolution of measure instrument. Thus, in the last two decades many researchers have concluded that roughness cannot be characterized by one or a limited number of discrete statistical values. Rather, it has been suggested that roughness should be characterized as a continuous function of scale. Indeed, a fully matching joint subjected to small shear displacements will be primarily influenced by small-scale roughness, whereas, the behavior of the same joint undergoing large shear movements will be governed by large-scale roughness.

3.2 GEOSTATISTICAL MODELS

The main idea of geostatistical methods is to relate the spatial variation among population densities to the distance lag. Geostatistics is therefore a statistical method that is particular useful in situation where a sample value is affected by it location and its relationship with its neighbors. The development of geostatistics began in the sixties (Matheron 1971) for the study of regionalized variables, where considerations on spatial continuity are essential for successful estimates. Geostatistics is generally based on the concept of variograms, which express the correlation between pairs of "points" (the values of the same variable at different positions in space) and provide information about the variability of the chosen property throughout the deposit, such as distances and directions of maximum and minimum continuities. The variograms merely describes the special relationship between the data points. Very often, in practice, the correlation *C(h)* between two variables *z(x)* and *z(x+h)* disappears when the distance *h* becomes too large (*C(h)=0* once |*h*|>*a*.) The distance *a* beyond which *C(h)* can be considered to be equal to zero is called "range" and it represents the transition from the state in which a spatial correlation exists to the state in which there is absence of correlation. In that case the semivariogram stops increasing and becomes more or less stable around a limit value called "sill" (Figure 3.2). The sill is approximately equal to the variance of the data. Such variograms, which are characterized by a sill value and a range, are called "transition models". The behavior of the semivariogram at distances comparable to the size of the domain determines whether the function is stationary or not. A function is considered stationary if it consists of small-scale fluctuations, compared to the size of the domain, about some well-defined mean value. The geostatistical process is a two-step procedure. The first is the calculation of the experimental variograms and the second is fitting a model to it.

The structural analysis is the selection and fitting of mathematical expressions to experimental variogram for the required first two moments of the regionalized variable. The form of these expressions comprises the model.

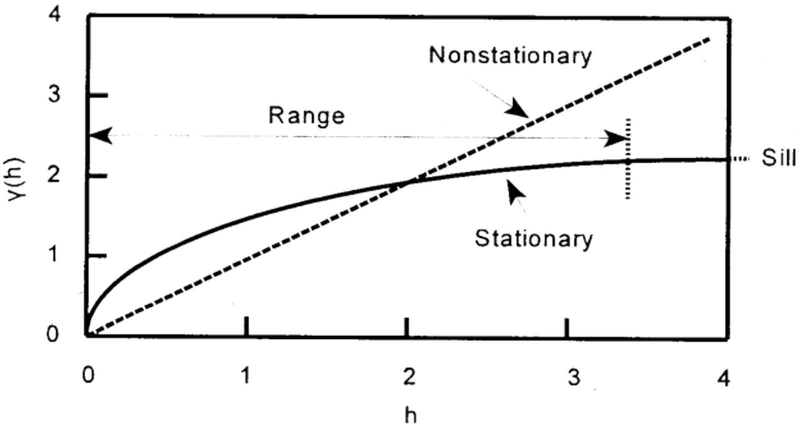

Figure 3.2 Semivariogram illustrating stationary and non stationary behavior.

Mean function	$m(h) = E\left[z(x)\right]$	
Covariance function	$R(h) = E\left[\left(z(x) - m(x)\right)\left(z(x') - m(x')\right)\right],$	$h = \|x -$
Linear model	$\gamma(h) = \alpha h,$	$\alpha > 0$
Spherical model	$\gamma(h) = \begin{cases} \left(\frac{3}{2}\frac{h}{a} - \frac{1}{2}\frac{h^3}{a^3}\right)\sigma^2, \\ \sigma^2 = \text{sill value,} \end{cases}$	$\forall h \in [0, a]$ $\forall h \geq a = \text{range}$
Exponential model	$\gamma(h) = \left(1 - \exp\left(-\frac{h}{a}\right)\right)\sigma^2$	
Gauss model	$\gamma(h) = \left(1 - \exp\left(-\frac{h^2}{a^2}\right)\right)\sigma^2$	
Power model	$\gamma(h) = \alpha h^{\theta},$	$\alpha > 0$ and $\theta \in \left]0, 2\right[$
Logarithmic model	$\gamma(h) = \log h$	
Nugget effect	$\gamma(h) = \begin{cases} C_0, \\ 0, \end{cases}$	$\forall h > 0$ $h = 0$

Table 3.2 Theoretical models currently used in structural analysis.

The two main characteristics of a stationary variogram are its behavior at the origin (parabolic, linear and nugget effect. See Figure 3.3), and the presence or the absence of a sill in the increase of $\gamma(h)$ (i.e. $\gamma(h)$ constant when $|h|>a$. See Figure 3.4) Thus the currently used theoretical models (Table 3.1) can be classified as:

1. Models with a sill (or transition models) and a linear behavior at the origin (spherical model and exponential model)
2. Models with a sill (or transition models) and a parabolic behavior at the origin (Gauss model)
3. Models without a sill where the corresponding regional function is only intrinsic and has neither covariance nor finite a priori variance (power model and logarithmic model)
4. Nugget effect.

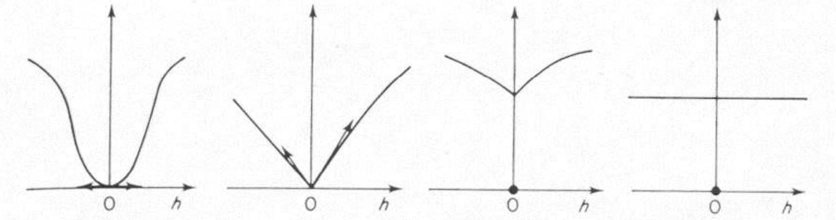

Figure 3.3 Behavior near the origin of the variogram. (a) Parabolic behavior; .(b) linear behavior; (c) nugget effect; (c) pure nugget effect.

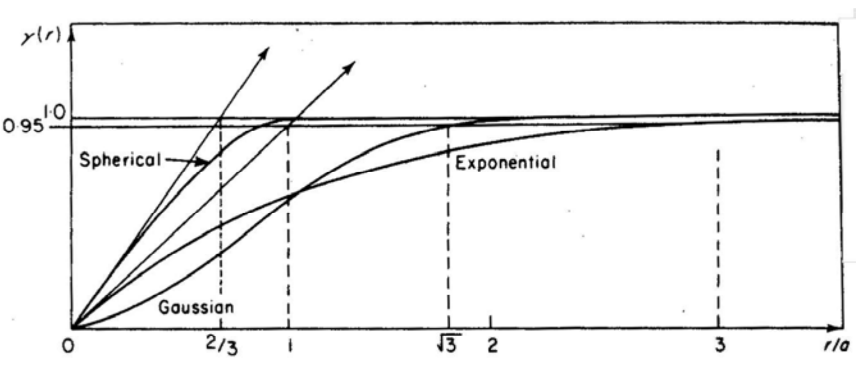

Figure 3.4 Models of semivariograms with a sill.

Geostatistical methods based on variograms are known as kriging. Kriging is the process of estimating value of specially distributed variable from adjacent values while considering the interdependence expressed in the semivariogram. The kriging process involves the construction of a weighted moving average equation which is used to estimate the true value of a regionalised variable at a specific domain. This equation is designed to minimized the effect of the relatively high variance of the sample values by including knowledge of the variance between the estimated point and other sample points within the range (Mohamed & Antia 1998). Kriging results to be a useful technique to densify point clouds of measured joint surfaces, to fill lack in measurements, and to estimate the elevation of the surface on a regular grid (Gentier et al. 2000).

3.3 FRACTAL MODELS

The importance of scale effect has lead many researchers to investigate the possibility of quantifying roughness of a surface or to estimating JRC by calculating the joint fractal dimension (*D*). Describing such irregular shapes using Euclidian geometry is difficult. Fractal geometry introduced by Mandelbrot (1983) may allow the description of such irregular shapes. Roughly speaking, fractal geometry is the geometry of irregular shapes. Fractals are functions that are continuous but not differentiable. The fractal dimension D has been used to characterize a feature with a fractal property. The fractal dimension is a fraction lying between the topological and Euclidian dimensions and describes the jaggedness or degree to which the fractal function fills up the Euclidian space. A linear profile across a rough surface may have a D between 1 (the topological dimension of a line) and 2 (the dimension of a Euclidian plane). Similarly, a rough surface may have a D between 2 and 3. Its dimension describes the degree of variation in a curve, a surface or a volume from its topological ideal. Fractal geometry allows the description of irregular forms that are more complex than the Euclidean shapes. As Mandelbrot wrote, “Clouds are not spheres, mountains are not cones, coastlines are not circles, and bark is not smooth, nor does lightning travel in straight line. They may be fractals.” In the past several years, fractal geometry has gradually become a tool for modeling natural structures.

In rock mechanics the assumption is that natural rock joint may be represented by self-similar (Hsiung et al. 1993, Lee et al. 1990, Wakabkykshi & Fukushige 1995) or self-affine fractal models (Lanaro 1999). In essence, a self-similar fractal is a geometric feature that retains its statistical moments to all scales. Self-affine fractals remain statistically similar only if they are scaled differently for profiles in different directions. Self-affine fractal models are generally thought to be more applicable to geological phenomena than self-similar fractal models (Kulatilake et al. 1997, Xie et al. 1997, Lanaro 2000).

Several methods have been suggested to estimate the fractal dimension of a rough profile: the divider method, the box-counting method (Kulatilake et al. 1995), the spectral method (Roko et al. 1997), and the variogram method (Ferrero et al. 1999). However, some of this work should be treated with caution (Den Outer et al. 1995, Sabbadini et al. 1995) as not all researchers have distinguished between self-similar and self-affine fractals (Kulatilake et al. 1995, Piggott & Elsworth 1995), and different methods of calculation can result in significant differences in numerical values of fractal parameters (Hsiung et al. 1993, Huang et al. 1992).

Derivation of relationships between fractal dimension and the more common roughness statistics based on the standard deviation of asperity angles or asperity heights have been used to try to provide a qualitative understanding of Barton’s empirical JRC-JCS model (Wakabkykshi & Fukushige 1995, Giani et al.). The same authors have also used fractals to describe the relationship between anisotropy and fracture mechanisms.

A new approach for describing fracture surfaces may come from the multi-fractal theory. (Xie et al. 1999) asserts that the multi-fractal spectra contain information related to fracture mechanism and structural properties that is not contained in conventional fractal analysis.

3.4 SUMMARY

Discontinuities have an important influence on the deformational behavior of rock systems. Properties of the discontinuities include orientation, extent, planarity, roughness and the strength of wall rock asperities. Roughness, which influences the friction angle, dilatancy and peak shear strength, refers to the local departures from planarity at both small and large scales. Consistent researches have been carried on the characterization of surface roughness.

To characterize how is rough a surface means to express the roughness with a number or a mathematical expression. Few methods have been suggested to characterize the surface roughness of natural rock joints. The work done so far has been limited to the characterization of surface roughness along linear profiles. These investigations have led to controversial findings (Huang et al. 1992, Hsiung et al. 1993, Odling 1994). In addition, since joint planes are three-dimensional, the quantification of surface roughness on the space is required. Indeed, roughness on natural rock joint planes is anisotropic. However, anisotropic roughness quantification is not addressed in literature. These clearly show our limited understanding on mathematical quantification of roughness of natural rock joints. Although precise methods for measuring the surface exist today (Chapter 3), neither of those systems can estimate a proper value for the roughness of surfaces. Thus, despite the considerable advances that have been made in measurement techniques, the relationship between joint roughness, dilation and shear behavior has only been solved at an empirical level and most of the new proposed parameters have been used to try to objectively quantify the JRC. Even though all these approaches are useful for describing profiles, they are not sufficient to capture the features necessary for characterizing three-dimensional roughness.

For example, (Ferrero et al. 1999) has shown that, on the same sample, JRC calculated, using Equation 3.2, for twenty profiles randomly chosen could assume values between 8 and 20. Therefore, the choice of the profile to use for estimating surface contribution to joint-shear strength may strongly affect the final result. Moreover, watching at the surface of sheared joints it appears that damage is not uniformly distributed, but it is located in function of the particular morphology of the joint and the direction of shearing. As well as shear strength of joint, damage location, and joint morphology are strongly dependent, it appears that only studying the entire surface, and not just one profile, it could be possible to understand its influence on the shear strength. Only recently, authors (Lanaro et al. 1998, Grasselli & Egger 2000a, Gentier & Hopkins 1997) have focused their attention on identifying three-dimensional parameters to quantify the relationship between of the surface roughness and shear strength. Incorporation of morphological data into shear models is the subject of next chapter.

4. Incorporating the effect of surface morphology into shear models

"Everything should be made as simple as possible but not simpler"
Albert Einstein

A different, and interesting approach, compared to the methods discussed in the previous chapter, to quantify the influence of surface features on the shear strength of rock joints is to directly study the effect of the geometry on shearing mechanisms. During shear tests under constant normal load the upper half of the joint moves crushing or overriding the asperities on the lower half of the sample.

This process has been studied by Ohnishi et al. (1996) who used digitized joint-surface profiles to simulate the shear behavior of rock joints. The proposed model uses the digitized profile data to produce stress-displacement curves that include dilatancy and shear stress relationships. It is assumed that the joints are rigid so they do not deform during the shearing. In the calculations, it is assumed that the joint is subjected to a small increment of shear displacement. The new position of the joint profile is then calculated, and it is then determined if there is any overlap with the lower joint surface. If there is overlapping, the upper block is “lifted” upward by an amount computed from the maximum slope of the asperities, which is determined from the measured data. If there is no contact between the profiles in the new position, the shear displacement is increased until contact is created. In this way, both shear and normal displacements are calculated allowing dilatancy to be estimated. However, it is not possible to characterize the behavior of the entire surface from one arbitrarily chosen profile.

4.1 INFLUENCE OF THREE-DIMENSIONAL SURFACE GEOMETRY ON SHEAR BEHAVIOR

The difficulty of characterizing the entire surface with individual profiles pointed to the need to perform laboratory investigations to relate the morphology of the joint to areas that are involved in shearing. On sheared samples in laboratory it was observed that the real contact area is only a small portion of the total one that is difficult to relate to a single profile. Moreover, the contact areas for the same rough surface (tests made on replicas) vary when changing shear direction and/or applied normal load (σ_n). Therefore, one of the current research topics is measuring and relating both the initial contact area and stress distribution, before shear displacement, to the damage zones that develop during shearing (Re & Scavia 1999, Nakagawa et al. 1999).

The geometry of the joint influences shearing at each stage. The initial contact area depends on the morphology. The closure depends on the contact-area distribution. The peak behavior, as well as the failure mode and the creation of damage, depend on the contact-area distribution. Gentier et al. (2000) state that the size, shape, and spatial distribution of damaged areas depend on the shear direction and the degree of stress and horizontal displacement. Obviously the damage increases as stress and displacement increase. They have found that little damage appears prior to the peak stress, and it occurs principally during the softening and residual phases of shearing. The locations of contacting asperities, during these phases, seem to correlate closely to the damaged areas that appear later. The common characteristic among all those contact areas is that they are located in the steepest zones facing the shear direction (Grasselli & Egger 2000a, Kimura & Esaki 1995) (Figure 4.1). The shape of the damage zones depends on the local geometry of the fracture surface, including the size and the shape of asperities as well as on the mechanical parameters of the rock.

4.2 MORPHOLOGICAL CHARACTERIZATION OF ROUGH JOINTS SUBMITTED TO SHEAR STRESS

For the research presented here, a large number of shear tests were performed on rock samples with "fresh" tensile joints. All the sheared joint surfaces present punctually spots on which the contact happened. The damage area distribution appears closely correlated to the morphology of the joint. Once the joint was closed, the impression was that it was completely mated.

Past researches prove that, for natural joints in rock, subjected to normal stress, the total contact area is typically much less than 70% of the joint surface (Hopkins 2000). Although, if this estimation is true for natural joints, that have a long geological history, "fresh" tensile

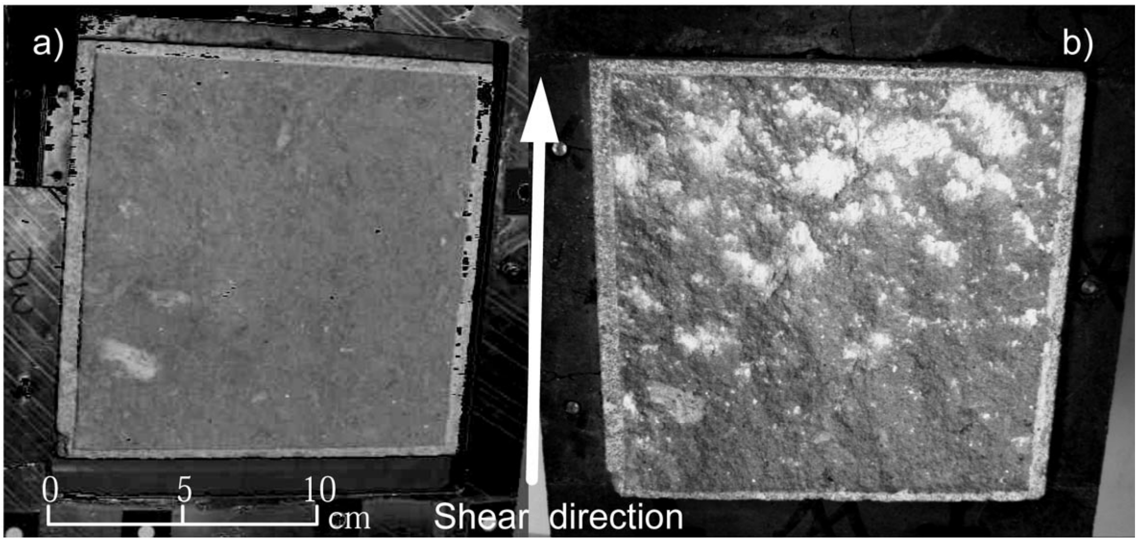

Figure 4.1 Picture of lower side of Magny limestone sample before (a) and after (b) shearing. Damage areas on sheared rock joint appear as white spots located on the part of joint with positive slope with respect to the shear direction.

joints have really less voids than natural fractures. Therefore, it is realistic to idealize the entire joint surface on contact once subjected to normal load. To verify these hypothesis three different tests were realized at the Lawrence National Laboratory in Berkeley and EMPA in Switzerland. The first test was to map the contact areas of one Carrara marble tensile joint and visually estimate the rate of contact area. To realize this experience, a thin lead foil (35 µm thick) was squeezed inside the joint under 1.3 MPa normal stress. The crude inspection of the deformed foil shows that contact was on most of the joint (Figure 4.2). It means that most of the void aperture inside the joint is lower than the thickness of the lead foil.

The second test was to compare the ultrasonic transmissibility of the sample having a joint, with the transmissibility of intact rock. Ultrasonic measurements result extremely sensitive to any change of stiffness of the joint. Although the shape of transmitted waves (100 kHz) results being the same, the comparison between amplitudes shows a difference up to 20% (Figure 4.3). This means that the presence of the joint affects the stiffness of the sample and shows that the contact is not perfect. The joint, even if it seems close at macroscopical scale, results open microscopically.

On the third test the void inside the joint was directly measured using x-ray computer tomography. One close joint, with a normal load of 50 N, was scanned and the data analyzed. The hardest problem was to handle the measurement noise caused by the density of the rock. The resulting map, with spatial resolution of 20 µm, shows the presence of a thin void network inside the joint.

Figure 4.2 Squeezed lead foil (35 µm). The areas not in contact are painted in red.

Comparing the results of all tests, it is possible to presume that "fresh" tensile joints, under normal load, can be considered very well mated. Furthermore, even if they are unmated at micro-scale, at the scale at which normally the joints are measured, it is correct affirming that it is possible, for modeling the initial condition of matching "fresh" tensile joints, subjected to normal load, to assume the entire joint in contact (100% contact). As shear load is applied, the asperities dipping face to the shear direction start to deform elastically, and areas inclined opposite to shear direction are detached (consequently, void appears perpendicularly to the direction of shearing). As long as, in laboratory tests, the average joint plane coincides with the shear plane, the contact at the beginning of shearing may be estimated on about 50% of entire surface.

The joint surfaces were mapped before and after shearing with a three-dimensional scanner (e.g. ATS system, see Chapter 3.4). The rough surfaces were reconstructed using a triangulation algorithm on measured point clouds. The algorithm, developed at ETHZ for automobile digital reconstruction, minimizes the number of triangles necessary for reconstructing the entire surface minimizing the error.

This approach results in a discretization of the joint surface as a finite number of triangles, whose geometric orientations are easy to calculate (based on the orientation of the normal vector to the triangle plane (***n***). See Figure 4.4). The accuracy of the reconstruction depends on the density of measurements; the denser the measurements the higher the accuracy of the reconstruction. This discretization of the joint surfaces is particularly advantageous for estimating the areas of the surfaces in contact during shearing.

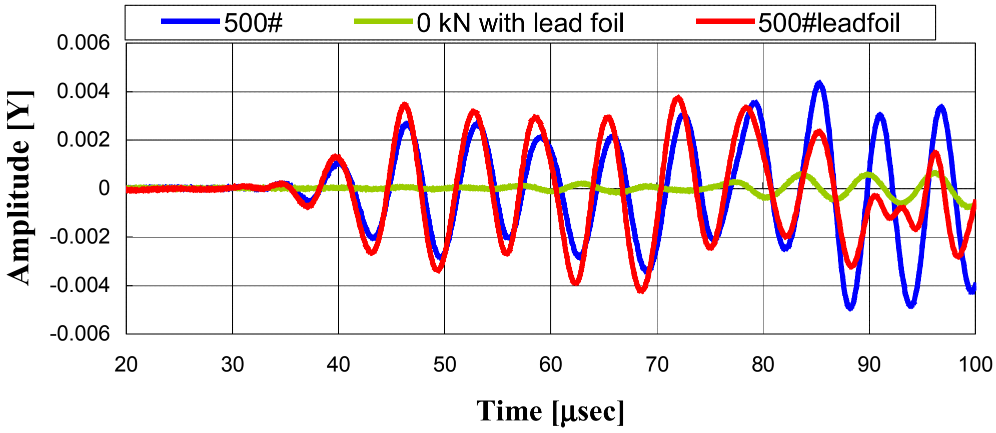

Figure 4.3 Comparison of wave transmissibility between intact rock and sample with one joint perpendicular to the transmission direction.

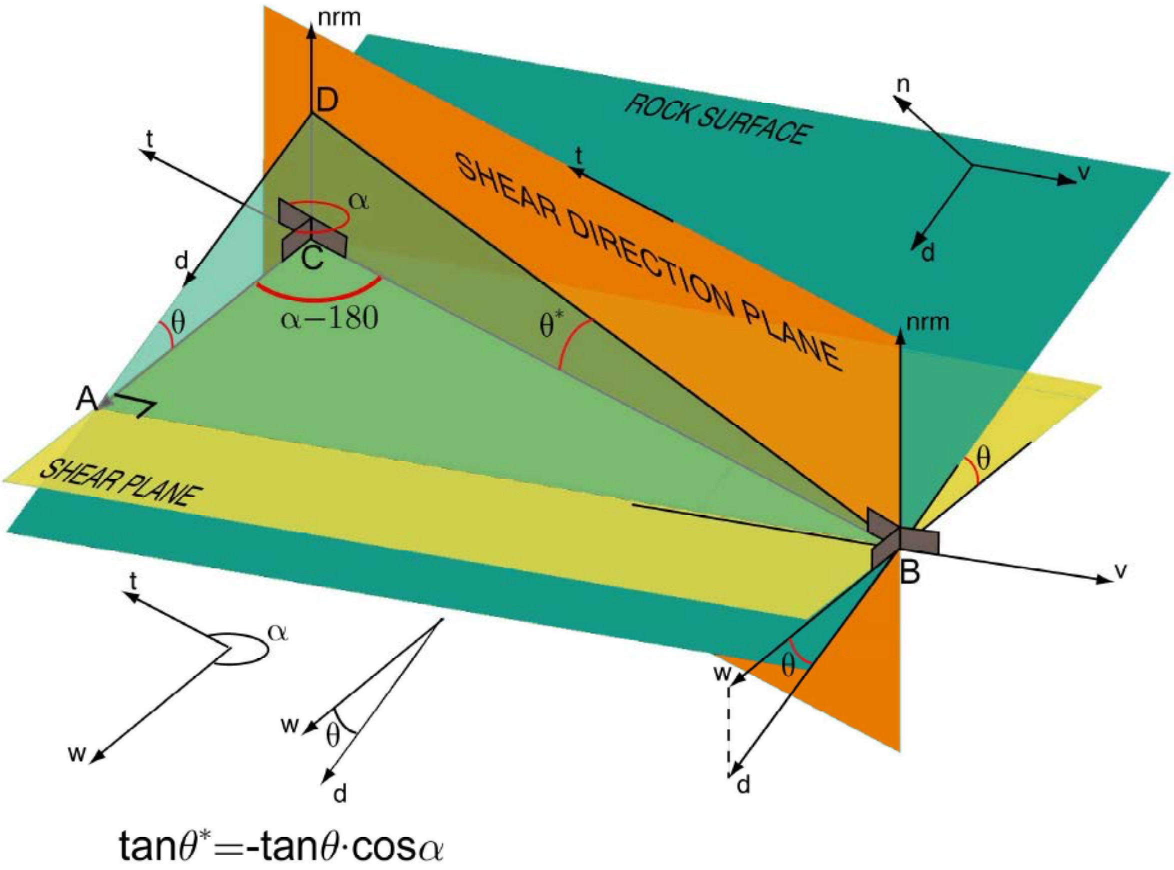

Figure 4.4 Geometrical identification of the apparent dip angles, in function of the shear direction.

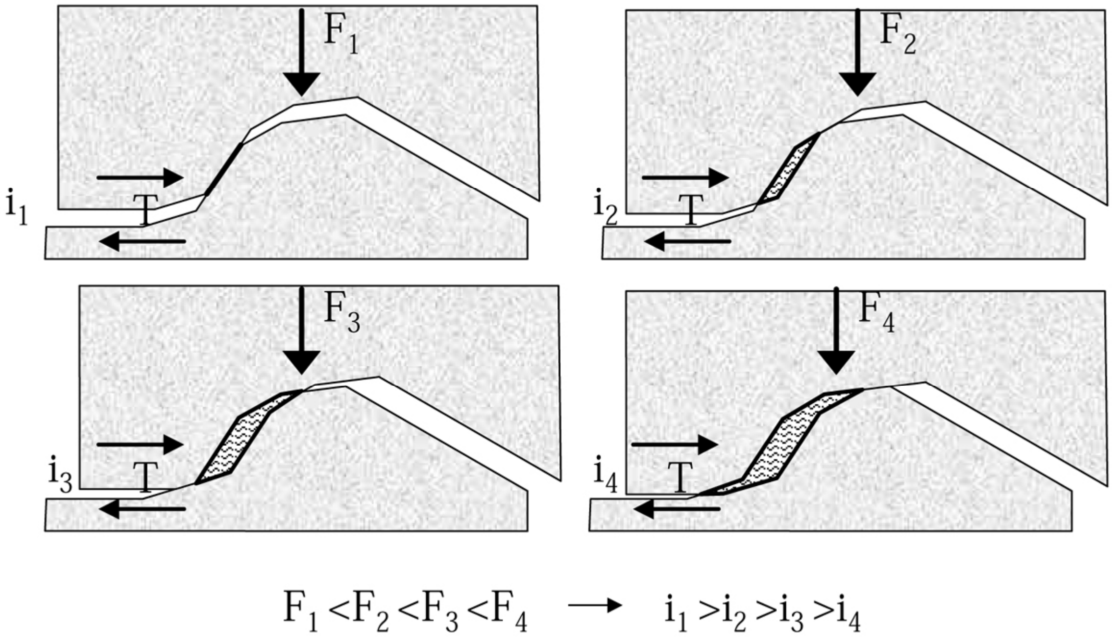

Figure 4.5 Boundary condition at the beginning of shearing.

To estimate the contact area, it is first necessary to specify the shear direction. It was postulated that contact could only occur on those triangles facing the shear vector (***t***). Moreover, since laboratory observations clearly show that only the steepest surfaces touch the other sample, the identification of the potential sliding areas only requires the determination of the areas which face the shear direction and which, among them, are steep enough to be involved. It should be noted that asperities with positive slope descending to the left (Figure 4.5) are treated for rightward shearing (when the upper half of the specimen is sheared rightward relative to the lower half), and negative asperities descending to the right for leftward shearing. For each triangle, the true dip vector (***d***) has been calculated and applied in the triangle center of gravity. Thus, each triangle surface orientation is uniquely identified by its azimuth angle and dip angle (Figure 4.4). Azimuth (α) is the angle between the true dip vector projection on the shear plane (***w***) and the shear vector (***t***), measured clockwise from ***t***. Dip (θ) is the angle between the shear plane and the triangle. Three-dimensional spatial plots of the steepest triangles faced towards the shear direction (Figure 4.6) have been possible using azimuth and apparent dip angles (θ^*) (Grasselli & Egger 2000a).

The apparent dip angle describes the contribution of each triangle inclination, projecting the dip angle along the vertical plane which contains the shear direction where:

$$\tan\theta^* = -\tan\theta \cdot \cos\alpha \, . \qquad 4.1$$

Based on the identification of the concept of threshold apparent dip angle, the shearing mechanism may be simplified by saying that, for any specified normal load, only the zones of the surface facing the shear direction, and steeper than a threshold inclination (defined as θ^*_{cr}) are involved in the shearing. Among these zones, the areas of the surface inclined exactly θ^*_{cr} will be just in contact, whereas the areas inclined more then θ^*_{cr} will be deformed, sheared or crushed, depending on the normal load applied. In this way it is possible to estimate the surface that might be in contact during shearing as a function of a threshold value of θ^*_{cr}. It is possible to indicate the areas of the joint inclined at the same or higher levels as θ^*_{cr}.

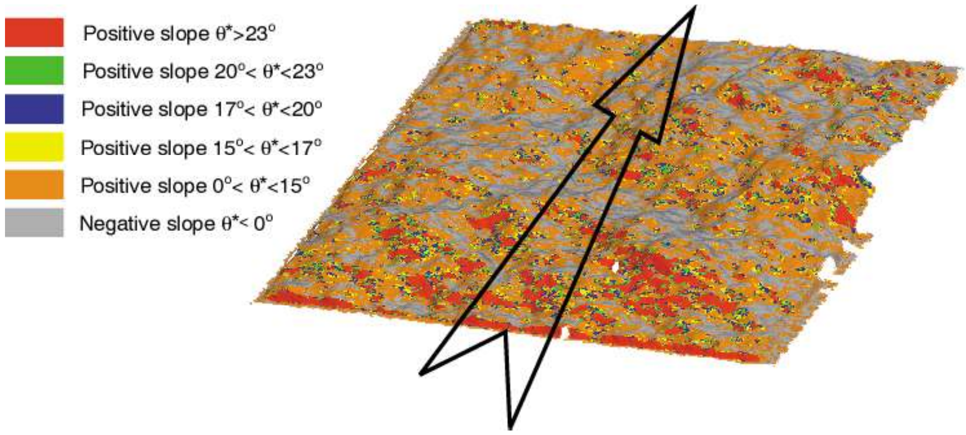

Figure 4.6 Three-dimensional distribution of the potential contact areas. Digitized image of a joint surface in a limestone test specimen. Areas with negative slope with respect to the shear direction are indicated in gray; these areas are not in contact during shearing. Areas with positive slope are indicated in colors that correspond to the local gradient.

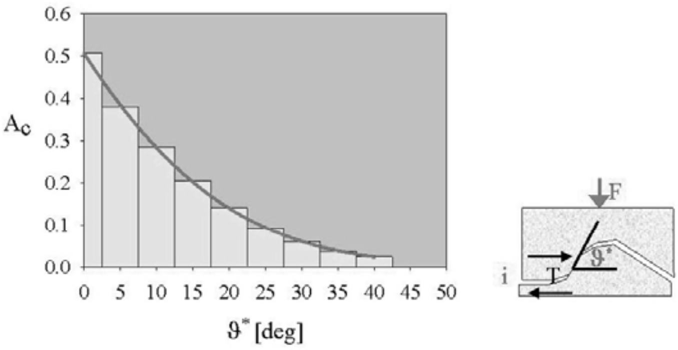

Figure 4.7 Plot of A_c versus θ^*.

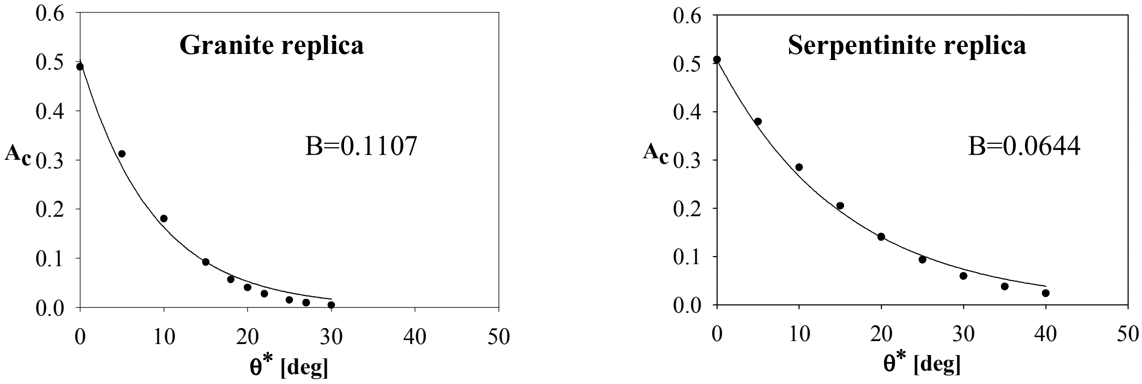

Figure 4.8 Relation between contact area ratio (A_c) and apparent dip inclination (θ^*) for two different surfaces using the first proposed equation.

Each of these areas are calculated and the sum is termed the total potential contact area (A_C); note that Ac depends on the specified value of the threshold dip angle θ^*. Thus, for each value of θ^*, it is possible to estimate the total area of the surface where contact is possible. To study the relationship between the potential contact area (A_c) and the corresponding minimum apparent dip angle, the digitized surface data was used to calculate Ac for several values of θ^* and plotted on the A_C-θ^* plane. The first approach in trying to quantify the relationship between Ac and θ^* was to fit these points (Figure 4.7) with an exponential function:

$$A_c = A_0 \cdot e^{\left(-B\cdot\theta^*\right)} \qquad 4.2$$

where A_0 is maximum possible contact area, and B is a “roughness” parameter, calculated using a best-fit regression function. The parameter B corresponds to roughness in that it controls the concavity of the curve (Figure 4.8), which describes the distribution of the apparent dip angles on the surface. B depends on the specified shear direction.

To explore whether alternative functional forms might provide a better fit to the data, the following, more complex, exponential law was applied:

$$A_c = a_0 \cdot e^{\left(\frac{-1}{2}\cdot\left(\frac{\theta^* - x_0}{b_0}\right)^2\right)} \qquad 4.3$$

where a_0, b_0 and x_0 are coefficients obtained with a best-fit regression on the data set. Although the fit parameters do not have any physical meaning, the above expression describes the experimental points better than the previous equation (Equation 4.2); i.e., the coefficient of correlation is closer to 1 (Table 4.1).

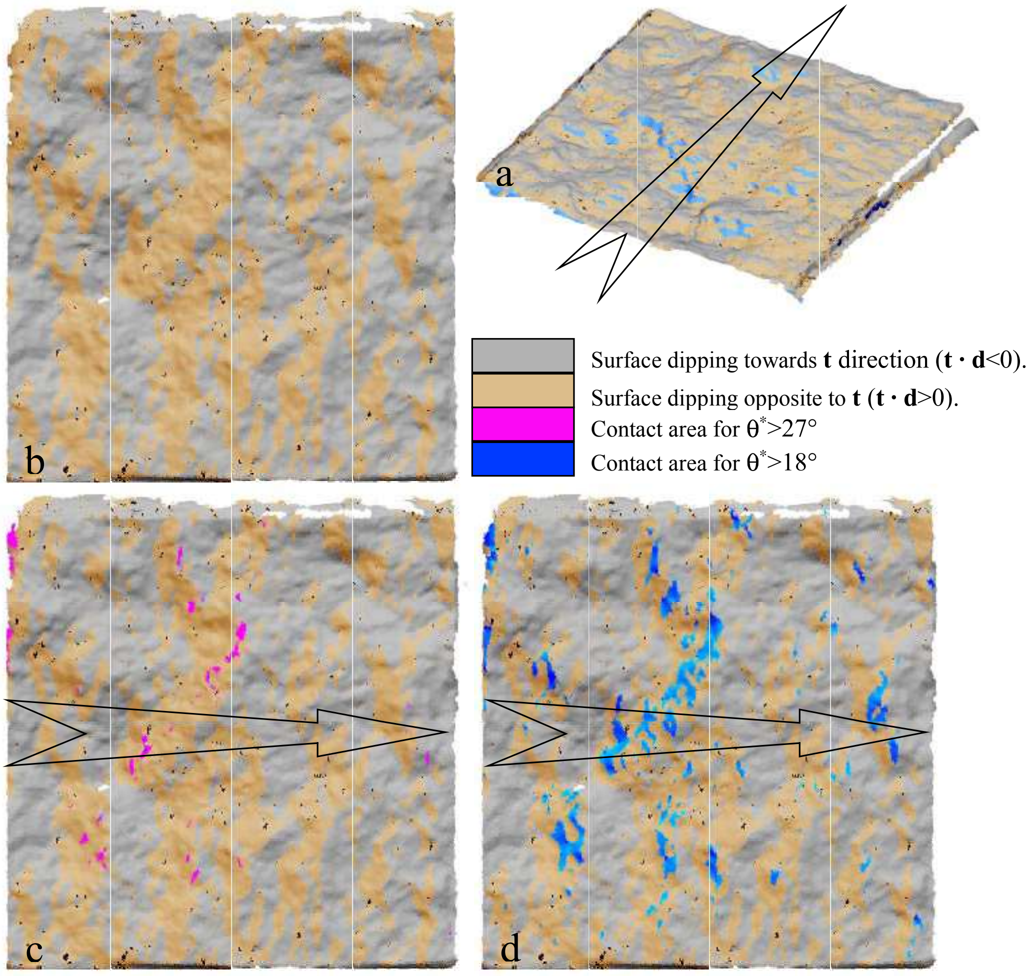

Figure 4.9 (a-b): Image representations of granite replica digitized surface. The areas dipping in the shear direction are gray and the regions dipping opposite to **t** (potential sliding areas) are orange: (c): Contact area with dip angle $\theta^*>27°$, corresponding to $\sigma_n/\sigma_c=0.049$ shear test moving in the direction of the arrow: (d): Contact area with dip angle $\theta^*>18°$, corresponding to $\sigma_n/\sigma_c=0.098$ shear test moving in the direction of the arrow.

Sample	A_0	B	r^2	a_0	b_0	x_0	r^2	A_0	C	θ^*_{max}	r^2
name	[-]	[-]	[-]	[-]	[-]	[-]	[-]	[-]	[-]	[deg]	[-]
C1	0.491	0.0992	0.9966	1.38	18.63	-26.84	0.9998	0.491	7.03	80	0.9988
C2	0.462	0.0815	0.9941	0.95	19.06	-20.78	0.9999	0.462	5.64	80	0.9991
C3	0.507	0.0812	0.9946	0.98	19.75	-22.74	0.9999	0.507	6.18	88	0.9977
C4	0.508	0.0883	0.9930	0.83	16.72	-16.46	1.0000	0.508	4.74	65	0.9971
C5	0.495	0.0835	0.9958	1.16	20.70	-27.02	0.9999	0.495	5.26	74	0.9989
C6	0.546	0.0903	0.9953	1.14	18.35	-22.29	0.9999	0.546	5.19	68	0.9984
C8	0.555	0.0906	0.9946	1.06	17.69	-20.22	1.0000	0.555	5.71	74	0.9979
G1	0.522	0.0942	0.9949	1.04	17.24	-20.18	0.9999	0.522	5.75	72	0.9975
G2	0.553	0.0906	0.9966	1.52	20.14	-28.58	0.9999	0.553	6.63	84	0.9986
G4	0.484	0.1108	0.9933	0.81	13.68	-13.97	1.0000	0.484	6.12	65	0.9967
G5	0.460	0.1103	0.9952	0.98	15.26	-18.80	0.9999	0.460	5.33	57	0.9989
G6	0.477	0.0996	0.9958	1.16	17.73	-23.67	0.9999	0.477	7.39	84	0.9985
G7	0.470	0.1013	0.9959	1.10	17.12	-22.29	1.0000	0.470	7.15	81	0.9980
G9	0.508	0.1167	0.9969	1.34	16.22	-24.17	1.0000	0.508	5.85	75	0.9986
Gn3	0.496	0.1482	0.9956	1.06	11.19	-13.73	0.9998	0.496	8.47	65	0.9970
Gn6	0.462	0.1350	0.9982	3.94	17.69	-36.70	0.9994	0.462	8.52	69	0.9993
Gn9	0.488	0.1475	0.9947	0.92	10.70	-11.99	0.9999	0.488	8.12	63	0.9966
Gn10	0.500	0.1341	0.9938	0.85	11.24	-11.61	0.9995	0.500	8.18	70	0.9953
Gn11	0.432	0.1538	0.9970	1.39	12.38	-18.91	0.9994	0.432	10.28	74	0.9979
Gn12	0.413	0.1830	0.9932	0.64	7.78	-7.31	1.0000	0.413	8.87	55	0.9953
Gn13	0.503	0.1401	0.9948	1.05	11.70	-14.11	0.9990	0.503	9.17	74	0.9958
M1	0.513	0.1430	0.9939	0.87	10.56	-10.93	0.9996	0.513	9.64	76	0.9954
M2	0.399	0.2061	0.9942	0.67	7.15	-7.25	1.0000	0.399	9.36	51	0.9961
M3	0.509	0.1916	0.9980	2.93	11.45	-21.44	0.9994	0.509	14.93	83	0.9987
M4	0.501	0.1521	0.9959	1.22	11.40	-15.13	0.9992	0.501	10.51	77	0.9967
M5	0.533	0.1655	0.9977	2.82	13.06	-23.88	0.9993	0.533	8.92	59	0.9989
M6	0.450	0.1659	0.9966	1.18	10.76	-14.91	0.9997	0.450	10.18	68	0.9978
M7	0.529	0.1757	0.9930	0.80	7.95	-7.23	0.9998	0.529	10.75	69	0.9938
M8	0.459	0.1634	0.9953	0.95	9.96	-11.98	0.9993	0.459	10.52	72	0.9961
M9	0.494	0.1930	0.9967	1.39	9.38	-13.46	0.9992	0.494	10.36	59	0.9977
M10	0.515	0.1430	0.9966	0.87	10.56	-10.93	0.9990	0.515	10.79	67	0.9972
M11	0.533	0.1623	0.9956	1.17	10.31	-12.94	0.9993	0.533	9.89	68	0.9968
M12	0.429	0.0979	0.9984	44.34	32.93	-98.30	0.9996	0.429	7.28	55	0.9975
ML1	0.573	0.1262	0.9955	1.23	13.31	-16.47	0.9999	0.573	7.25	66	0.9977
ML2	0.481	0.1457	0.9922	0.81	9.73	-8.83	1.0000	0.481	5.66	55	0.9985
ML3	0.523	0.1348	0.9964	1.39	13.33	-18.55	0.9995	0.523	7.81	66	0.9977
S1	0.497	0.0692	0.9961	1.31	25.93	-36.33	0.9997	0.497	4.99	83	0.9994
S2	0.497	0.0606	0.9973	2.53	35.27	-63.97	0.9994	0.497	4.58	86	0.9989

Table 4.1 Comparison among results obtained fitting measurements with the three proposed empirical descriptions of the potential contact area. All the three expressions are able to describe closely the surface (r^2 close to unit). The power expression was chosen because its parameters have an evident mechanical meaning.

Although these equations provide good fits to the data, they are unappealing in the sense that as A_c ranges between 0 and A_0, θ^* ranges between 0 and infinity. The realistic upper bound on θ^* is equal to $\theta^*_{\max}$. To overcome this problem, a third equation was derived:

$$A_c = A_0 \cdot \left(\frac{\theta^*_{\max} - \theta^*}{\theta^*_{\max}} \right)^C \qquad 4.4$$

where, as before, A_0 is the maximum possible contact area, $\theta^*_{\max}$ is the maximum apparent dip angle in the shear direction, and C is a "roughness" parameter, calculated using a best-fit regression function, which characterizes the distribution of the apparent dip angles over the surface. C and $\theta^*_{\max}$ depend on the specified shear direction. The upper limit of the curve where it intersects the y-axis is A_0; the curve intersects the x-axis at $\theta^*_{\max}$. This equation is preferable to the previous two (Equations 4.2 and 4.3) in that θ^* is bounded by 0 and $\theta^*_{\max}$ for A_c between A_0 and 0. Laboratory tests show that natural rock surfaces present $\theta^*_{\max}$ in a range between 20 and 90 degrees.

The curves defined by equation 4.4 are concave; the shape parameter C determines the concavity of the curve. Relatively high values of C correspond to high concavity, which, in turn, corresponds to surfaces with a relatively low degree of "roughness" in the sense that there are more triangles with low inclination compared to the maximum value; i.e. for a fixed A_0 and $\theta^*_{\max}$, increased concavity (high values of C) indicates a smooth surface with relatively few steeply dipping triangles in the shear direction.

The parameters in Equation 4.4 (A_0, C, and $\theta^*_{\max}$) were estimated using measured data for 39 surfaces and six rock types (described in detail in the following chapter). The estimated values obtained using equations 4.2 and 4.3, are reported in Table 4.1. Once again, the equation provides a good fit to the measured data. Estimated curves are shown in **Error! Reference source not found.** for granite and serpentinite surfaces.

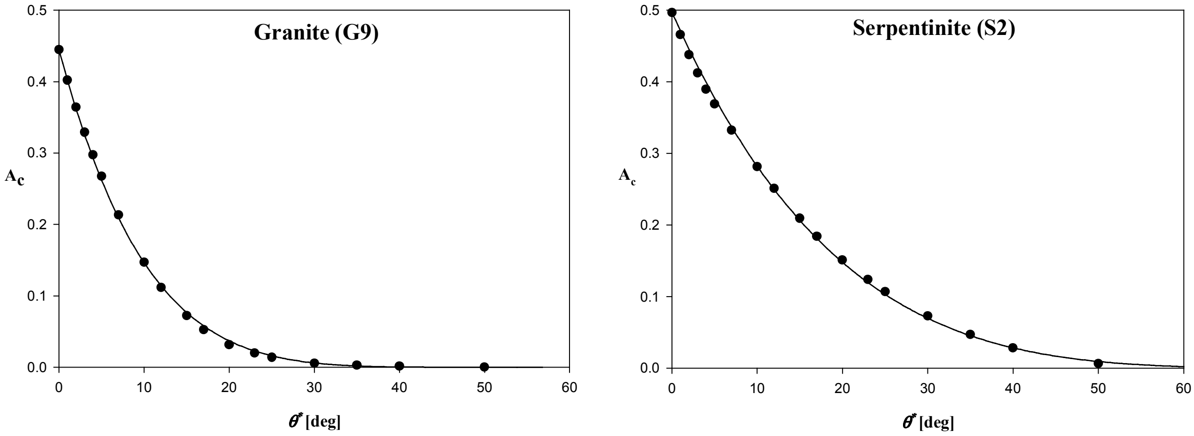

Figure 4.10 Relation between contact area ratio (A_c) and apparent dip inclination (θ^*) for two different surfaces using the third proposed equation.

These curves are representative of those obtained for the other surfaces; the r^2 values obtained for all surfaces are reported in Table 4.1.

4.3 EVOLUTION OF SURFACE PARAMETERS WITH SHEARING

To gain some understanding of how surfaces change with shearing, surface parameters for several samples were measured before and after shear tests. The surfaces of four samples were measured before and after shearing to obtain surface parameters. Shearing causes two general types of damage: crushing and shearing of asperities. One would expect shearing of asperities to occur at peak shear stress, at those asperities with the steepest inclinations. In this case, $\theta^*_{\max}$, which results in a corresponding decrease in *C*. (see Table 4.2). *C* also decreases because the angularity of the sheared surface is more uniform. The more uniform roughness is reflected by an increase in the ratio $\theta^*_{\max}/C$ with shearing. The parameter A_0, which is the maximum potential contact area for the shear direction, changed very little during shearing.

Sample name	A_0 [-]	C [-]	$\theta^*_{\max}$ [deg]	r^2 [-]	$\theta^*_{\max}/C$ [deg]
C2 (fresh)	0.462	5.64	80	0.9991	14.19
C2 (sheared)	0.462	4.19	65	0.9994	15.51
G9 (fresh)	0.508	5.85	75	0.9986	12.81
G9 (sheared)	0.493	4.85	65	0.9985	13.40
M12 (fresh)	0.429	7.28	55	0.9975	7.55
M12 (sheared)	0.405	7.14	55	0.9970	7.71
ML2 (fresh)	0.481	5.66	55	0.9985	9.73
ML2 (sheared)	0.466	5.55	55	0.9987	9.91

Table 4.2 Evolution with shearing cycles for the parameters of the surface characteristic curve.

4.4 APPLYING THE RESULTS TO THE FIELD

The close agreement (Table 4.1) between the curves derived from equation 4.4 and the measured data suggests the possibility of defining functional relationships between potential contact area and the minimum apparent dip angle. The obvious question is how such relationships would be applied in the field, since they require knowledge of A_0, C and $\theta^*_{\max}$. Based on the samples studied here, the values of these parameters tend to be characteristic for specific rock types, indicating that it might be possible to determine ranges for each rock type based on laboratory measurements of representative samples.

For each of the six rock types studied, several fracture surfaces were analyzed to obtain an indication of the variability in surface characteristics for fractures generated under identical conditions. Measured values obtained for maximum possible contact area during shearing (A_0)

and maximum dip angle with respect to the shear direction ($\theta^{*}_{\max}$) are reported in Table 4.1. As described above, from A_0 and $\theta^{*}_{\max}$ it is possible to determine the concavity parameter C in equation 4.4. For each of the surfaces analyzed, $\theta^{*}_{\max}/C$ was calculated and the values are reported in Figure 4.11. The figure shows the variability in this parameter for each rock type, and also shows that it is possible to differentiate between some of the rock types. For example, the gneiss and marble samples tended to be smoother than the granite and limestone samples ($\theta^{*}_{\max}/C$ describes the change of angularity across the surface; low values correspond to high concavity, which, in turn, indicates relatively few steeply inclined areas). Although many more measurements would have to be made to have the necessary confidence to use these data in the field, the results suggest the potential to be able to adopt these parameters to capture the relevant geometrical features of fractures in specific rock types.

Other important issues in using laboratory data to predict field conditions include scale effects, and any differences between naturally occurring fractures and those studied in the laboratory. As described in the next chapter, the test specimens used here were induced tensile fractures. Thus, an important consideration is how the behavior of these “fresh” joints is different from in situ fractures.

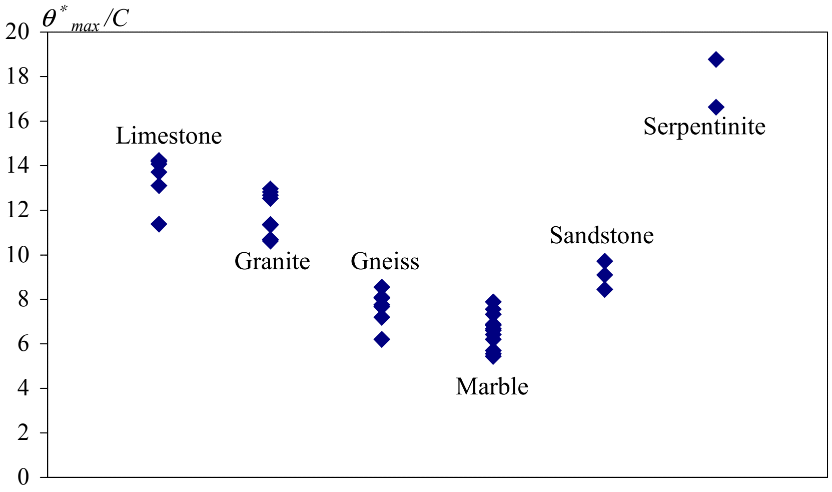

Figure 4.11 Range of values that the parameters of the surface characteristic curve can assume for each tested rock type

Rock	A_0		C		$\theta^{*}_{\max}$		$\theta^{*}_{\max}/C$	
type	Min	Max	Min	Max	Min	Max	Min	Max
Gneiss	0.413	0.503	8.12	10.28	55	74	6	9
Tarn granite	0.460	0.553	5.33	7.39	57	84	11	13
Magny limestone	0.462	0.555	4.74	7.03	65	88	11	14
Carrara marble	0.399	0.533	7.28	14.93	51	83	5	8
Sandstone	0.481	0.573	5.66	7.81	55	66	8	10
Serpentinite	0.497	0.497	4.58	4.99	83	86	17	19

Table 4.3 Range of values that the parameters of the surface characteristic curve can assume for each tested rock type in the considered shear direction.

Although many more measurements would have to be made to have the necessary confidence to use these data in the field, the results suggest the potential to be able to use these parameters to capture the relevant geometrical features of fractures in specific rock types.

4.5 CONCLUSIONS

Because the geometry of roughness influences the size and distribution of contact areas during shearing, it has to be considered the most important geometrical boundary condition for explaining this process. In addition, the size, shape, and spatial distribution of damaged areas depend on the shear direction, the degree and distribution of stress, and horizontal displacement. It is obvious that damage increases with increasing stress and displacement. The experimental results described here indicate that no damage appears prior to the peak stress; damage occurs principally during the softening and residual phases of shearing. In addition, it appears that areas where shearing of asperities can be observed correspond to areas where there were contacting asperities at peak shear stress. A possible interpretation is that it is the breaking of asperities at peak shear stress that initiates sliding. The common characteristic among all damaged areas is that they are without exception located in the steepest zones facing the shear direction (Figure 4.1). The shape of the damage zones depends on the local geometry of the fracture surface, including the size and shape of the asperities, as well as on the mechanical parameters of the rock.

In order to estimate the position of the damaged areas that will occur during shearing, it is first necessary to specify the shear direction. Only the triangles facing the shear vector ($\boldsymbol{t}$) provide shear resistance. The concept of a threshold apparent dip angle was introduced to locate and estimate the contact area during shearing. It was argued that only the zones of the surface facing the shear direction, and steeper than a threshold inclination (defined as θ^{*}_{cr}), are involved in the shearing. Three empirical relationships between the potential contact area (A_c) and the minimum apparent dip inclination (θ^{*}) were proposed. The close agreement between the experimentally measured data and all of these empirical descriptions of the potential contact area, as a function of the minimum apparent dip angle, suggests that it is possible to predict the damage areas that will appear during shearing by choosing the proper threshold value for θ^{*}. For several reasons, the third expression (Equation 4.4) is the most suitable to be employed: it gives realistic values of Ac for the minimum and maximum values of θ^{*} [0, and $\theta^{*}_{\max}$, respectively], its correlation to experimental data is extremely good (see Table 4.1), and the parameters in the equation are easy to calculate and closely related to the specific geometry of the joint surface.

To apply the results presented here to field applications would require many more measurements. However, the results suggest the potential to use the surface parameters to capture the relevant geometrical features of fractures in specific rock types. More specifically, the close agreement (Table 4.1) between the curves derived from equation 4.4 and the measured data suggests the possibility of defining functional relationships between potential contact area and the minimum apparent dip angle. The obvious question is how such relationships would be applied in the field, since they require knowledge of A_0, C and $\theta^*_{\max}$. Based on the samples studied here, the values of these parameters tend to be characteristic for specific rock types, indicating that it might be possible to determine ranges for each rock type based on laboratory measurements on representative samples.

Other important issues, in using laboratory data to predict field conditions, include scale effects (summarily discussed in the last chapter), and any differences between naturally occurring fractures and those studied in the laboratory. As described in the next chapter, the test specimens used here were induced tensile fractures. Thus, an important consideration is how the behavior of these “fresh” joints is different from in situ fractures. The results of experiments in which surface parameters were measured before and after shear tests give some indication of how these parameters change during shearing, and, thus, how they would likely be different for in situ fractures. In general, as would be expected, damage induced by shearing results in a more uniform surface roughness.

5. Shear tests

"Experiments should be reproducible — they should all fail in the same way."
Murphy law

One of the primary objectives of this work is to better understand the frictional behavior of joints under shear loads, including the creation of damage zones. In Switzerland, there is concern that sliding along joints under dams could lead to stability problems. Generally, shearing of rock joints occurs in-situ under a variety of boundary conditions. However, it is possible to identify two different characteristic behaviors:

The first condition, where the joint can freely dilate (e.g. rock slope), is duplicated in the laboratory by keeping the normal force constant (CNL) under the shearing test; the second condition, where the joint is constrained and any dilatancy activates additional normal load (e.g. foundation piles or a block in a rock mass), is simulated in laboratory by keeping the normal stiffness constant (CNS) during the shearing.

For studying the joint behavior under the foundations of dams, it is reasonable to think that the high water pressure against the face of the dam produces shearing along fractures under the foundations. Depending on the orientations of the joint sets and their depth, each joint is free to dilate and it is subjected to normal load in the range of 0.2-5.0 MPa. To study these conditions, it has been judged that the most appropriate laboratory experimental set-up is the CNL shear test. Therefore, to study the frictional response of rock joints, more than fifty constant-normal-load direct-shear tests were performed on both replicas of tensile joints, and induced tensile fractures for seven rock types. The main experimental results are summarized in this chapter and presented in full in the enclosed CD.

The advantage of using replicas is that they make it possible to independently study the two parameters that most strongly influence shear behavior: normal load and the morphology of the joint surfaces. Using replicas of the same joint, the influence of normal load on peak shear strength was investigated. Using replicas of different joints, fixing the normal load, the influence of morphology was studied.

The advantage of using rock-joint samples, rather than mortar replicas, is that they allow to test rock types commonly found underground and in foundations works and to investigate the influence of different mechanical parameters on the shear strength and the failure mechanism. Seven different types of rocks have been used during this study.

5.1 SAMPLE PREPARATION

5.1.1 *Preparation of rock samples*

Tensile joints were induced using a three-point bending configuration on rectangular rock specimens 30-cm tall with a 15-cm-square base. The location of the joint plane was controlled by sawing a 5-mm-deep groove around each sample.

After creating the joint, the two halves of the original block were placed in their original position, closing the joint. The sample was then grouted into a steel shear box, leaving 25 mm of void space around the joint plane. The space around the sample is necessary to permit room for instrumentation required to measure and record the movement of the joint during shear test. The sample is then left for 48 hours to let the grout drying. Three steel cylinders are cast in the concrete of the upper and lower sample side to allow precise positioning of the frame that is used as reference for surface measurements (Figure 5.1) (See Chapter 3).

5.1.2 *Rock samples*

Seven different types of rocks have been used during this study:

- sandstone (Burdigalian molasses) that comes from the region of Fribourg (Switzerland). It is a cemented detrital sediment predominantly of quartz grains, the grades of the latter being those of sand. Other components are feldspars and black micas. The grains are angular and cemented with calcium carbonate;
- Yellow Magny limestone (Crinoidal limestone, Jurassic, Bajocian stratum) that comes from Cote d’Or (France). It is a rock composed in great part of crystalline joints of encrinites, with Foraminifera, corals, and mollusks. Its aspect is yellow, slightly mottled, with medium grain and high porosity;
- Pont du Gard limestone (Miocenic molasse limestone) that comes from Languedoc Roussillon region (France). It is a rock composed of organic grains and debris, cemented with calcium carbonate. Its aspect is light gold, and with large grain and shells. It is extremely porous rock;
- Carrara marble that comes from Apuane Alps (Italy). It is a highly metamorphic rock composed essentially of calcite. The fusion and re-crystallization of calcium carbonate with residual clay produces its typical aspect of white-ivory rock with small faded gray veins;
- Tarn granite that comes from the region of Tarn (France). It is a rock composed of biotite quartz and feldspar with medium grain texture;

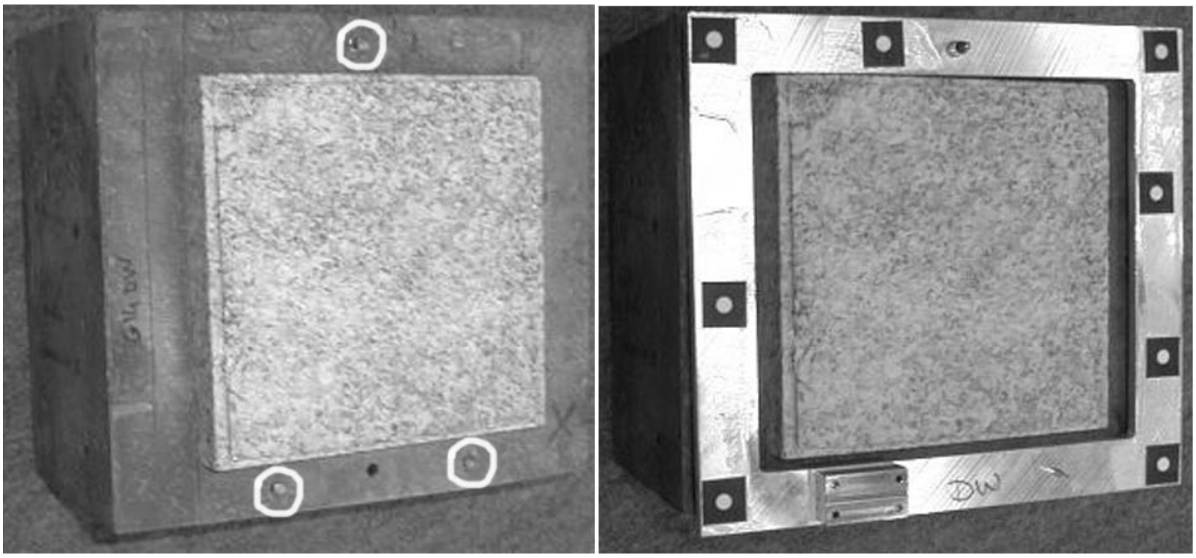

Figure 5.1 On the left picture it is possible to see the three steel cylinders cast in the concrete around the rock sample. They allow precise positioning of the aluminum frame on which the reference targets have been fixed (right picture) that are used for surface measurements.

- serpentinite that comes from Valtellina region (Italy). It is a rock consisting of serpentine minerals derived from the alteration of previously existing olivine and pyroxene. Its aspect is dark green with an accentuated schistosity;
- gneiss which comes from the region of Erstfeld (Switzerland). It is a coarsely crystalline, banded metamorphic rock composed of white, black mica, feldspar, and biotite. It presents an accentuated schistosity.

Even though sandstone, Magny limestone, granite, Carrara marble are classified as isotropic rocks, joints in these rocks vary widely in terms of surface morphology.

Joints in sandstone are generally similar and tend to be very smooth and flat. Based on visual inspection, the joint roughness appears invariant with respect to direction (isotropic roughness).

Joints in Magny limestone display randomly anisotropic roughness with significant micro-roughness.

Joints in granite also exhibit randomly anisotropic roughness with micro-roughness characterized by the size of the crystals composing the rock. The surface of the joint appears to be composed of flat surfaces with well-defined edges. These joint surfaces are particularly well suited for representation using the triangulation algorithm presented in Chapter 5.

Joints of Carrara marble exhibit randomly anisotropic roughness with substantial waviness and micro-roughness.

Gneiss and serpentinite are metamorphic rocks and contain planes of schistosity that result in anisotropic rock properties and a reduction in shear resistance parallel to the schistosity planes.

To study the shear anisotropy of these rocks, samples were created with joints both perpendicularly and parallel to the schistosity planes.

Gneiss joints are generally smooth when they coincide with the schistosity plane; they tend to have a fine saw-tooth shape when they are perpendicular to the schistosity plane.

In contrast to joints in all other rock types studied, serpentinite joints exhibit a characteristic anisotropic “sinusoidal” pattern.

The morphology of joints in Pont du Gard limestone appears to depend solely on the microstructure of the rock. The roughness is randomly anisotropic and substantial undulations are common. The micro-roughness is determined by the size of shells present in the matrix.

5.1.3 *Mechanical parameters*

The mechanical properties of each rock type were determined through uniaxial, Brazilian and tri-axial tests on core samples that were 42-mm in diameter and 110-mm in height. To measure the basic-friction angle, direct cyclic shear tests on saw-cut dry surfaces were executed for each type of rock (Operating Mode LMS+LMR ER.610). The mean values are reported in Table 5.1.

Material	Symbol	α	ρ	σ_c	σ_t	σ_c/σ_t	E	ϕ_b	ϕ_r	c_r
		[deg]	*[t/m³]*	*[MPa]*	*[MPa]*	*[-]*	*[GPa]*	*[deg]*	*[deg]*	*[MPa]*
Gneiss	Gn	0	2.66	160	3.5	46	45.9	36	43	4.9
Gneiss	Gn	30	2.66	60	-	-	21.1	36	40	2.4
Gneiss	Gn	90	2.65	184	9.5	19	37.4	36	40	1.7
Tarn granite	G	-	2.70	173	8.8	20	48.4	34	51	0.8
Magny limestone	C	-	2.19	25	2.4	10	14.9	36	38	4.5
Pont du Gard limestone	CpG	-	1.94	5	1.0	5	3.6	37	32	1.3
Carrara marble	M	-	2.69	87	9.2	9	29.6	37	50	1.3
Sandstone	ML	-	2.15	10	0.7	15	25.4	37	40	1.0
Serpentinite	S	0	2.74	166	6.0	28	76.8	39	50	5.7
Serpentinite	S	90	2.75	74	16.3	5	39.4	39	49	5.6
Masterflow replica	R	-	2.10	47	5.4	9	16.4	35	-	-

Table 5.1 Mechanical properties of rocks used in shear tests.

5.1.4 *Construction of replicas*

The decision to use replicas was made to allow us to investigate empirical relationships among normal-load, peak-shear strength and damage zones. The assumption that replicas made from the same cast have identical surfaces permits us to perform several shear experiments on joints with the same morphology.

To validate and generalize this approach, casts were made of five different rock joints: one gneiss joint (Gn2), two granite joints (G8 and G2) and two serpentinite joints (S1 and S2).

Furthermore, tests were also carried out in different directions to analyze the influence of the roughness-anisotropy on the frictional resistance (the proposed correlation of these results with the analytical description of the joint is presented in Chapter 7.)

5.1.5 *Casting modulus*

A large number of different materials for moulds have been used in the past such as two-components silicon rubber (Chryssanthakis & Barton 1990, Olsson 1998), sand-epoxy, silicon elastomer (Archambault et al. 1995). In this study, based on past extensive test-experience at LMR, Vinamold® rubber has been used. The molding material has been chosen for its satisfactory reproduction of rough surfaces.

For each mould, the original joint has been cleaned with water, for helping the rubber to be detached, and placed into a steel box. The two surfaces were separated by a special frame produced with a numerical milling-machine (precision ±1/100 mm), that has been used both to assure the horizontality of the average joint-plane, and to stiffen the mould.

The rubber has been liquefied heating up to 160ºC for 10 hours. The flowing rubber has been poured into the room between the two sides of the open joint. After a minimum of 12

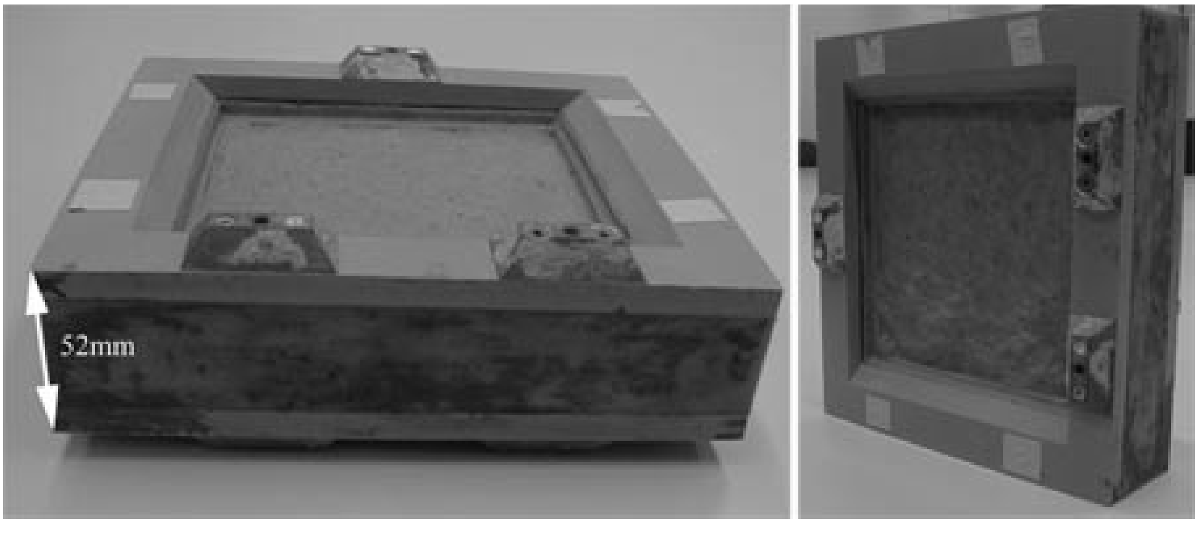

Figure 5.2 Each mould presents two PVC frames separated by one layer of Vinamold® rubber. The thickness of the mould is 52 mm and the negatives of the two sides of the joint are spaced 22 mm.

hours, the steel box has been opened and the mould could be easily detached. Each mould has a thickness of 52 mm (Figure 5.2).

5.1.6 *Preparation of concrete replicas*

The concrete used for the replicas was a pre-mixture high strength concrete, Masterflow 928, which was already largely experimented in past laboratory tests at the LMR. Its grain size is in the range of 0 and 3 mm and it does not present shrink. The water/cement ratio of 0.17 has been chosen on the basis of past experience. The concrete has been carefully mixed with water during 4 minutes. The result was an extremely fluid and homogeneous concrete that has been poured into the molding box where the joint mould had been previously fixed into a special PVC box (Figure 5.4). On the frame of the mould, six steel cylinders, three for each side, had been placed into their compartment. Their positions on the two blocks are specular and the distance between each couple is exactly 30 mm. They were used as references for repositioning the measurement-frame during the surface digitizing-process (Figure 5.5).

After a minimum of 12 hours, the surrounding PVC box was removed and the replicas could be easily detached from the mould. The replicas had a thickness between 6 up to 15 centimeters, depending on the production-series. The first and the second type were realized filling all the 15 centimeters thickness of the steel shear boxes. For the others, based on laboratory comparative tests on flat joints, it has been chosen to use a normal, cheaper pozzuolanic concrete for the bottom of the sample, producing Masterflow joint-moulds only 6 cm thick (Figure 5.3). To reduce the thickness means reducing the weight on the casting modulus, and therefore, its elastic deformation. This deformation made unmated replicas of mated joints. However the comparison between two different reproductions of the same face of the joint results identical. The adopted procedure to fabricate replica is inadequate to reproduce exactly the rock joint but is able to produce identical joints. As the idea was to fix the morphology of the surface, the procedure has been kept valid as well as the shear tests on those replicas.

Figure 5.3 The two different types of replicas produced.

5.1.7 *Mechanical parameters of concrete-replicas*

The mechanical properties of replicas were determined, using the same adopted procedure as for the rocks, through uniaxial, Brazilian and tri-axial tests on core samples that were 54-mm in diameter and 110-mm in height, and direct cyclic shear tests on saw-cut dry surfaces. The mean values are reported in Table 5.1

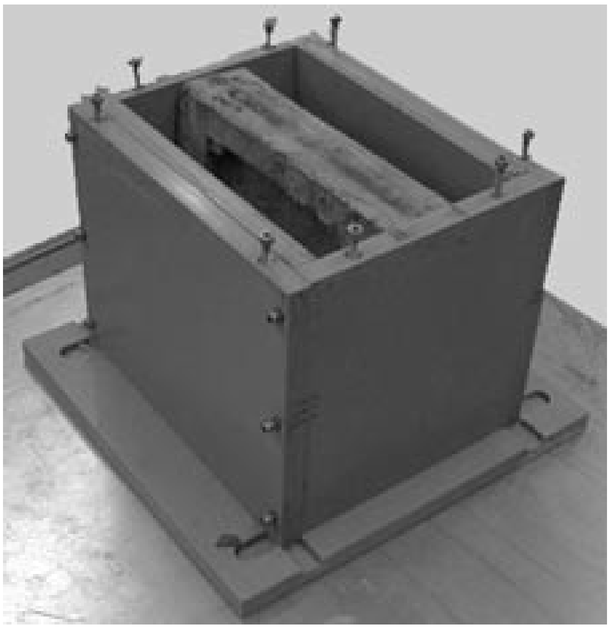

Figure 5.4 PVC molding box used to produce Masterflow concrete replicas. It is possible to see the joint mould positioned in the middle of the box.

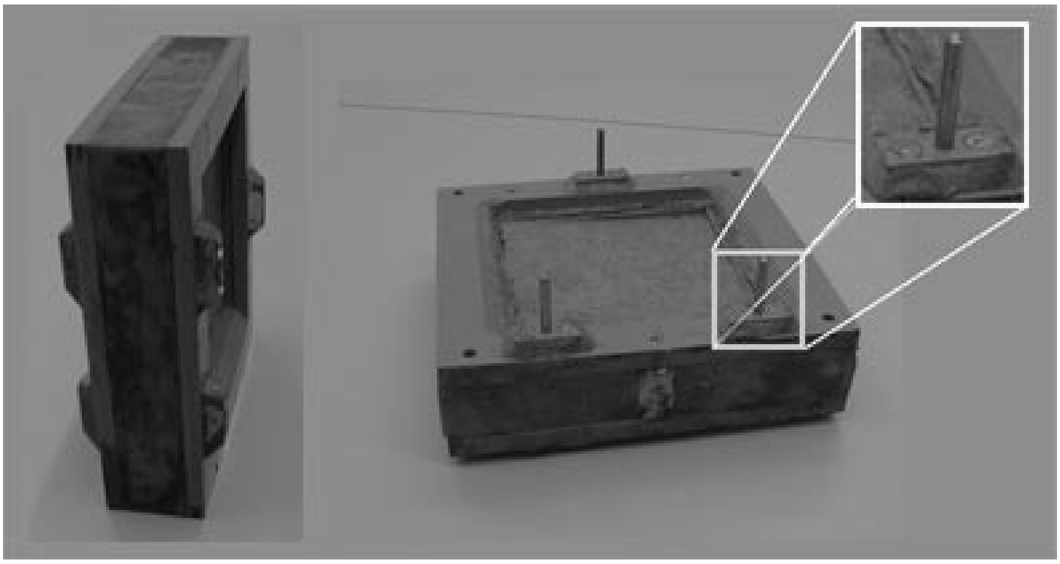

Figure 5.5 On the frame of the mould, six steel cylinders, three for each side, had been placed into their compartment. Their positions on the two blocks are specular and the distance between each couple is exactly 30 mm. They have been used as references for repositioning the measurement-frame during the surface digitizing-process

Figure 5.6 The shear box used to make the experimental tests. Both servo-hydraulic equipment and LDTV are controlled using a PC equipped with an acquisition data system.

5.2 TEST SET-UP FOR DIRECT SHEAR TEST

5.2.1 *Description of the shear apparatus*

The direct shear tests were performed with a servo-hydraulic equipment (Figure 5.6). Specimens of jointed rock are fixed into the upper and lower shear boxes and simultaneously subjected to normal and shearing stresses. In principle, the equipment is a shear box inside a

stiff load frame. Shear and normal loads are applied by hydraulic jacks equipped with servo-valves. The loading capacity of the jacks is 2000 kN for the normal force (Amsler D79) and 150 kN for the shear force (W+B NS/PA 19). The normal load is transferred to the sample via a spherical junction and the horizontal motion is guided by a precision linear bearing (Figure 5.7f), which is designed for low friction and a single degree of freedom (translation only). This insures that the upper sample holder can move during shearing with a minimum of friction and bending moment.

Detailed vertical and horizontal measurements of the shear box displacements are provided by 4 vertical short-stroke inductive LDVT (HBM-W5K) and 1 horizontal long-stroke LDVT (HBM-W10K), positioned near the joint of the specimen, directly linked to the sample (Figure 5.7d-e). Dilatancy, shear displacement and rotations are accurately measured and recorded using a PC equipped with an acquisition data system (HBM-DCM 9012).

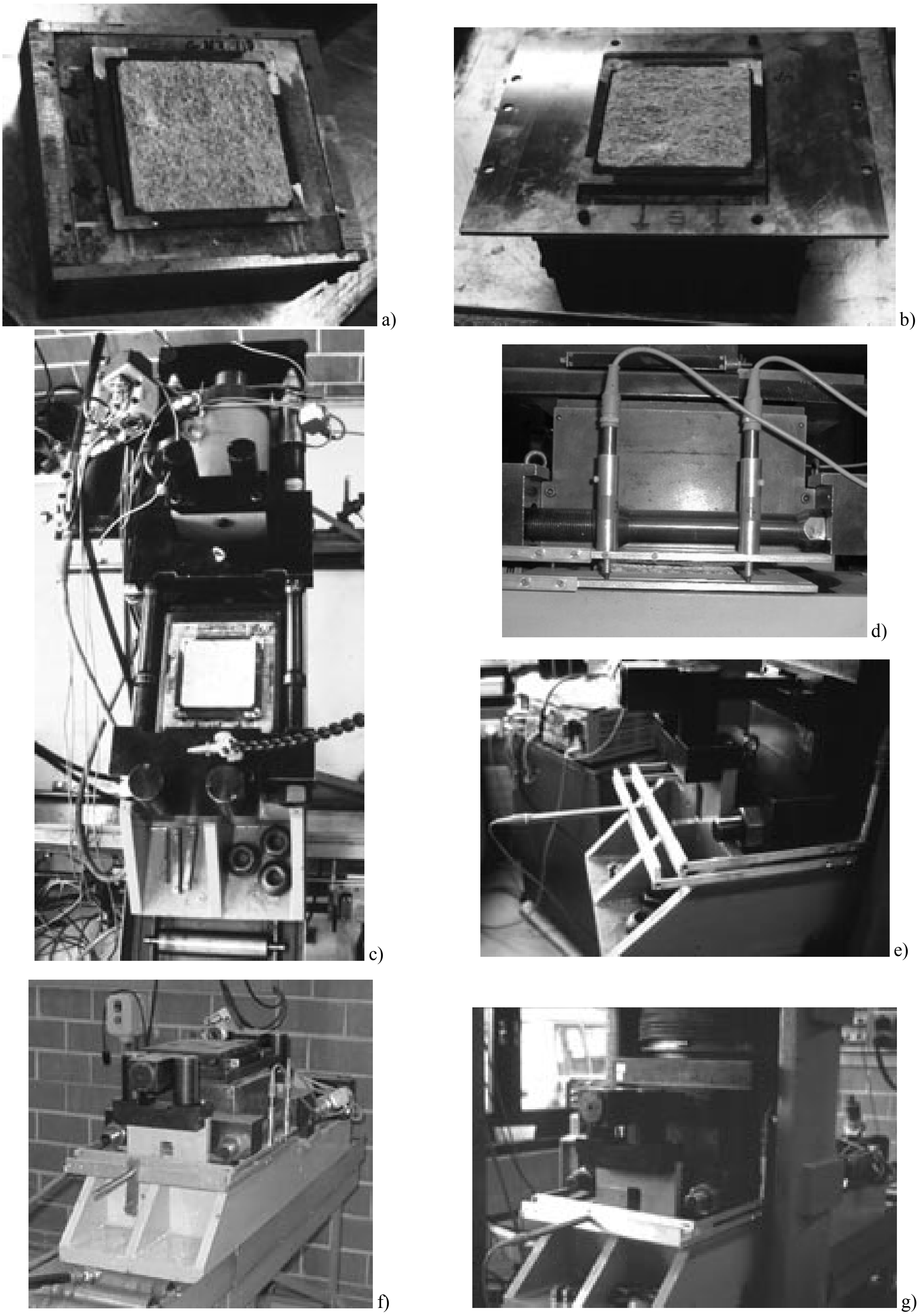

Figure 5.7 Proceeding for the set-up of laboratory shear tests: a) the rock sample is confined into a steel frame, in order to avoid failure along edges of the sample; b) aluminum frame used to position all LDVT directly at the initial joint shear plane. It is not subjected to any load, therefore all its displacements exactly describe the joint movement; c) the lower shear box is positioned into the shear load frame; d) two of the four LDVT used to measure the vertical motion of the sample; e) horizontal LDVT used to measure the displacement along shear direction; f) both shear boxes are positioned. It is possible to see on the top of the upper sample the linear bearing that insures a movement during shearing with a minimum friction and bending moment; g) the shear frame is positioned under the vertical press and the test is ready to start.

5.2.2 *Set-up procedure for shear tests*

The study has been performed assuring a fresh and mated joint at the beginning of the test. To set the initial position of the sample, the two halves of the joint are matched together manually. As the joints are fresh tensile fractures, this procedure results easy

and precise enough for our purpose. For each constant normal load (CNL) shear test the following values are recorded:

- morphology of the surface on a grid of 0.3 mm by 0.3 mm;
- normal load on the joint plane;
- shear load, parallel to the joint plane;
- horizontal displacement along the shear direction;
- vertical displacement (dilatancy) of the upper part of the sample with respect to the lower one, measured in four points (Figure 5.7e).

Trying to avoid failure along the edges of the sample (Figure 5.8) due to the effect of stress concentrations and of tensile stresses at the boundary (Hopkins 2000), the rock-joints have been squeezed into two steel frames, one on each part of the sample (Figure 5.7a); replicas are instead produced with a lateral ridge around the outside edge.

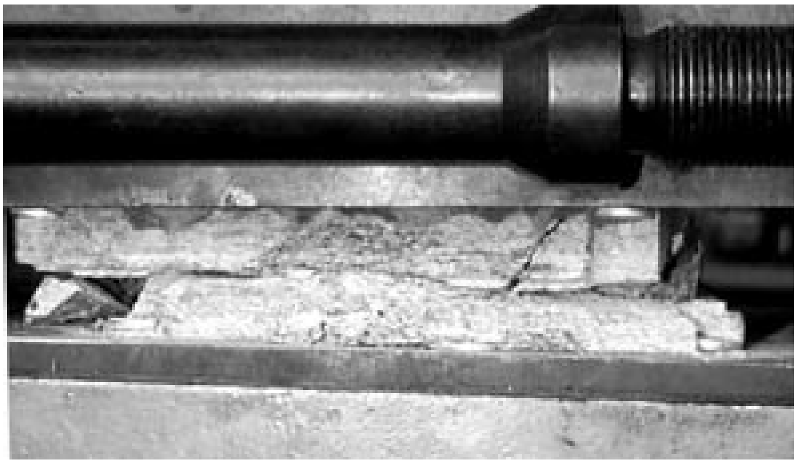

Figure 5.8 During the shearing, important failures can occur along the edges of the sample due to the effect of stress concentrations and of tensile stresses at the boundary

5.3 SHEAR TEST RESULTS

For direct-shear tests under constant normal load, it is possible to measure the horizontal and vertical displacements across the joint at fixed time-steps for any applied stress.

5.3.1 *Shear load-horizontal displacement curve*

If the shear load is plotted against the horizontal displacements, a load-displacement curve is obtained. For most rock joints the load-displacement curve takes approximately the form of Figure 5.9.

The actual behavior of sheared full-matched rock-joints may be described more completely as follows. The load-displacement curve, Figure 5.9, divides into five regions: (1) QA, in which it is slightly convex upwards, corresponds to a closure of the joint; (2) AY, a nearly linear portion, corresponds to the elastic behavior of the joint subjected to compression and shear; (3) YP, in which it is concave downwards, reaching a maximum at P, corresponds to the initiation and progression of local micro-cracks on the contact areas until the failure; (4) a falling region PD corresponds to the transient post-peak behavior; (5) DR, in which it is nearly horizontal, corresponds to the ultimate/residual friction of the joint.

In the first two regions, QA, and AY, the behavior is nearly elastic; a slight hysteresis may be observed, but loading and unloading in this region does not produce irreversible changes in the structure or properties of the rock-joint (tests C4.0 and C5.0). The point Y, at which the transition from elastic to irreversible behavior takes place, is known as the yield point and the corresponding stress as the yield stress. From its nature it is difficult to measure with any

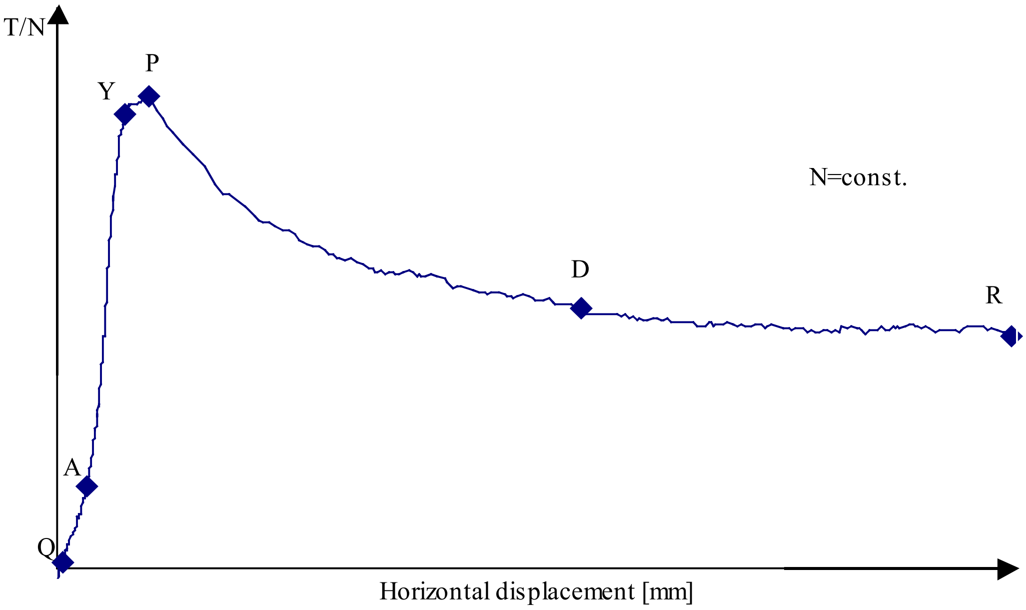

Figure 5.9 Typical load-horizontal displacement curve for a constant normal load shear test.

accuracy.

In the third region, YP, the slope of the load-displacement curve decreases progressively to zero with increasing stress. In this region irreversible changes are induced in the rock.

The fourth region, PD, begins at the maximum, P, of the stress-strain curve and is characterized by a negative slope. The presence and importance of this region depends on the rock type. It is possible to identify two different behaviors: ductile and brittle (Figure 5.10). A material is said to be in a ductile state or ductile under conditions in which it can sustain permanent deformation without losing its ability to resist load. The peak is difficult to uniquely identify and the peak shear strength is extremely close to the residual strength. A material is said to be in a brittle state or brittle under conditions in which its ability to resist load decreases with increasing deformation.

The region PD, characteristic of brittle behavior, shows a sudden loss of strength that is usually totally obscured by the instability of the machine-specimen system, which results in violent failure of the material very near to the point P. Therefore, the brittleness of a material can be defined as the magnitude of the greatest slope of the falling portion PD (Figure 5.9). The maximum ordinate of the shear stress vs. displacement curve at P is known as shear peak strength and denoted by τ_p.

The process of failure is regarded as a continuous one, which occurs progressively throughout the brittle region PD, in which the rock steadily deteriorates. Failure thus begins at the maximum ordinate P of the curve, and the criteria for failure attempt to predict the beginning of failure under more general conditions. In actual testing it frequently happens that sudden failure occurs at some point of the curve PD with complete loss of cohesion across a

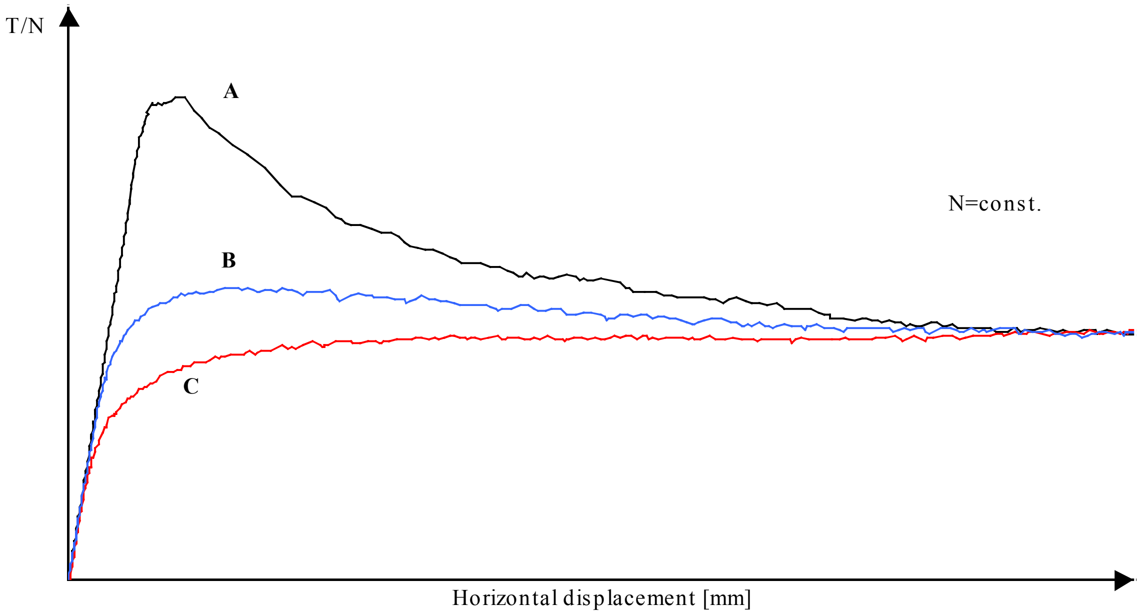

Figure 5.10 The shear behavior of a rock joint submitted to constant normal load can assume all shapes from curve A to curve C. Type A is typical for brittle rocks. The peak value is easily identified and an abrupt drop of strength follows the peak. Curve type C is the typical response of ductile behavior. It presents no peak. The transition between brittle and ductile behavior can be schematized by type B on which the shear-stress curve reaches a maximum and then quietly goes to the residual value of resistance, without any sudden loss of strength.

plane, and this is known as brittle fracture. In conventional testing machines, because of the instability of the machine-specimen system, brittle fracture occurs spontaneously at a point very near to P, so that in such cases failure and fracture become synonymous. However, in stiff testing machines, and in underground rock systems in which stress is applied through a rock mass which behaves as a stiff system, the ability of partially failed rock in the region PD to withstand load is of the greatest importance (Jaeger & Cook 1971).

5.3.2 *Shear tests on concrete replicas of tensile rock joints*

By testing artificial rough joints at low normal stresses, it was found that the shearing occurs by overriding the asperities, which remain unbroken. At higher normal stresses, the asperities start to be sheared and the dilation angle becomes smaller. The dilation is entirely replaced by shearing at a sufficiently high normal stress. The experimental curves (Figure 5.11) show, for the same morphology, the growth of the peak shear load (T_p) with increasing normal force (N). Figure 5.12 evidences that, when the normal force increases, the ratio T_p/N progressively decreases and, beyond a critical normal load, which corresponds to σ_n/σ_c=0.2, it tends to the constant value T_r/N (T_r is the residual shear resistance).

Experimentally it has been proven that increasing the applied normal load (σ_n) the absolute value of peak shear strength increases (Figure 5.11). However with increasing σ_n the ratio τ_p/σ_n decreases (Figure 5.12). The effect of roughness on the shear strength is indeed more pronounced in the range of low normal effective stress (Flamand 1998). Beyond a critical normal load, which has been evaluated corresponding to σ_n/σ_c=0.2, τ_p/σ_n tends to a constant value (ultimate or residual shear resistance).

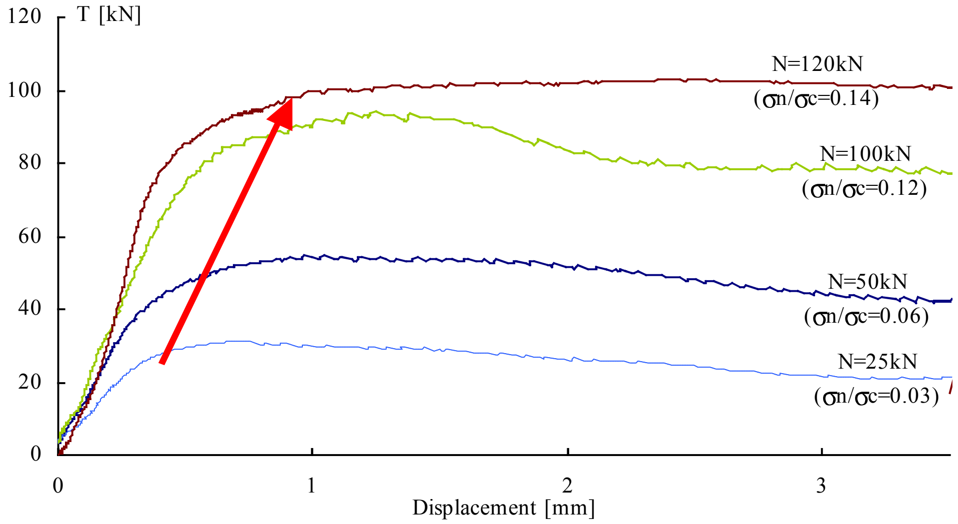

Figure 5.11 Several shear tests have been executed on different samples with the same morphology (replicas of G2 granite tensile joint). Plotting the shear force vs. the horizontal displacement, test results evidence that sensible growth in shear resistance and a stiffer response of the joint follow the increasing of the applied normal load.

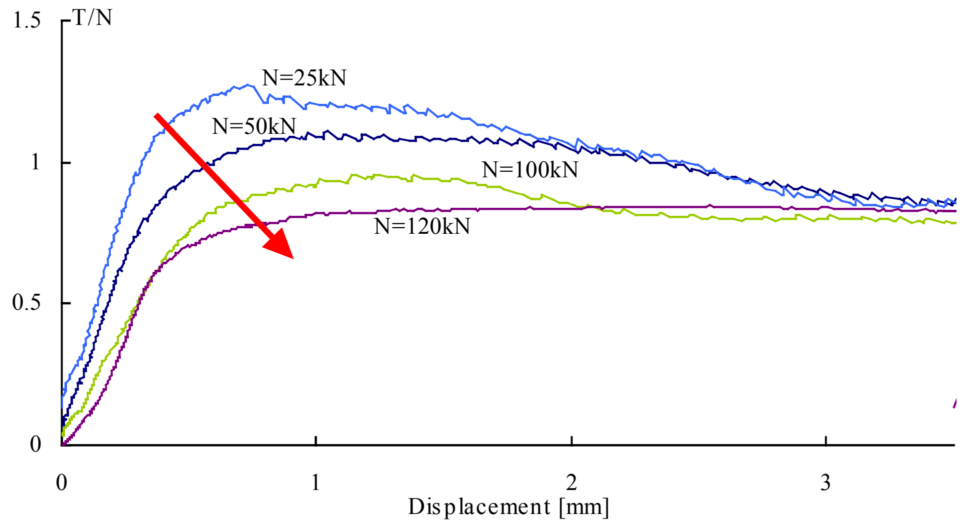

Figure 5.12 Plotting T/N vs. horizontal displacement for test results on replicas of G2 granite tensile joint, it is possible to remark that increasing of the applied normal load, the ratio T/N progressively decreases, and, beyond a critical normal load (σ_n/σ_c=0.2) T/N tends to a constant value.

5.3.3 *Directional shear tests to show the anisotropy in shear strength (tilt tests)*

The assumption that shear strength depends on the direction of the motion was verified shearing identical surfaces in different directions. Therefore it was chosen to use replicas in order to have the same initial conditions for each test. Furthermore, tilt tests have been realized in four different directions to confirm the results obtained during shear tests. The

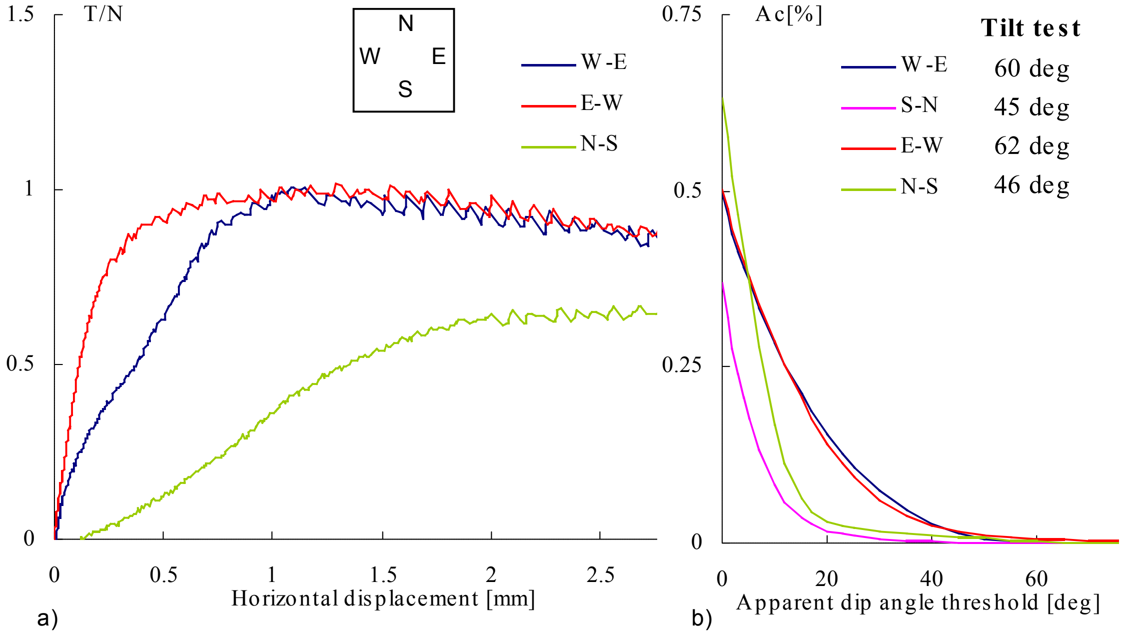

Figure 5.13 Replicas of serpentinite joint (S2) have been sheared in three different directions (a): from W to E, in the reverse direction (E-W) and perpendicularly (N-S). The experimental results show that, for joints with this surface, the strength along the axis W-E is the same for both directions, whereas the joint is weaker in the axis N-S. Analyzing of the surface (b) show that along the axis W-E the contribution is equal in both directions whereas is definitely lower in the perpendicular direction. Tilt tests results confirm this tendency.

comparison among shear strength values, obtained during laboratory tests, and morphological parameters, calculated from surface measurements, results in a strict correlation. These experimental results confirm that the shear strength of rock joints is directionally anisotropic, and validate the approach for the description of the surface morphology proposed in Chapter 5.

Shear tests on tensile rock joints

45 shear tests have been realized on fresh tensile rock joints. The shear behavior depends on the nature of the rock. It is possible to identify, for the normal load range tested (σ_n/σ_c=0.01÷0.4), the following types of behavior: ductile for Pont du Gard limestone, Magny limestone and sandstone; semi-ductile for Carrara marble; brittle for gneiss, granite and serpentinite.

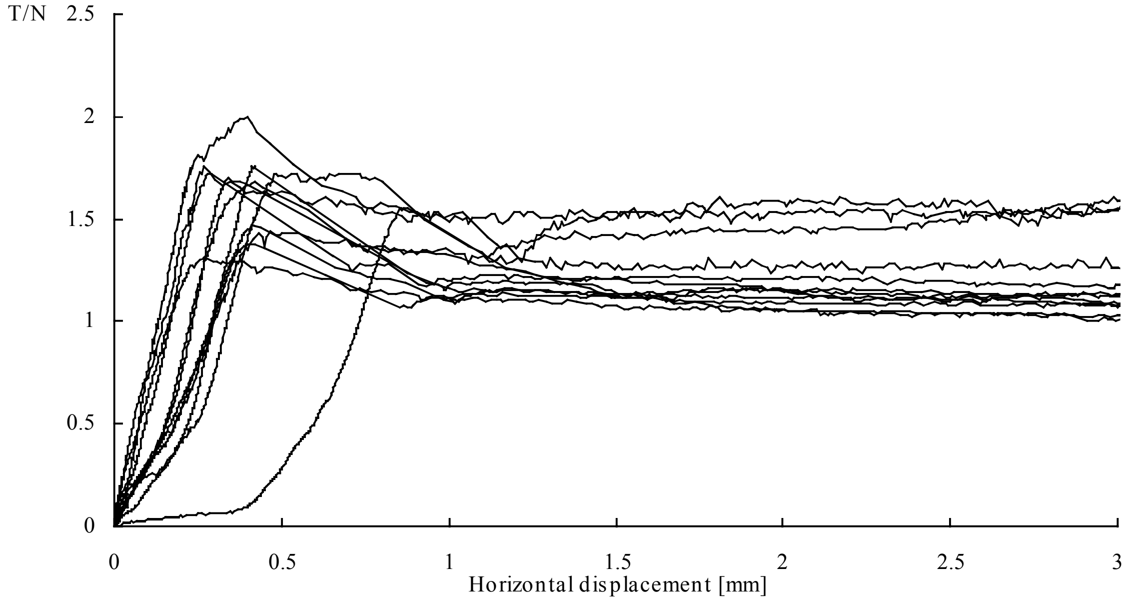

Sample	A_0	C	$\theta^*_{\max}$	l_x	l_y	α	u_p	N	σ_n/σ_c	T$_p$	T/N	ϕ_p	ϕ_r	k$_{s\,50\%}$
name	[-]	[-]	[deg]	[mm]	[mm]	[deg]	[mm]	[kN]	[-]	[kN]	[-]	[deg]	[deg]	[mm^{-1}]
M1	0.513	9.64	76	140	140	-	0.41	17	1.0%	34	2.0	63	54	7.2
M2	0.399	9.36	51	140	140	-	0.27	34	2.0%	44	1.3	53	46	6.0
M3	0.509	14.93	83	140	140	-	0.50	17	1.0%	24	1.4	55	52	4.2
M4	0.501	10.51	77	140	140	-	0.88	74	4.3%	114	1.5	57	47	3.9
M5	0.533	8.92	59	140	140	-	0.29	51	3.0%	87	1.7	60	49	7.8
M6	0.450	10.18	68	140	140	-	0.44	51	3.0%	84	1.6	59	48	7.6
M7	0.529	10.75	69	140	140	-	0.44	74	4.3%	109	1.5	56	46	3.9
M8	0.459	10.52	72	140	140	-	0.39	75	4.4%	126	1.7	59	48	7.4
M9	0.494	10.36	59	140	140	-	0.42	51	3.0%	88	1.7	60	47	4.4
M10	0.515	10.79	67	140	140	-	0.27	17	1.0%	30	1.8	60	57	5.7
M11	0.533	9.89	68	70	140	-	0.45	84	9.9%	115	1.4	54	45	7.6
M12	0.429	7.28	55	140	140	-	0.55	35	2.1%	60	1.7	60	58	6.6

Figure 5.14 Shear test realized on Carrara marble samples.

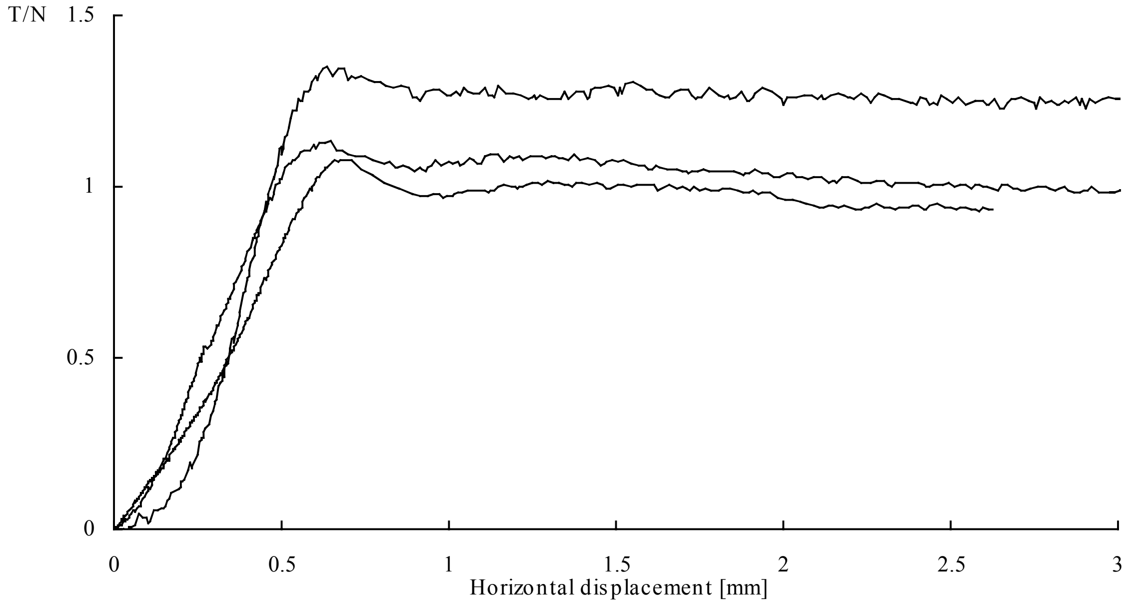

Sample	A_0	C	θ^*_{max}	l_x	l_y	α	u_p	N	σ_n/σ_c	T_p	T/N	ϕ_p	ϕ_r	$k_{s\,50\%}$
name	[-]	[-]	[deg]	[mm]	[mm]	[deg]	[mm]	[kN]	[-]	[kN]	[-]	[deg]	[deg]	[mm^{-1}]
ML1	0.573	7.25	66	140	140	-	0.65	20	10.2%	27	1.4	53	51	4.1
ML2	0.481	5.66	55	140	140	-	0.67	81	41.3%	87	1.1	47	43	2.1
ML3	0.523	7.81	66	140	140	-	0.67	41	20.9%	46	1.1	48	45	1.9

Figure 5.15 Shear test realized on sandstone samples.

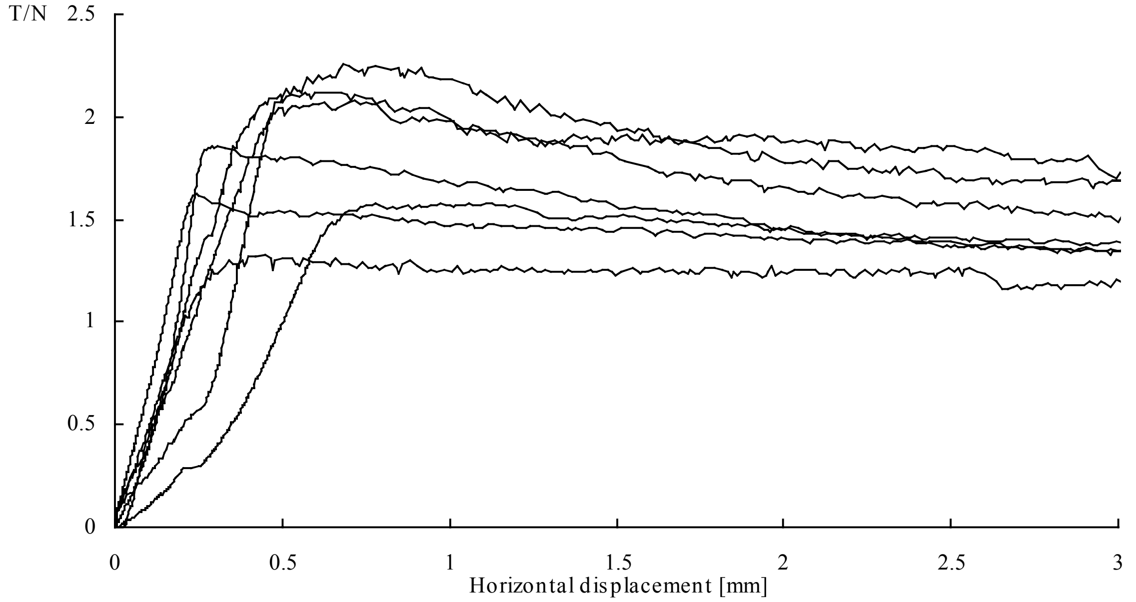

Sample	A_0	C	θ^*_{max}	l_x	l_y	α	u_p	N	σ_n/σ_c	T_p	T/N	ϕ_p	ϕ_r	$k_{s\,50\%}$
name	[-]	[-]	[deg]	[mm]	[mm]	[deg]	[mm]	[kN]	[-]	[kN]	[-]	[deg]	[deg]	[mm^{-1}]
C1	0.491	7.03	80	140	140	-	0.50	21	4.3%	44	2.1	65	60	8.2
C2	0.462	5.64	80	140	140	-	0.52	21	4.3%	42	2.0	64	56	5.2
C3	0.507	6.18	88	140	140	-	0.53	73	14.9%	107	1.5	56	51	4.0
C4	0.508	4.74	65	140	140	-	0.31	48	9.8%	90	1.9	62	53	9.4
C5	0.495	5.26	74	140	140	-	0.24	61	12.4%	98	1.6	58	53	7.1
C6	0.546	5.19	68	140	140	-	0.58	20	4.1%	41	2.1	65	59	7.4
C8	0.555	5.71	74	140	140	-	0.74	61	12.4%	95	1.6	57	53	3.5

Figure 5.16 Shear test realized on sandstone samples.

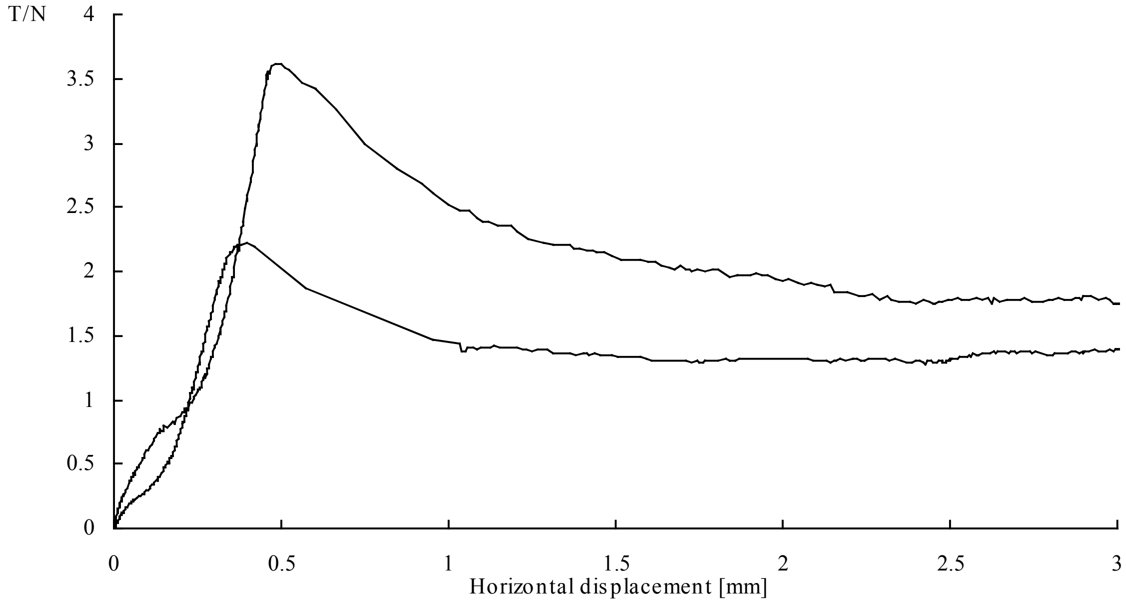

Sample name	A_0 [-]	C [-]	$\theta^*_{\max}$ [deg]	l_x [mm]	l_y [mm]	α [deg]	u_p [mm]	N [kN]	σ_n/σ_c [-]	T_p [kN]	T/N [-]	ϕ_p [deg]	ϕ_r [deg]	$k_{s\,50\%}$ [mm^{-1}]
S1	0.497	4.99	83	140	140	0	0.40	38	1.2%	83	2.2	66	53	9.9
S2	0.497	4.58	86	140	140	0	0.50	19	0.6%	67	3.5	75	61	12.3

Figure 5.17 Shear test realized on serpentinite samples.

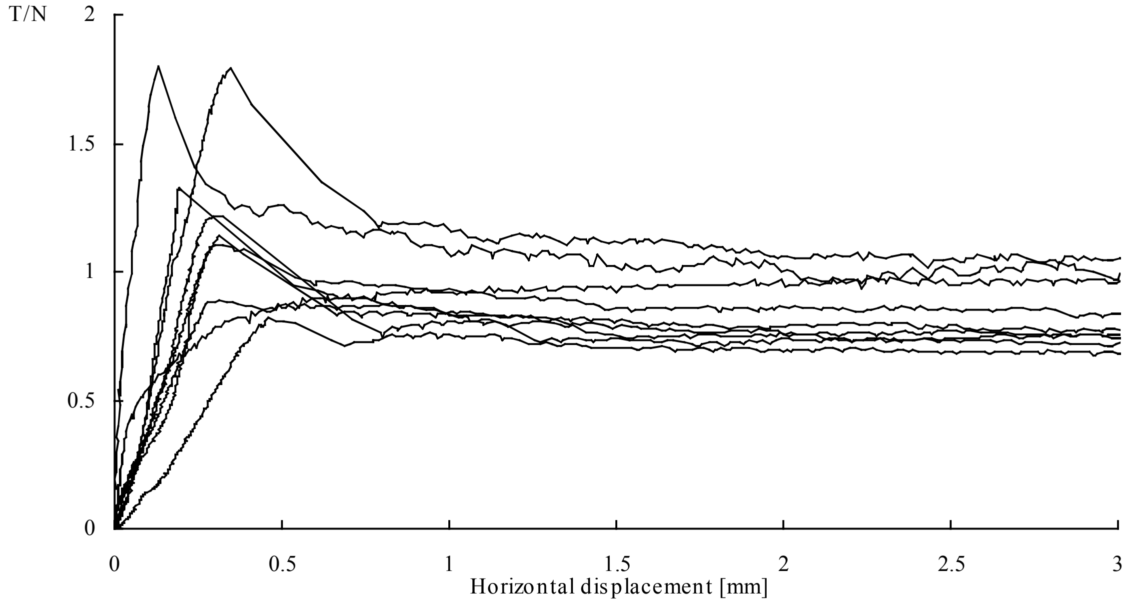

Sample name	A_0 [-]	C [-]	$\theta^*_{\max}$ [deg]	l_x [mm]	l_y [mm]	α [deg]	u_p [mm]	N [kN]	σ_n/σ_c [-]	T_p [kN]	T/N [-]	ϕ_p [deg]	ϕ_r [deg]	$k_{s\,50\%}$ [mm^{-1}]
Gn3	0.496	8.47	65	140	140	90	0.31	52	1.4%	46	0.9	42	38	3.2
Gn6	0.462	8.52	69	140	120	0	0.35	32	1.2%	58	1.8	61	46	7.4
Gn9	0.488	8.12	63	140	140	90	0.31	69	1.9%	79	1.1	49	37	5.7
Gn10	0.500	8.18	70	140	140	90	0.35	70	1.9%	76	1.1	48	40	3.4
Gn11	0.432	10.28	74	140	140	90	0.30	69	1.9%	84	1.2	51	37	4.9
Gn12	0.413	8.87	55	130	130	90	0.48	69	2.2%	56	0.8	39	35	2.2
Gn13	0.503	9.17	74	140	140	90	0.20	51	1.4%	68	1.3	53	36	9.6

Figure 5.18 Shear test realized on gneiss samples.

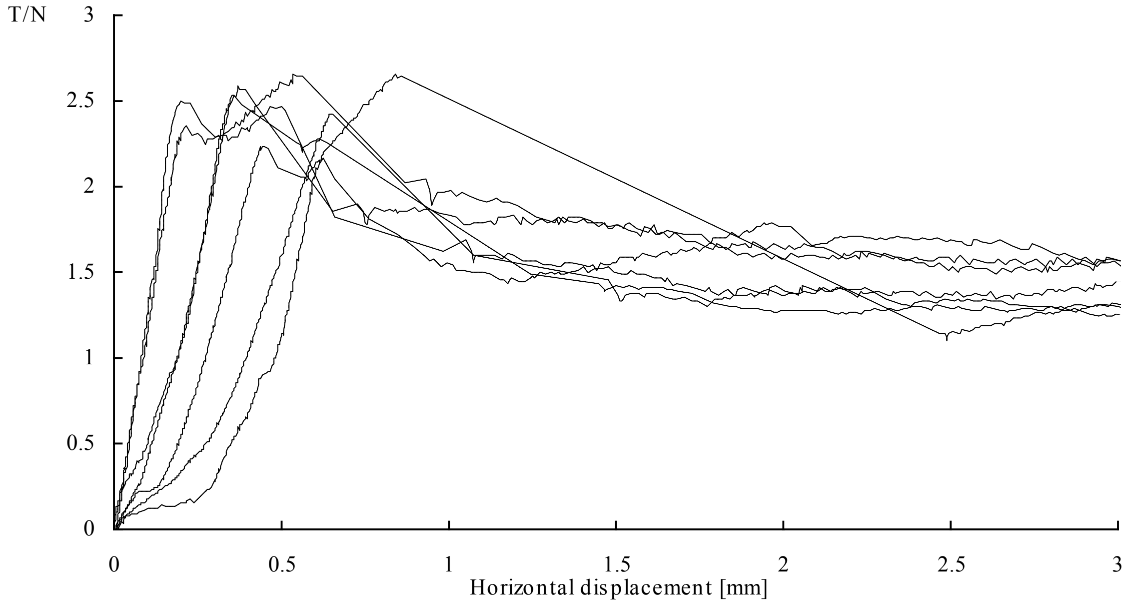

Sample name	A_0 [-]	C [-]	$\theta^*_{\max}$ [deg]	l_x [mm]	l_y [mm]	α [deg]	u_p [mm]	N [kN]	σ_n/σ_c [-]	T_p [kN]	T/N [-]	ϕ_p [deg]	ϕ_r [deg]	$k_{s\,50\%}$ [mm^{-1}]
G1	0.522	5.75	72	140	140	-	0.38	45	1.3%	113	2.5	68	51	9.6
G2	0.553	6.63	84	140	140	-	0.65	45	1.3%	109	2.4	68	53	5.7
G4	0.484	6.12	65	140	140	-	0.49	43	1.3%	94	2.2	65	52	7.3
G5	0.460	5.33	57	140	140	-	0.62	22	0.6%	48	2.2	65	54	6.4
G6	0.477	7.39	84	140	140	-	0.38	22	0.6%	57	2.6	69	57	9.2
G7	0.470	7.15	81	140	140	-	0.23	22	0.6%	55	2.5	68	57	15.1
G9	0.508	5.85	75	140	140	-	0.56	22	0.6%	59	2.7	69	57	13.8

Figure 5.19 Shear test realized on Tarn granite samples.

5.3.4 *Cycles of shear tests on the same sample*

In order to study the answer of a joint to cyclic loads, several series of multiple shear tests have been executed both on rock and replica samples.

It has been remarked that the residual friction measured after 3 mm shearing during the first cycle (called ultimate friction) is higher than that of the following. And all them tend to the same residual value (called residual friction) (Figure 5.23).

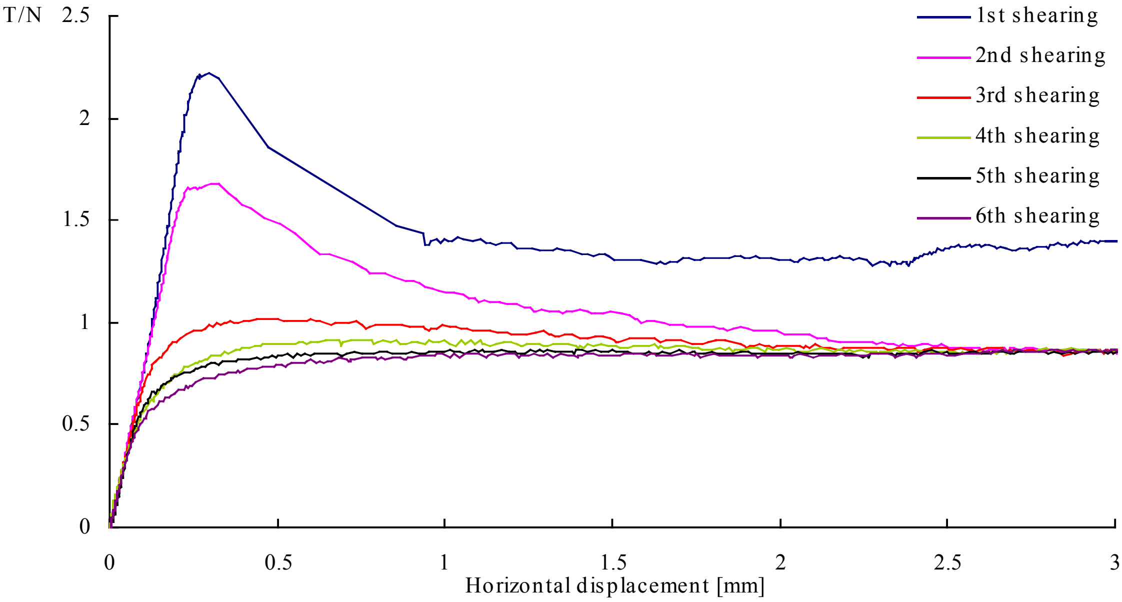

Sample	A_0	C	$\theta^*_{\max}$	l_x	l_y	α	u_p	N	σ_n/σ_c	T_p	T/N	ϕ_p	ϕ_r	$k_{s\,50\%}$
S2	[-]	[-]	[deg]	[mm]	[mm]	[deg]	[mm]	[kN]	[-]	[kN]	[-]	[deg]	[deg]	[mm^{-1}]
1st cycle	0.497	4.58	86	140	140	0	0.4	38	1.2%	83	2.2	66	53	9.9
2nd cycle	-	-	-	140	140	0	0.37	38	1.2%	63	1.7	59	40	12.6
3rd cycle	-	-	-	140	140	0	0.46	38	1.2%	39	1.0	46	41	7.1
4th cycle	-	-	-	140	140	0	0.49	38	1.2%	34	0.9	42	41	6.8
5th cycle	-	-	-	140	140	0	0.5	38	1.2%	32	0.8	41	41	7.7
6th cycle	-	-	-	140	140	0	0.53	38	1.2%	30	0.8	40	40	7.1

Figure 5.20 Multiple shearing on the same serpentinite sample (S2) under a constant normal load of 2 MPa. After 5 mm of shear displacement, the sample was repositioned at the origin and sheared again. This procedure can explain the presence of peak for only the first two tests. As the contact areas are all the time the same and the normal load does not increase, when the micro-roughness has been completely sheared (after 2 cycles), the sample "slides" on a patch of flat, inclined surfaces.

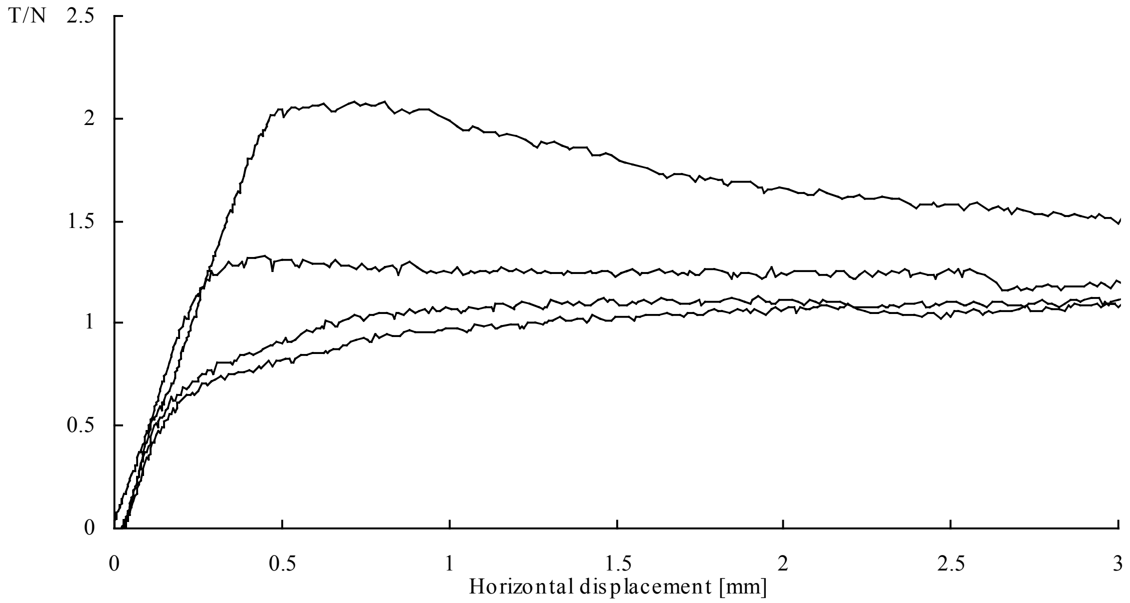

Sample	A_0	C	θ^*_{max}	l_x	l_y	α	u_p	N	σ_n/σ_c	T_p	T/N	ϕ_p	ϕ_r	$k_{s\,50\%}$
C2	[-]	[-]	[deg]	[mm]	[mm]	[deg]	[mm]	[kN]	[-]	[kN]	[-]	[deg]	[deg]	[mm^{-1}]
1st cycle	0.462	5.64	80	140	140	-	0.52	21	4%	42	2.0	64	56	5.2
2nd cycle	0.462	4.19	60	140	140	-	0.42	20	4%	26	1.3	53	50	5.5
3rd cycle	-	-	-	140	140	-	0.75	20	4%	20	1.0	48	48	4.3
4th cycle	-	-	-	140	140	-	0.85	20	4%	19	0.9	48	48	4.4

Figure 5.21 Multiple shear test realized on Magny limestone sample (C2).

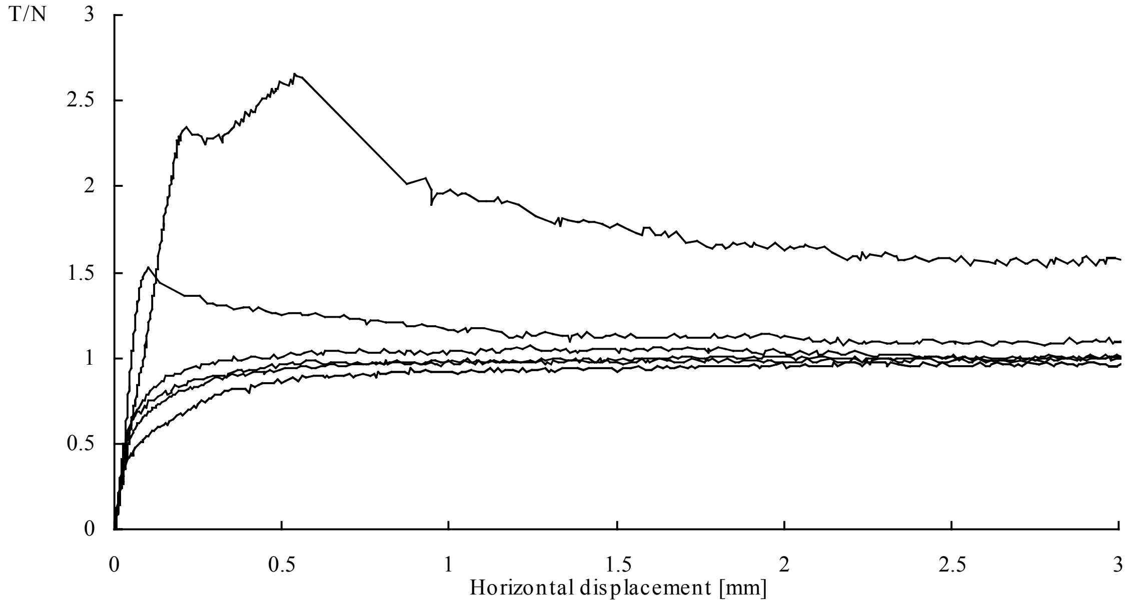

Sample	A_0	C	θ^*_{max}	l_x	l_y	α	u_p	N	σ_n/σ_c	T_p	T/N	ϕ_p	ϕ_r	$k_{s\,50\%}$
G9	[-]	[-]	[deg]	[mm]	[mm]	[deg]	[mm]	[kN]	[-]	[kN]	[-]	[deg]	[deg]	[mm^{-1}]
1st cycle	0.508	5.85	75	140	140	-	0.56	22	0.6%	59	2.7	69	57	13.8
2nd cycle	0.493	4.85	65	140	140	-	0.1	22	0.6%	34	1.5	57	47	23.7
3rd cycle	-	-	-	140	140	-	0.34	23	0.7%	23	1.0	46	46	16.5
4th cycle	-	-	-	140	140	-	0.49	23	0.7%	22	0.9	46	46	16.3
5th cycle	-	-	-	140	140	-	0.68	33	1.0%	31	0.9	46	46	12.3
6th cycle	-	-	-	140	140	-	0.55	22	0.6%	20	0.9	46	46	12.8

Figure 5.22 Multiple shear test realized on Tarn granite sample (G9).

This difference can be explained by shearing of micro-roughness on contact areas. During the second shearing, as the shear-test starts again from the same position, most of the contact areas have already been sheared before. The difference between the ultimate strength of a joint and the residual resistance could be used to quantify the influence of the micro-roughness on the joint friction. Even if only few shear tests have been realized with horizontal displacement larger than five millimeters, their results show constant light decrease of the friction value to the residual strength (Figure 5.23). Thus, it is possible to argue that the ultimate friction will decrease to the residual strength for large displacements also during the first cycle. If this result will be confirmed on further studies, it will have interesting implications for the role that dry gauge plays during shearing.

Experimentally it is evident that, shearing several times the same fresh mated joints, only the first and eventually the second test present a peak (**Error! Reference source not found.**). For the others it is possible to identify just a yield point and a residual value for the shear strength.

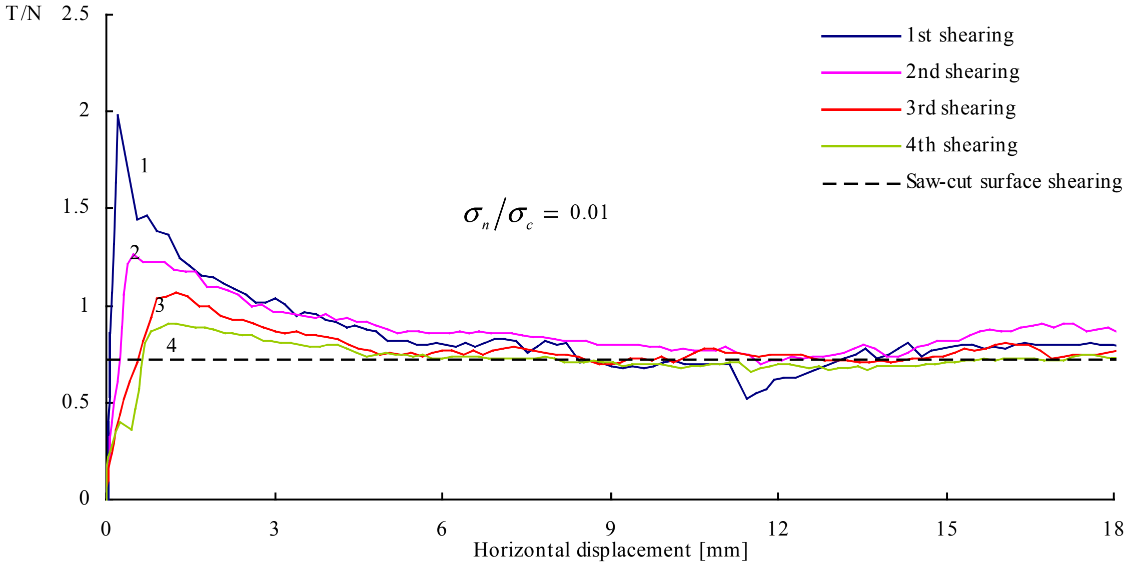

Figure 5.23 Multiple shearing on the same gneiss sample (Gn2) under a constant normal load of 2 MPa. After 20 mm of shear displacement, the sample was repositioned at the origin and sheared again.

5.3.5 *Shear stiffness of the joint*

For most rock-joints, sheared in laboratory, the load vs. displacement curve is approximately linear up to the yield point. This may be represented by the equation:

$$\frac{\tau}{\sigma_n} = k_s \cdot u \qquad 5.1$$

where the constant k_s [mm^{-1}] is called shear stiffness.

The definition of shear stiffness implies that if the joint is loaded with a shear force lower than the one corresponding to the yield point, and subsequently unloaded, the same path as given by Equation 5.1 is traversed. Even all the energy stored in the specimen while loading is released during unloading. In laboratory shear tests, there is no unique shear stiffness, but for any value of τ, the slope of the tangent to the curve identifies the local shear stiffness. To define a unique value, the average shear stiffness of a rock joint has been defined as the inclination of the tangent at the curve in the point corresponding to 50% of the peak shear strength (Figure 5.24).

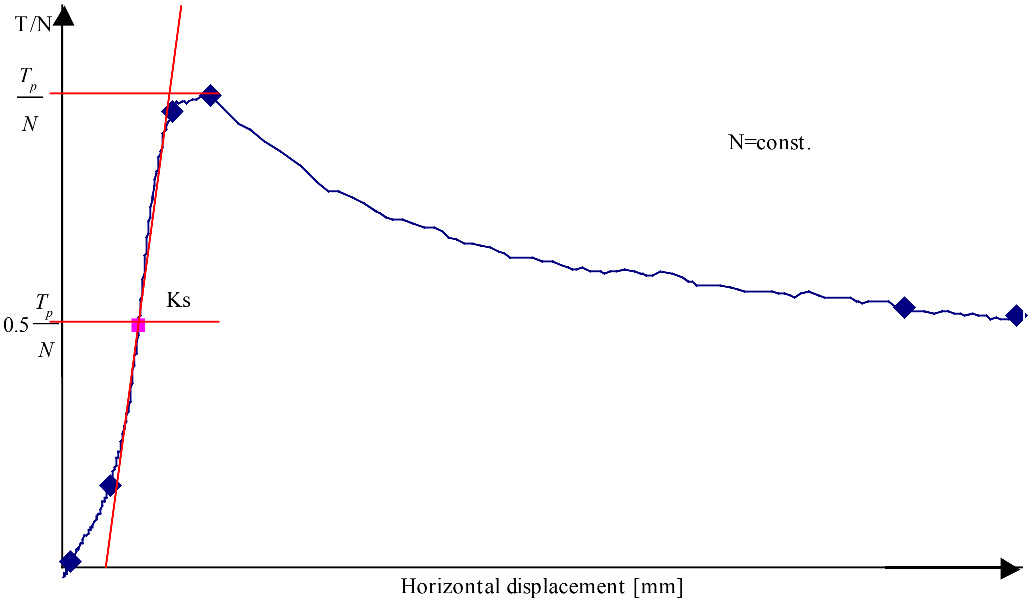

Figure 5.24 The average shear stiffness is defined as the tangent to the T/N vs. horizontal displacement curve, calculated at 50% of the peak shear strength value.

5.3.6 *Movement of the sample during the shear test*

During the shear test the upper part of the joint, submitted to both normal and shear load, slides over the lower part. As the joint is rough, the surface features impose an important constraint to the trajectory of the upper surface. Historically it has been considered by measuring only the vertical displacement of the sample (dilatancy), ignoring its rotation because it has been assumed that rotation is prevented by the stiffness of the shear apparatus. The first to point the importance of even small rotation (e.g. 0.1 degree) of one part of the sample was Boulon (1995) who tried to avoid any rotation of the sample using a conceptually new shear machine. Our experimental setup was equipped with four vertical displacement transducers in order to measure the position of the upper half of the sample during the test, calculating the dilatancy at the center of the sample and the rotations around the shear direction (roll) and around the direction on the shear plane normal to shear direction (pitch) (Figure 5.25). Rotation around the vertical axis (yaw) was discarded by the particular experimental set up. Roll and pitch rotations, even if their values are extremely small, greatly affect position and size of the areas damaged during the shearing, and, consequently, the shear strength of the joint, as well as its normal and shear stiffness.

When rock joints in nature are free to dilate they are also free to rotate. Therefore, it is important to consider also the rotations, and not only dilatancy, when shearing of rock joints is modeled.

Experimentally we can remark, contrary to literature, that for the mated fresh joint we tested, no important normal displacement (dilatancy or contractancy) was measured before reaching the peak strength. However, rotations of the sample are recorded also before the peak. The reasons are that:

- only one vertical measurement is generally recorded, thus it is not possible to determine if measured displacements are due to vertical translation or to rotations;

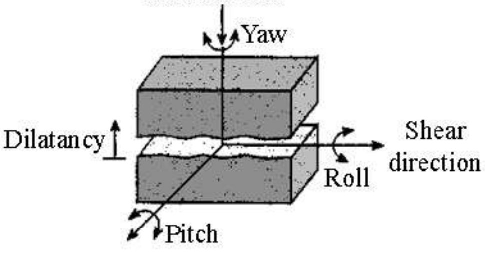

Figure 5.25 The four vertical measurements (Figure 5.7f) permit to define the position of the shear plane during the test and to calculate the dilatancy of the center of the sample and the rotation around the shear direction (roll) and around the direction on the shear plane normal to shear direction (pitch). Rotations around the vertical axis (yaw) are discarded because the shear set up permits only horizontal motion, in the direction of shear, guided by a precision linear bearing (Figure 5.7f). As yaw rotations are discarded, only one horizontal measurement result sufficient to completely determine the motion of the sample during shearing (Figure 5.7e).

- during the loading phase, the sample is not in rotational equilibrium;
- stress redistribution caused by the particular surface morphology increases the rotational disequilibrium.

5.4 DISCUSSION AND REMARKS

Mechanical behavior of replicas results closely related to cement properties. Cement is ductile and it plasticizes more than rock, therefore damage areas appear deformed and furrowed by sand grains present in the concrete mixture. Furthermore, the "matching ratio" of replicas is lower than that of fresh tensile joints in rock. Therefore, mechanical results obtained with replica samples are only qualitatively confirmed by tests on rock joint samples. Replicas results seem useful to simulate the mechanical behavior only for ductile rocks (with no peak). For brittle rocks marked peaks are indeed measured during laboratory shear tests, especially if fresh tensile fractures employed. Another important aspect, coming from the analysis of experiments, is a substantial difference between the measured residual frictional angle and the base one observed shearing tensile rock joints and not found using replicas. The easiest explanation to those disagreements can be related both to the difference in micro-roughness of the joint surface between rock joints and replicas and to the mating of the two sides of the joint. Tensile rock joints indeed result to match better than replicas. Experimentally it has been found a directional dependency for shear strength that results quite well evidenced by the surface characteristic curve proposed in Chapter 4.2. Analysis of vertical measurements done during laboratory test shows the presence of dilatancy and rotation of the sample. These observations, compared to the image of the sheared joint surfaces, evidence the importance that also little rotations, that happen during shearing, have on the contact area distribution, and, therefore, on the damage location.

6. Constitutive model for shear strength of rock joints

"The behaviour of macroscopic systems is generally described by non-linear laws. The non-linear laws may explain irreversible phenomena like instabilities, dualism, unevolving societies, cycles of growth and decay of societies. The linear laws are only linear approximation of the non linear laws at a point in time and space"
Ilya Prigogine

The experimental results of rock joints, observed in laboratory tests or field experiments, provide raw data under specific test conditions. These data provide the basis for determining the joint behavior. A general mathematical model must be developed to represent the mechanical behavior of the rock joints under general loading paths and histories, such that the universal laws of classical solid physics are always satisfied. Such models serve as constitutive models for rock joints and they are utilized as predictors of complete histories of stresses and displacements of rock joints in various numerical methods and computer programs under general loading conditions. In view of the extreme complexity of joint behavior, usually only part of the most important aspects of the rock joint behavior, most often resulted from laboratory tests, can be approximately represented in a constitutive model. These are usually relations between stresses and displacements (or their increments). Constitutive models are often conceived intuitively from conceptual models obtained as typical behavior of rock joints under laboratory test conditions.

The formulations of constitutive models follow basically two approaches: the empirical approach and the theoretical approach. In the empirical approach, a constitutive model is obtained either by curve fitting to laboratory results or from conceptual mathematical functions. The constants appearing in these models may or may not have physical meanings and can only represent rock joint behavior under special test conditions. The empirical constitutive models obtained in this manner can provide practical solutions to engineering problems so long as the parameters lie within the range covered by laboratory tests or their reasonable extrapolations. However, the model developed might not conform to physical laws commonly accepted as axioms in all branches of classical solid physics. Moreover, as the range of validity of the parameters in empirical models cannot be completely covered by laboratory experiments or field measurements, it is necessary to made extrapolations, which may introduce some errors whose significance may become unpredictable. In such circumstances, the model will lose both its physical basis and practical utility.

The theoretical approach, on the other hand, is based on a formal description of joint behavior on which basic laws of classical solid physics must be obeyed as the first priority. The models are usually formulated using theories of different branches of solid mechanics. However, models formulated by this approach may suffer from the limitation brought about by that fact that today no existing mathematical theory of classical solid physics or mechanics can conveniently represent, even approximately, all aspects of rock joint behavior. Some less important aspects of the joint behavior must be ignored and the developed model must be validated against laboratory test data.

The behavior of rock joints under certain experimental conditions, therefore, is the common foundation for both approaches. In the follow paragraphs the term "joint" will be used to describe all the natural discontinuities in rock having zero tensile strength (100% persistence, thus no rock bridges), an absence of soft infilling, and no previous history of displacement. Under external loads, sliding along the joints is likely to occur. Due to the presence of the asperities at the joint surfaces, dilatation usually accompanies the shearing process. The asperities of the joint walls have finite strength, they degrade during the shearing process. Dilation of the joint will diminish at the later stages of the shearing. During this process, gouge material is being produced by the damage of the asperities.

Several criteria have been proposed in past to identify the strength of a joint (see Chapter 2). They delineate the state of stress that separates pre-sliding and post-sliding of the joint. The simplest constitutive model for rock joints is perhaps the Coulomb friction law in which the joint behavior is simply characterized by a single value of friction angle. Some more complicated joint models appeared later accompanying the development of numerical methods. Notable among them are Barton empirical model (Barton & Choubey 1977), Amadei-Saeb's analytical model (Amadei et al.) and Plesha's theoretical model (Plesha 1987). All of them are two-dimensional models. However, among all the models proposed in literature, Barton's criterion is the only that is currently used in practice. Its approach is based on the choice of the correct value for the morphological parameter: the joint roughness coefficient (JRC). To estimate the proper JRC value for a surface several methods have been proposed in literature. However, none of them results able to always predict the correct value of JRC. Moreover, there are a number of unsolved problems with regard to their validity. JRC estimation by visual comparison with 10 standard profiles is prone to be subjective; on the other side, back analysis of shear results is not useful to previously estimate JRC (our ultimate goal is to evaluate τ_p using known parameters and not to estimate JRC knowing τ_p). Other methods proposed in literature like fractal analysis or statistics are controversial. Another important remark is that JRC estimation methods are based on analysis of only a single profile in the direction of shearing, hence they do not take into account the real three-dimensional geometry of the joint, whereas it has been shown in Chapter 5 that shearing strictly depends on contact area location and distribution (3D).

To show the veridicality of these hypotheses, three different profiles from different samples have been randomly extracted in the shear direction. JRC has been estimated both with visual comparison and with back analysis (JCS=σ_c). The results clearly confirm that it is not easy to uniquely estimate JRC value using current suggested methods (Figure 6.1).

Sample	**Profile**	**JRC** *visual comparison*	**JRC** *back analysis*
C2 (y=25 mm)		16-18	20
C2 (y=50 mm)		14-16	20
C2 (y=75 mm)	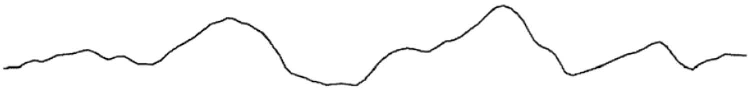	14-16	20
G2 (y=25 mm)		12-14	18
G2 (y=50 mm)	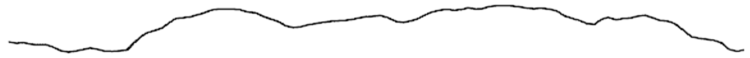	8-10	18
G2 (y=75 mm)		14-16	18
M2 (x=25 mm)		8-10	12
M2 (y=50 mm)		8-10	12
M2 (y=75 mm)		8-10	12
S2 (y=25 mm)		18-20	17
S2 (y=50 mm)		18-20	17
S2 (y=75 mm)	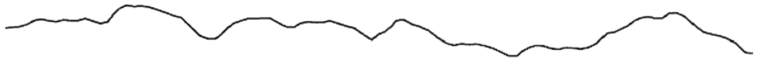	18-20	17
	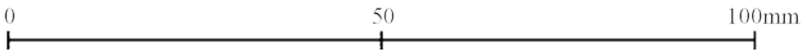	**Scale**	

Figure 6.1 JRC estimation of profiles extracted from four samples.

Thus, the challenge today is to provide either a new model able to estimate accurately the joint shear strength, or to incorporate new, easily measured parameters into the expression of shear strength, e.g. objective estimation of JRC.

6.1 PEAK-SHEAR-STRENGTH BEHAVIOR FOR REPLICAS

To begin to study the resistance of jointed rock to shear stress, a series of direct-shear tests were carried out. Concrete replicas of an induced joint in rock (Chapter 5) were employed at this stage of the research. The advantage of using replicas is that they allow us to independently study the two parameters that most strongly influence shear behavior: normal load and surface morphology. Using replicas of the same surface, morphological parameters are constant, thus allowing us to investigate the influence of normal load on peak shear strength. Moreover, using replicas of different surfaces and performing experiments under the same applied normal load, allowed the influence of surface morphology to be examined.

In agreement with results obtained by other researchers (Flamand, 1998), the effect of surface roughness on shear strength was found to be more pronounced for relatively low values of effective stress. By testing rough joints in replicas at extremely low values of normal stress, it was found that shearing occurs by overriding the asperities, which remain unbroken. At higher values of normal stress, the asperities begin to be sheared. The experimental curves (Figure 5.11) show that for the same morphology, there is an increase in peak shear strength (T_p) with increasing normal force (N). Figure 5.12 shows that as the applied normal force is increased, the ratio of shear-to-normal load (T_p/N) progressively decreases and, beyond a critical normal load, which is approximately $\sigma_n/\sigma_c=0.2$, tends toward a constant value equal to T_r/N, where T_r is the residual shear resistance. This means that the role of surface morphology in shear resistance decreases with increasing normal load. When there is no applied normal load, the normal force acting on the joint is that resulting from the weight of the sample itself, and in this case the ratio of shear-to-normal load is maximum. The maximum peak-friction angle corresponds to this loading condition. Thus, the relationship between the ratio of shear-to-normal load and peak-friction angle is given, according to Coulomb’s expression, by:

$$\frac{\tau_p}{\sigma_n} = \tan\left(\phi_p\right) \qquad 6.1$$

However, the experimental results presented here show that the peak friction angle never exceeds values larger than 65-80 degrees, depending on the morphology of the joint. This is consistent with results presented by other researchers; e.g., Barton (1977) suggests that the maximum peak-friction angle be fixed at a value of 70 degrees for design purposes. Thus, an expression for peak-shear strength should approach a finite value as the applied normal load approaches zero.

The study of the experimentally derived curves of τ_p/σ_n versus σ_n/σ_c (see Figure 6.2) shows that peak-shear strength decreases from a maximum finite value to a constant residual value, and that the curves have a negative-exponential shape. Taking into account these considerations and the test results, which suggest the overall shape of the curve, the following expression for peak shear strength was proposed (Grasselli & Egger 2000b):

$$\tau_p = \sigma_n \cdot \tan\left(\phi_r'\right) \cdot \left[1 + e^{\frac{-\theta^*_{\max}}{A_0 \cdot C} \cdot \frac{\sigma_n}{\sigma_c}}\right] \qquad 6.2$$

where τ_p is the peak shear strength of the joint; σ_n is the applied average normal stress; σ_c is the compressive strength of the intact material obtained from a standard uniaxial test; ϕ'_r is the residual friction angle (measured after a standard displacement of 5 mm); A_0 is the maximum potential contact area for the specified shear direction; θ^*_{max} is the maximum apparent dip angle with respect to the shear direction; and C is the roughness parameter defined in Chapter 4.2.

The expression inside the brackets in equation 6.2 goes to two as the argument in the exponential term goes to zero. The argument in this term approaches zero if either θ^*_{max} or σ_n approach zero. However, in practice, θ^*_{max} is confined to a range of approximately 20 to 90 degrees (see discussion in Chapter 4.2). With respect to σ_n, as described in detail above, the minimum value occurs when there is no applied normal load, in which case the normal stress

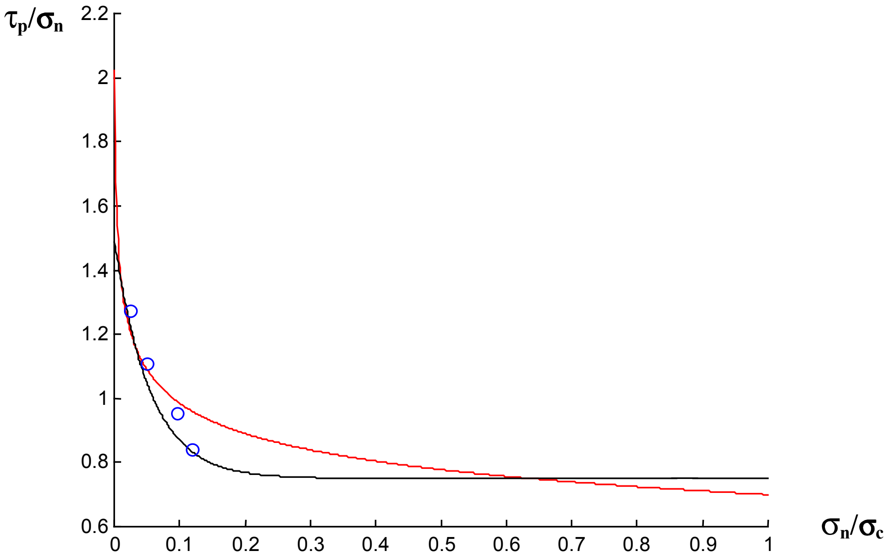

Figure 6.2 Comparison between the proposed model (black) and Barton's equation (red) to fit the experimental points obtained in laboratory tests on replicas of one tensile granite sample.

is that resulting from the weight of the sample itself. In this condition, as σ_n approaches zero, it is possible to show that:

$$\lim_{\sigma_n \to 0}\left(\frac{\tau_p}{\sigma_n}\right) = 2\cdot\tan\left(\phi_r^{'}\right) = \tan\left(\phi_p\right) \quad \rightarrow \quad \phi_p = 65^\circ \sim 80^\circ \qquad 6.3$$

Equation 6.2 was derived based on the results of experiments performed on replicas of the same granite joint. It was, therefore, necessary to perform additional tests on different joints to determine if the expression was generally applicable. Shear tests were next conducted on a replica of a joint in serpentinite, and on a replica of the same granite joint used for the first series of experiments, except that the shear direction was reversed. The surface parameters were measured as described in Chapter 4.2. The shear strength of each joint was predicted using equation 6.2, and the predicted values were found to agree very closely with the measured values (Figure 6.3).

The predicted values from equation 6.2 for the granite replica data were then compared to those calculated using Barton's (1977) peak-shear-strength criterion (Figure 6.2). The value of JRC needed to use Barton's formulation was determined from a least squares best fit to the experimental data (a value of JRC=9.5 was estimated). Since the joint was in intact rock, a value of JCS=σ_c was used along with the estimated value of JRC to plot Barton's equation on the τ_p/σ_n vs. σ_n/σ_c plane. The results obtained using Barton's formulation are compared to those obtained with equation 6.2 in Figure 6.2. The comparison shows that the values obtained with equation 6.2 result in a better fit to the experimental data. In addition, the equation does not over-estimate the peak shear strength; this is a problem that sometimes occurs in applying Barton's approach.

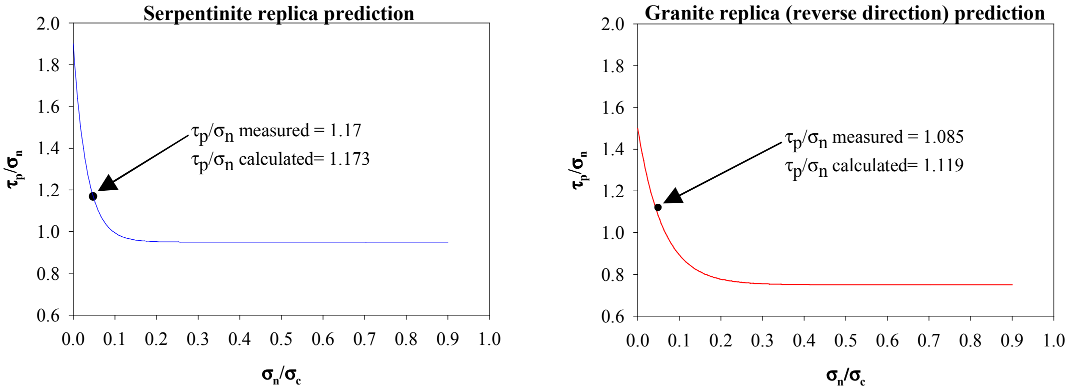

Figure 6.3 Comparison between the τ_p/σ_n values obtained from shear tests and those calculated using equation 6.2. Both replicas have been produced with the same type of concrete.

6.2 FAILURE MODES AND IMPLICATIONS FOR PEAK SHEAR STRENGTH

The method for predicting the peak shear strength of joints in replicas proposed in the previous section (Equation 6.2) had to be modified for use on fractures in rock. Observations of the surfaces of several sheared rock joints indicated that the breaking of individual asperities was governed by tensile failure rather than compressive failure. For example, the failure planes tended to be rough, and it was possible to observe intact fragments sheared from the surface (particularly evident on surfaces where shearing was interrupted after small shear displacements). This result is consistent with results published by Fishman (1990) and Armand (2000). Thus, it appears that tensile strength may be a far more important parameter than compressive strength in quantifying the peak shear resistance of rock joints. This conclusion was important in deriving a more general expression for peak shear strength that holds for both mortar replicas and rock joints.

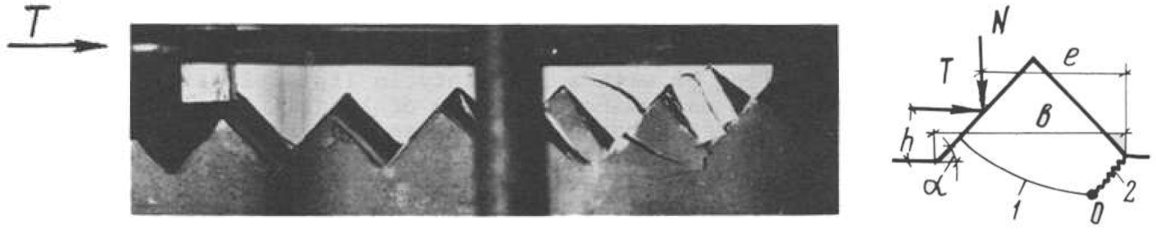

a) b)

Figure 6.4 a) View of failed model (Fishman 1990). b) Scheme of failure of asperities under the action of normal and shear load (Fishman 1990).

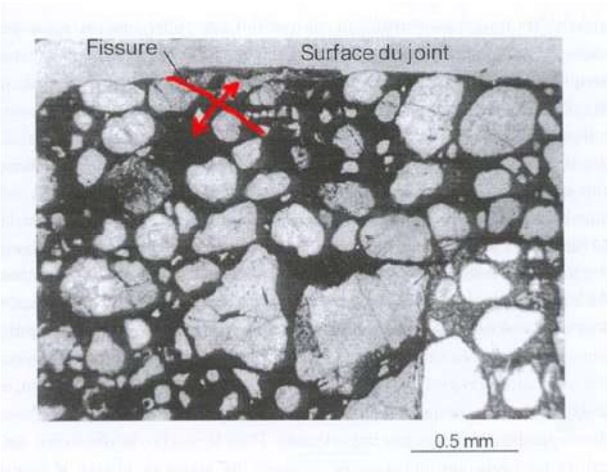

Figure 6.5 Tensile fracture produced during shearing (Armand 2000).

6.3 PEAK SHEAR STRENGTH CRITERION

In deriving a general expression for peak shear strength, a primary consideration was based on the observation that the general mechanical behavior of rock joints is similar to that of mortar replicas. Thus, equation 6.2 was judged to be a good starting point. A second consideration was the importance of using the tensile strength of the rock rather than compressive strength (see discussion in section 6.2). The first step was to directly substitute tensile strength for compressive strength in equation 6.2:

$$\tau_p = \sigma_n \cdot \tan\left(\phi_r^{'}\right) \cdot \left[1 + e^{\frac{-\theta_{\max}^*}{A_0 \cdot C} \cdot \frac{\sigma_n}{\sigma_t}}\right] \qquad 6.4$$

The fit with experimental data obtained with the resulting equation was judged insufficient; more specifically, the equation consistently underestimated peak shear strength. In the next step, a parameter P was introduced in the denominator of the argument to the exponential expression:

$$\tau_p = \sigma_n \cdot \tan\left(\phi_r^{'}\right) \cdot \left[1 + e^{\frac{-\theta_{\max}^*}{P \cdot A_0 \cdot C} \cdot \frac{\sigma_n}{\sigma_t}}\right] \qquad 6.5$$

Multiple least-squares regression using the data obtained for all 39 rock-joint samples was used to estimate the parameter P, and a value of 9.0 was obtained. Interestingly, in trying to determine the appropriateness of the new expression for joints in mortar replicas, it was observed that the ratio of σ_c/σ_t for the mortars used in the replicas is equal to 9.0. Therefore, the argument in the exponential term in equation 6.5 reduces to the expression in equation 6.2, and the equations are exactly the same. Note that this is not the case for replicas made in concrete with different material properties.

Thus, for induced joints in the rock types and mortar replicas used here, the following expression for peak shear strength is proposed:

$$\tau_p = \sigma_n \cdot \tan\left(\phi_r^{'}\right) \cdot \left[1 + e^{\frac{-\theta_{\max}^*}{9 \cdot A_0 \cdot C} \cdot \frac{\sigma_n}{\sigma_t}}\right] \qquad 6.6$$

where τ_p is the peak shear strength of the joint; σ_n is the applied average normal stress; σ_t is the tensile strength of the intact material obtained with standard Brazilian test; $\phi_r^{'}$ is the residual friction angle (after a standard displacement of 5 mm); A_0 is the maximum potential contact area for the specified shear direction; $\theta^*_{\max}$ is the maximum apparent dip angle with respect to the shear direction; C is the roughness parameter derived in section 4.2; and 9.0 is the value estimated for the constant P, determined by a least-squares fit for a multiple regression on data from 39 surfaces and six rock types. Equation 6.6 can be written as:

$$\tau_p = \sigma_n \cdot \tan\left(\phi_r'\right) \cdot [1 + g] \qquad 6.7$$

where the term g quantifies the contribution to peak shear strength by parameters related to the surface morphology of the joint; i.e., g is given by:

$$g = e^{\frac{-\theta^*_{\max}}{9 \cdot A_0 \cdot C} \cdot \frac{\sigma_n}{\sigma_t}} \qquad 6.8$$

The predictions of peak shear strength made with equation 6.6 (Table 6.1) match well with the experimental results obtained in laboratory tests (Figure 6.6). However, since the objective of this study is to develop a simple method for estimating joint shear strength, equation 6.6 is not entirely satisfactory because it requires an estimate of the residual friction angle (ϕ_r') for each sample. However, analysis of the laboratory results lead to the hypothesis that ϕ_r' is a function of the basic friction angle of the material, and the surface roughness of the specific joint. In a following section, an empirical relationship is proposed to estimate ϕ_r' (Equation 6.15).

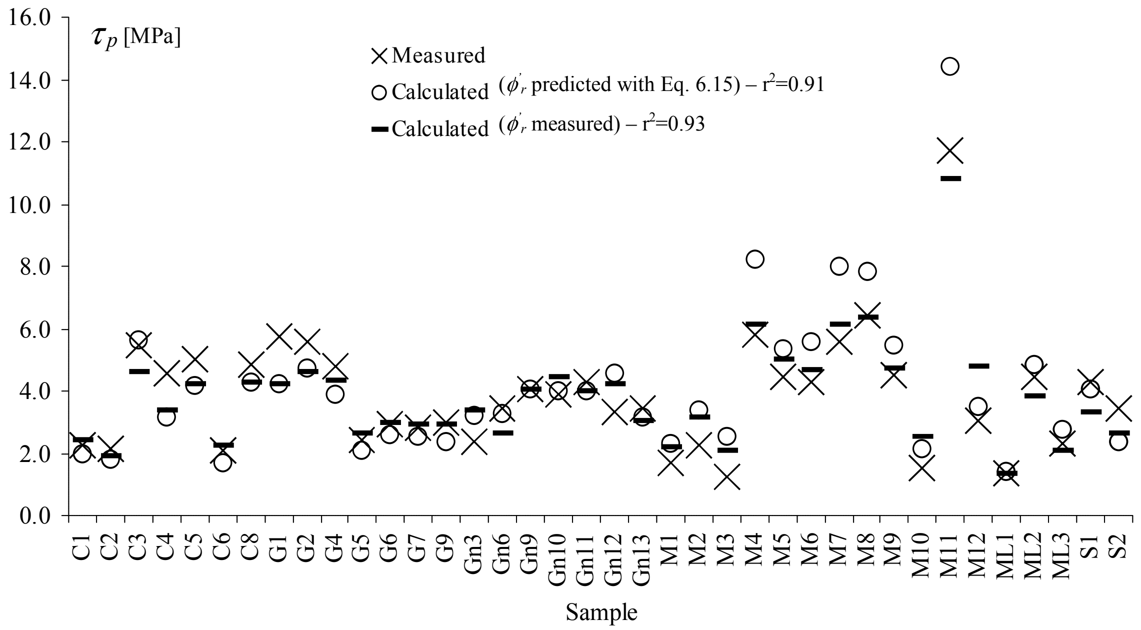

Figure 6.6 Peak shear strength predicted (Equation 6.6) and measured during the laboratory experiments.

Sample name	σ_c [MPa]	σ_t [MPa]	σ_n [MPa]	l_x [mm]	l_y [mm]	α [deg]	A_0 [-]	C [-]	$\theta^*_{\max}$ [deg]	$\phi_{r\ measured}$ [deg]	$\phi_{r\ calculated}$ [deg]	$\tau_{p\ measured}$ [MPa]	$\tau_{p\ calculated}$ [MPa]
C1	25	2.4	1.07	140	140	-	0.491	7.03	80	60	55	2.2	2.0
C2	25	2.4	1.07	140	140	-	0.462	5.64	80	56	54	2.1	1.8
C3	25	2.4	3.72	140	140	-	0.507	6.18	88	51	56	5.5	5.7
C4	25	2.4	2.45	140	140	-	0.508	4.74	65	53	51	4.6	3.1
C5	25	2.4	3.11	140	140	-	0.495	5.26	74	53	53	5.0	4.2
C6	25	2.4	1.02	140	140	-	0.546	5.19	68	59	52	2.1	1.7
C8	25	2.4	3.11	140	140	-	0.555	5.71	74	53	53	4.9	4.3
G1	173	8.8	2.30	140	140	-	0.522	5.75	72	51	51	5.7	4.2
G2	173	8.8	2.30	140	140	-	0.553	6.63	84	53	54	5.6	4.7
G4	173	8.8	2.19	140	140	-	0.484	6.12	65	52	49	4.8	3.9
G5	173	8.8	1.12	140	140	-	0.460	5.33	57	54	47	2.4	2.1
G6	173	8.8	1.12	140	140	-	0.477	7.39	84	57	53	2.9	2.6
G7	173	8.8	1.12	140	140	-	0.470	7.15	81	57	53	2.8	2.5
G9	173	8.8	1.12	140	140	-	0.508	5.85	75	57	51	3.0	2.4
Gn3	184	9.5	2.65	140	140	90	0.496	8.47	65	38	37	2.4	3.2
Gn6	160	3.5	1.90	140	120	0	0.462	8.52	69	46	52	3.4	3.3
Gn9	184	9.5	3.52	140	140	90	0.488	8.12	63	37	37	4.0	4.0
Gn10	184	9.5	3.57	140	140	90	0.500	8.18	70	40	37	3.9	4.0
Gn11	184	9.5	3.52	140	140	90	0.432	10.28	74	37	37	4.3	4.0
Gn12	184	9.5	4.08	130	130	90	0.413	8.87	55	35	37	3.3	4.6
Gn13	184	9.5	2.60	140	140	90	0.503	9.17	74	36	37	3.5	3.2
M1	87	9.2	0.87	140	140	-	0.513	9.64	76	54	55	1.7	2.3
M2	87	9.2	1.73	140	140	-	0.399	9.36	51	46	48	2.3	3.4
M3	87	9.2	0.87	140	140	-	0.509	14.93	83	52	57	1.2	2.5
M4	87	9.2	3.78	140	140	-	0.501	10.51	77	47	55	5.8	8.2
M5	87	9.2	2.60	140	140	-	0.533	8.92	59	49	51	4.4	5.4
M6	87	9.2	2.60	140	140	-	0.450	10.18	68	48	53	4.3	5.6
M7	87	9.2	3.78	140	140	-	0.529	10.75	69	46	53	5.6	8.0
M8	87	9.2	3.83	140	140	-	0.459	10.52	72	48	54	6.4	7.9
M9	87	9.2	2.60	140	140	-	0.494	10.36	59	47	51	4.5	5.4
M10	87	9.2	0.87	140	140	-	0.515	10.79	67	57	53	1.5	2.2
M11	87	9.2	8.57	70	140	-	0.533	9.89	68	45	53	11.7	14.4
M12	87	9.2	1.79	140	140	-	0.429	7.28	55	58	49	3.0	3.5
ML1	10	0.7	1.02	140	140	-	0.573	7.25	66	51	52	1.4	1.4
ML2	10	0.7	4.13	140	140	-	0.481	5.66	55	43	50	4.5	4.9
ML3	10	0.7	2.09	140	140	-	0.523	7.81	66	45	53	2.3	2.7
S1	166	6.0	1.94	140	140	0	0.497	4.99	83	53	58	4.3	4.0
S2	166	6.0	0.97	140	140	0	0.497	4.58	86	61	59	3.4	2.4

Table 6.1 Comparison among the peak shear strengths obtained experimentally in laboratory tests (see section 5.3) and the values calculated with the equation 6.6.

6.4 HORIZONTAL PEAK SHEAR DISPLACEMENT

Horizontal peak shear displacements, measured in the experiments on joints of 140 mm length, were found scattered in the range between 0.27 mm and 0.65 mm. Observing the experiment plots of shear strength versus horizontal displacement it was remarked that often the beginning of the test was characterized by the fact that the joint was not totally mated. Therefore a small displacement occurred before the joint was able to provide all its strength. Thus the horizontal peak shear displacement can be expressed as the sum of two contributions:

$$u_p = a + \Delta u_p \qquad 6.9$$

where a is the horizontal displacement necessary to mate the joint (when the joint is assumed "fresh", it principally depends on the experimental set up); and Δu_p is the horizontal deformation of the joint before the peak. Subtracting this mating displacement from the total peak displacement, it was experimentally observed that, on the samples tested, Δu_p is almost constant. Therefore, if it is assumed the joint that is completely mated, it is possible to write, for the first cycle, that:

$$u_p = \Delta u_p = 0.27 \sim 0.65 mm \qquad 6.10$$

6.5 JOINT SHEAR STIFFNESS

Observing the experimental curves, as the joint is mated, it is possible to affirm that the joint deforms linearly up to the peak shear stress. (see section 5.3.5). Therefore, a linear relation is used to describe the shear stiffness, k_s (defined in section 5.3.5):

$$k_s = \frac{1}{\Delta u_p} \cdot \frac{\tau_p}{\sigma_n} \qquad 6.11$$

where τ_p is the peak shear strength of the joint; σ_n is the applied average normal stress; and Δu_p is the horizontal deformation of the mated joint before the peak.

6.6 RESIDUAL SHEAR STRENGTH CRITERION

A negative slope of the stress-strain curve characterizes the post-peak behavior. Consequently the shear strength of a joint falls to a constant value that corresponds to the ultimate/residual friction resistance of the joint. The presence and importance of residual strength region depends on the rock type. It is possible to identify two different behaviors: ductile and brittle that is evidenced by the difference between peak and residual strength values. Anyway, the process of failure has to be regarded as a continuous one, which begins at peak and occurs progressively throughout the entire post peak and residual region in which the rock steadily deteriorates. The residual strength is reached after a horizontal displacement that is possible to synthesize as:

$$u_r = a + \Delta u_p + \Delta u_r \qquad 6.12$$

where a is the horizontal mating displacement, Δu_p is the horizontal deformation of the joint before the peak, and Δu_r is the horizontal displacement that the joint needs to fall from the peak to the residual state. Experimentally it was noticed that, for samples with same dimensions (140 mm length), Δu_r could be assumed as a value between 1.5 and 5 mm:

$$\Delta u_r = 1.50 \sim 5mm \qquad 6.13$$

As the joint has reached its residual state, the ratio between shear and applied normal loads is constant, thus it is reasonable to write that:

$$\frac{\tau_r}{\sigma_n} = \tan\left(\phi_r^{'}\right) \qquad 6.14$$

where τ_r is the residual shear strength of the joint; σ_n is the applied average normal stress; and ϕ'_r is the residual friction angle (after standard displacement of 5 mm).

It is possible to measure ϕ'_r directly in laboratory executing one direct shear test on whatever joint of the same rock studied. However, shearing different joints (with the shear plane parallel to the average joint plane) of the same rock type, it was proved that the ratio between residual shear strength and applied normal load is roughly dependent from the surface morphology. Thus, it is possible to argue that the residual friction angle is function just of the rock basic friction angle and of the morphological parameters of the joint.

The laboratory tests show that in general, the lower bound for the residual friction angle is given by the value of the basic friction angle of the material itself. In fact, the effect of surface roughness is to increase the residual friction angle. Thus, using the basic friction angle for the material is a conservative estimate of the lower bound. The spatial distribution and magnitude of the roughness directly influence the residual friction angle. The internal geometry of the rock itself, e.g., schistosity, also has an important effect. This is important because, for example, shearing gneiss along a schistosity plane results in a residual friction angle equal to the basic friction angle. Thus, the starting point for deriving an empirical expression for the residual frictional angle was the basic friction angle. An important consideration was incorporating the three parameters proposed in section 4.2 that describe the surface morphology: A_0, C, and $\theta^*_{\max}$. The functional form for incorporating these parameters was determined by experimenting with different expressions and comparing the results to experimental data. There is a lot of scatter in the experimental data, so the following empirical relationship is at best a rough approximation:

$$\phi_r' = \phi_b + \left(C \cdot A_0^{1.5} \cdot \theta_{\max}^* \cdot \left(1 - A_0^{\frac{1}{C}} \right) \right)^{\cos\alpha} \qquad 6.15$$

where ϕ_b is the basic friction angle; A_0 is the maximum potential contact area for the specified shear direction; $\theta^*_{\max}$ is the maximum apparent dip angle of the surface with respect to the shear direction; C is the roughness parameter (Section 4.2); and α is the angle between the schistosity plane and the normal to the joint. If the rock does not exhibit schistosity, α is assumed to be equal to zero (α=0).

Equation 6.15 can be written more simply as:

$$\phi_r' = \phi_b + \beta \qquad 6.16$$

where β represents the contribution of the roughness to the residual friction angle that, according to the shear tests results, takes on values in the range between 15 and 24 degrees:

$$\beta = \left(C \cdot A_0^{1.5} \cdot \theta_{\max}^* \cdot \left(1 - A_0^{\frac{1}{C}} \right) \right)^{\cos\alpha} = 15^o \sim 24^o \qquad 6.17$$

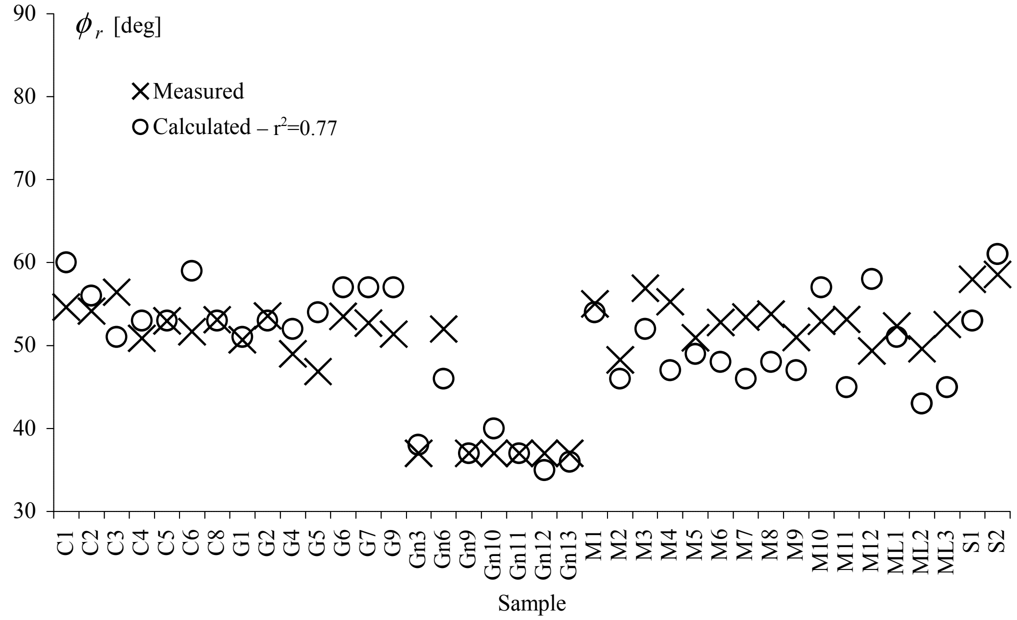

Figure 6.7 Residual friction angle (ϕ_r') predicted (Equation 6.15) and measured during the laboratory experiments.

6.7 CONSTITUTIVE MODEL FOR MATED ROCK JOINTS

The considerations made in the last paragraphs lead to the formulation of a model able to summarize the shear strength provided by the joint, under constant normal load conditions, at each state of displacement:

$$\begin{cases} \dfrac{\tau}{\sigma_n} = 0 & 0 \le u \le a \\ \dfrac{\tau}{\sigma_n} = k_s \cdot (u-a) = \dfrac{1}{\Delta u_p} \cdot \dfrac{\tau_p}{\sigma_n} \cdot (u-a) & a \le u \le u_p \\ \dfrac{\tau}{\sigma_n} = \dfrac{\tau_r}{\sigma_n} + \dfrac{\tau_p - \tau_r}{\sigma_n} \cdot \dfrac{u_p}{u} & u > u_p \end{cases} \qquad 6.18$$

This expression approaches the residual strength for values of displacement larger than u_r:

$$\frac{\tau}{\sigma_n} \approx \frac{\tau_r}{\sigma_n} \qquad u > u_r \qquad 6.19$$

The agreement between the constitutive model and the experimental results is good (Figure 6.8).

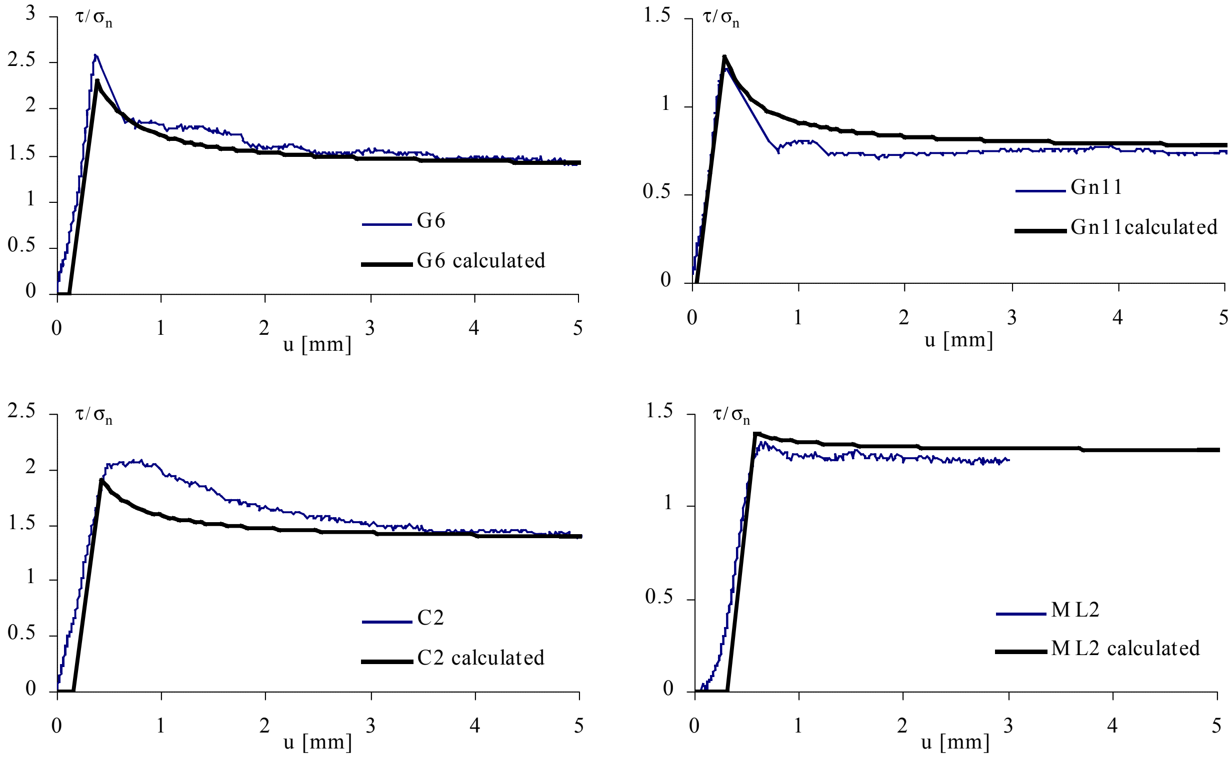

Figure 6.8 Comparison between laboratory experiments results and proposed constitutive model (Equation 6.18).

Sample name	i [deg]	u_p [mm]	a [mm]	$k_{s\ \mathrm{measured\ 50\%}}$ [mm^{-1}]	ϕ_b [deg]	$\phi_{r\ measured}$ [deg]	$\phi_{r\ calculated}$ [deg]	$JRC_{back\ analysis}$ [deg]	$JRC_{calculated}$ [deg]
C1	12.0	0.50	0.23	8.2	36	60	55	20.9	18.8
C2	15.5	0.52	0.25	5.2	36	56	54	20.2	17.2
C3	8.4	0.53	0.26	4.0	36	51	56	23.8	25.0
C4	8.9	0.31	0.04	9.4	36	53	51	25.6	16.0
C5	8.5	0.24	0.00	7.1	36	53	53	24.5	19.2
C6	9.5	0.37	0.10	7.4	36	59	52	20.5	16.6
C8	7.3	0.74	0.47	3.5	36	53	53	23.6	19.9
G1	11.5	0.38	0.11	9.6	34	51	51	18.2	14.6
G2	15.9	0.65	0.38	5.7	34	53	54	17.9	16.0
G4	10.6	0.45	0.18	7.3	34	52	49	16.3	14.0
G5	13.4	0.62	0.35	6.4	34	54	47	14.3	12.5
G6	16.0	0.38	0.11	9.2	34	57	53	15.9	14.9
G7	14.2	0.23	0.00	15.1	34	57	53	15.6	14.6
G9	12.6	0.56	0.29	13.8	34	57	51	16.1	14.1
Gn3	15.5	0.31	0.04	3.2	36	38	37	6.7	8.0
Gn6	13.5	0.35	0.08	7.4	36	46	52	8.5	12.4
Gn9	7.9	0.31	0.04	5.7	36	37	37	1.8	7.5
Gn10	12.0	0.35	0.08	3.4	36	40	37	9.1	7.2
Gn11	8.1	0.30	0.03	4.9	36	37	37	3.1	7.3
Gn12	5.4	0.48	0.21	2.2	36	35	37	12.5	7.4
Gn13	6.8	0.20	0.00	9.6	36	36	37	7.4	7.9
M1	11.1	0.28	0.01	7.2	37	54	55	13.0	16.1
M2	4.8	0.27	0.00	6.0	37	46	48	11.7	15.3
M3	7.5	0.50	0.23	4.2	37	52	57	16.6	17.0
M4	7.4	0.88	0.61	3.9	37	47	55	13.5	20.8
M5	9.2	0.29	0.02	7.8	37	49	51	9.2	17.8
M6	7.6	0.44	0.17	7.6	37	48	53	9.0	18.3
M7	5.2	0.44	0.17	3.9	37	46	53	14.8	20.4
M8	5.7	0.39	0.12	7.4	37	48	54	15.0	19.9
M9	5.8	0.42	0.15	4.4	37	47	51	14.3	18.0
M10	10.7	0.27	0.00	5.7	37	57	53	13.7	15.6
M11	3.6	0.45	0.18	7.6	37	45	53	16.4	22.2
M12	7.9	0.55	0.28	6.6	37	58	49	15.2	15.4
ML1	7.6	0.65	0.38	4.1	37	51	52	16.3	17.5
ML2	1.7	0.67	0.40	2.1	37	43	50	27.2	32.8
ML3	0.4	0.67	0.40	1.9	37	45	53	16.3	23.0
S1	15.1	0.40	0.13	9.9	39	53	58	15.0	13.1
S2	25.2	0.50	0.23	12.3	39	61	59	17.0	12.9

Table 6.2 Comparison among results obtained experimentally in laboratory tests (see section 5.3) and the values calculated with the proposed equations (Equation 6.15 for ϕ_r and Equation 6.26 for JRC).

6.8 OBJECTIVE QUANTIFICATION OF JRC

One of the most interesting challenges in studying shear strength of rock joint is to quantify in an objective manner the JRC coefficient that Barton proposed in order to take into account the resistance contribution provided by the specific morphology of the studied joint. Barton's criterion for peak shear strength is expressed as:

$$\tau_p = \sigma_n \cdot \tan\left(\phi_b + JRC \cdot Log_{10}\left(\frac{JCS}{\sigma_n}\right)\right) \qquad 6.20$$

Considering that the peak shear strength value is unique for the same experiment, it is possible to equal equation 6.7 and equation 6.20 obtaining:

$$\tan\left(\phi_b + JRC \cdot Log_{10}\left(\frac{JCS}{\sigma_n}\right)\right) = \tan\left(\phi_r^{'}\right) \cdot [1+g] \qquad 6.21$$

It follows that:

$$\phi_b + JRC \cdot Log_{10}\left(\frac{JCS}{\sigma_n}\right) = \arctan\left(\tan\left(\phi_r^{'}\right) \cdot [1+g]\right) \qquad 6.22$$

Therefore JRC can be expressed as:

$$JRC = \frac{\arctan\left(\tan\left(\phi_r^{'}\right) \cdot [1+g]\right) - \phi_b}{Log_{10}\left(\frac{JCS}{\sigma_n}\right)} \qquad 6.23$$

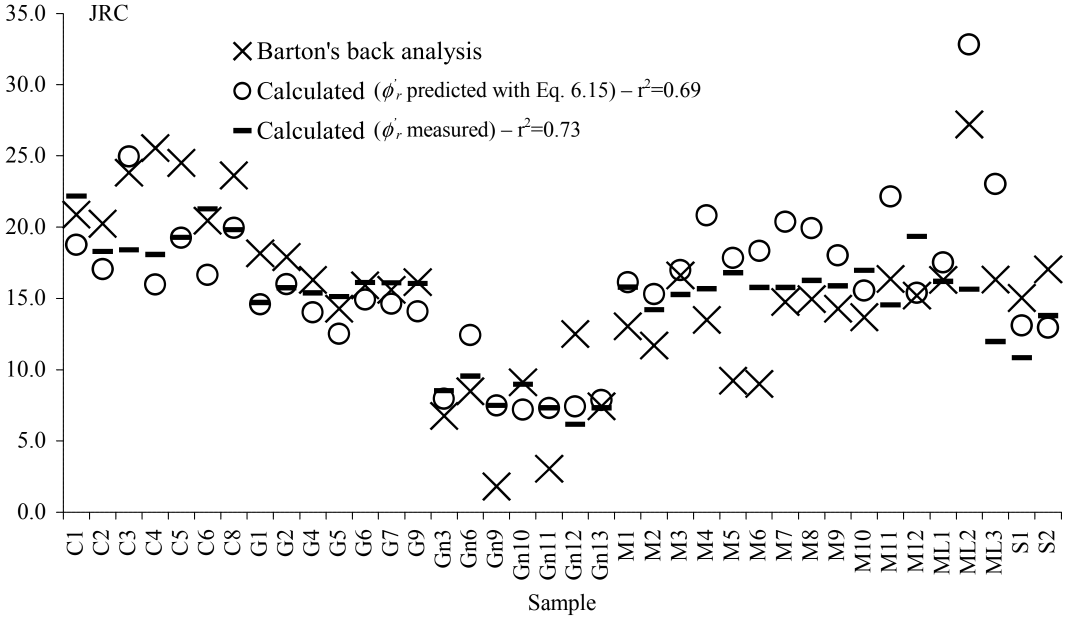

Figure 6.9 JRC predicted (Equation 6.26) and measured during the laboratory experiments.

As the considered joints are “fresh”, it results that:

$$JCS = \sigma_c \tag{6.24}$$

Hence:

$$JRC = \frac{\arctan\left(\tan\left(\phi_r^{'}\right)\cdot[1+g]\right)-\phi_b}{Log_{10}\left(\dfrac{\sigma_c}{\sigma_n}\right)} \tag{6.25}$$

Substituting g with Equation 6.8, and $\phi_r^{'}$ with Equation 6.15, it is obtained that:

$$JRC = \frac{\arctan\left(\tan\left(\phi_b + \left(C\cdot A_0^{1.5}\cdot\theta_{\max}^{*}\cdot\left(1-A_0^{\frac{1}{C}}\right)\right)^{\cos\alpha}\right)\cdot\left[1+e^{\frac{-\theta_{\max}^{*}}{9\cdot A_0\cdot C}\cdot\frac{\sigma_n}{\sigma_t}}\right]\right)-\phi_b}{Log_{10}\left(\dfrac{\sigma_c}{\sigma_n}\right)} \tag{6.26}$$

The comparison between the JRC values calculated with back analysis of the experimental tests and those obtained with the equation 6.26 is good (Figure 6.9). The advantage of this approach to quantify JRC is that the three-dimensionality of the surface is considered and the analysis is hence not only reduced to a single profile.

6.9 CONCLUSIONS

An empiric constitutive law relating stress and displacements was proposed to model joints sheared under constant normal load conditions.

From experiment results it was observed that at the beginning of the test the joint is often not perfectly mated, therefore the initial relative position of the two walls of joint is considered with the parameter *a* that is the horizontal displacement necessary to mate the joint (when the joint is assumed “fresh”, it principally depends on the experimental set up). The assumption of linear pre-peak behavior (elastic deformation) is based on the observations of the laboratory tests. The value of the peak shear strength is expressed in function of the material tensile strength, the load conditions, the basic friction angle and the morphological description of the surface (see section 4.2).

The residual shear strength of the joint is evaluated as function of surface morphology and basic friction angle. Residual strength results similar for each type of rock and it is reached rapidly after peak. Experimentally it was remarked that 5 mm after the peak, the joint strength has already reached its residual state. The residual friction angle for a real joint reflects pure frictional behavior, as well as the basic friction angle expresses the resistance of clean planar surfaces. Nevertheless, the real joint can mate and contains gauge material originating from the failure of surface asperities. It follows that, for clean un-weathered joints, residual strength is higher than basic friction resistance.

The proposed constitutive model results able to describe experimental shear tests realized both on replicas and fresh rock joints. Moreover, the parameters required in the model can be easily obtained through standard laboratory tests.

The peak shear criterion is also used to estimate the JRC value. The expression obtained to evaluate the joint roughness coefficient results generally able to predict the JRC calculated by back analysis of shear tests.

In the current research no attention was spent in order to investigate the influence of the scale on the shearing. The results have validity only in the range of the samples tested in laboratory (σ_n/σ_c=0.01÷0.4 and σ_c/σ_t=5 ÷46). Further studies are needed to explore the applicability of the proposed model to in situ conditions.

7. Conclusions

"For centuries scientists have been working toward that goal. I have been lucky and persistent enough to make some contributions to this magnificent quest"
Sheldon Lee Glashow

Discontinuities have an important influence on the deformational behavior of rock systems. Joints, bedding planes, faults, and other recurrent planar fractures radically alter the behavior of rock. As joints are generally not randomly distributed, their effect is to create pronounced anisotropy in the properties of the rock mass, in particular, anisotropy of strength.

Determining a general criterion to estimate the shear strength of rough rock joints is a problem that has been investigated for many years. Numerous shear models have been proposed over the last several decades to relate shear strength to measurable joint parameters. While these models have improved our understanding of rock-joint behavior, their limitations have to be recognized.

One of the most important challenges is introducing three-dimensional joint morphology into shear-strength expressions.

To accomplish this requires not only the ability to measure and characterize surface roughness, but also the ability to express roughness as a number (e.g., JRC) or a mathematical expression. Technological advancements are making it increasingly possible to measure and characterize surfaces in three dimensions. Therefore, the challenge today is finding ways to quantify three-dimensional surface characteristics and incorporating new parameters into expressions of shear strength. To be useful, these expressions must provide accurate estimates of peak-shear strength, based on parameters easily measured under both laboratory and in-situ conditions. Among all the models proposed in the literature, Barton's criterion is the only one that is currently used in practice. The approach is based on choosing a value for the morphological parameter: the joint roughness coefficient (JRC). Several methods for estimating the JRC value have been proposed in the literature. However, none of them is able to consistently provide accurate values, in large part because of fracture anisotropy, which makes it difficult to capture three-dimensional geometry in measuring a single profile. This problem points to the importance of three-dimensional characterization of surface roughness.

Since the geometry of roughness influences the size and distribution of contact areas during shearing, which, in turn, determines the stress distribution across the surface and the damage that will occur, it has to be considered the most important geometrical boundary condition for explaining the shearing process.

One of the primary objectives of this work is to better understand the frictional behavior of joints under shear loads, including the creation of damage zones.

It is argued that in order to locate and estimate the contact area during shearing, it is only necessary to consider zones on the surface facing the shear direction, and steeper than a threshold inclination. It is obvious that damage increases with increasing stress and displacement. Moreover, the size, shape, and spatial distribution of damaged areas depend on shear direction, the degree of stress, and horizontal displacement.

The experimental results described here indicate that no damage appears prior to peak stress; damage occurs principally during the softening and residual phases of shearing. In addition, it appears that areas where shearing of asperities can be observed correspond to areas where there were contacting asperities at peak shear stress. A possible interpretation is that it is the breaking of asperities at peak-shear stress that initiates sliding. The common characteristic among all damaged areas is that they are without exception located in the steepest zones facing the shear direction. The shape of the damage zones depends on the local geometry of the fracture surface, including the size and shape of the asperities, as well as on the mechanical parameters of the rock. An important conclusion from the experimental work is that the tensile strength of the rock is more important than the compressive strength in predicting peak shear strength. An empirical relationship between maximum potential contact during shearing and the minimum apparent dip inclination (θ^*) is proposed (Section 4.2). The close agreement between this empirical description of the potential contact area, as a function of the minimum apparent dip angle involved in shearing, and experimental results suggests the ability to predict the real contact areas involved in shearing by choosing the proper threshold value for θ^*. The obvious question is how such relationships would be applied in the field, since they require knowledge of the maximum potential contact area for the specified shear direction (A_0), the maximum apparent dip angle with respect to the shear direction (θ^*_{max}), and the roughness parameter (C) defined in Chapter 5.2.

Based on the samples studied for the research presented here, the values of these parameters tend to be characteristic for specific rock types, indicating that it might be possible to determine ranges for each rock type based on laboratory measurements of representative samples. Although many more measurements would have to be made to have the necessary confidence to use these data in the field, the results suggest the potential to be able to adopt these parameters to capture the relevant geometrical features of fractures in specific rock types.

In addition, a critical further step is to find an expression to quantify contact area across the joint that describes how contact varies during shearing and with changes in applied normal load.

The research described here suggests that those areas of the surface facing the shear direction with steepest inclination govern the mechanical behavior of joints up to and including peak shear stress. Furthermore, it appears possible to define a threshold inclination angle that is key for establishing the relationship between the applied normal stress and peak shear stress.

To study the frictional response of rock joints and its dependence on surface parameters, more than fifty constant-normal-load direct-shear tests were performed on both replicas of tensile joints, and induced tensile fractures in seven rock types (Chapter 1). The experimental results demonstrated that shear strength depends on the direction of shearing, which reflects anisotropy of surface roughness. The analysis of the experimental data leads to the conclusion that the mechanical results obtained with the replicas are only qualitatively similar to the test results obtained for rock-joint samples. The mechanical behavior of the mortar replicas was found to be much more ductile than the mechanical response of the rock samples. Furthermore, the “matching ratio” of the replicas was lower than that of the tensile joints in rock, which were extremely well mated. Therefore, it appears that the results obtained with mortar replicas are only able to quantitatively simulate the mechanical behavior of joints in ductile rocks, which exhibit no marked peak in shear strength. In contrast, joints in brittle rocks exhibit marked peaks in strength when measured during laboratory shear tests, especially for fresh tensile fractures such as those tested and reported on here.

Analysis of vertical measurements made during laboratory test shows the presence of dilatancy and rotation of the sample. These observations, analyzed in conjunction with images of sheared joint surfaces, provide strong evidence of the importance of even small rotations in determining the spatial distribution of contact areas during shearing, and, therefore, on the location of damage zones.

Based on the empirical description of potential contact area and observations of sheared surfaces, a new constitutive law relating stress and displacements, was proposed to model joints sheared under constant normal load (CNL) conditions in laboratory tests (see section 6.7). It was shown that this constitutive model is able to describe experimental shear tests for both replicas and fresh rock joints. Moreover, the parameters required to apply the model can be easily obtained through standard laboratory tests. From the literature, it appears that CNL and constant normal stiffness (CNS) tests have the same behavior up to peak shear stress; therefore, this approach may be valid for both boundary conditions up to peak stress. The proposed model was also used to calculate values of the joint roughness coefficient (JRC) (see section 6.8). The expression obtained to evaluate the joint roughness coefficient gave results that were in close agreement with JRC values calculated by back analysis of shear tests. Estimating JRC using parameters from the empirical description of potential contact area has the advantage of giving a value that incorporates characteristics of the entire surface, rather than those of only a single arbitrary profile.

The results presented here suggest that surface geometry can be captured by measurable surface parameters that, in turn, can be used to predict peak shear strength. As discussed in the following section, to apply these results in the field will require many more laboratory tests to determine how much variability there is in the parameters for each rock type, and how the parameters depend on scale. It is also necessary to determine how the mechanical behavior of natural joints is different than that of the induced tensile fractures studied here. This means understanding how all of the various processes that natural fractures are exposed to over time change fracture surfaces and mechanical properties.

8. Perspectives

"Ciò che fa progredire la scienza é l'immaginazione e non sono i numeri."
Anonymous

The work presented here suggests several avenues for both laboratory and field research. Rapidly changing technology is opening the door to not only high-resolution surface characterization in the laboratory, but also to new approaches that may allow joints to be characterized in situ. The approach described herein for measurement and analysis of surface data would benefit from refinements that would make it easier to use by engineers in the field; e.g., developing a user friendly software to analyze the measurement data and to calculate directly the surface parameters for the imposed shear direction.

The ultimate objective is to be able to use the results presented here to help practicing engineers to estimate peak shear strength of rock joints in situ. Being able to characterize joints in the field, as described above, is only the first step. The easiest case is where fracture surfaces are exposed (e.g., dam foundations) so that can be analyzed directly. Unfortunately, this is rarely the case. More often, only fracture traces are available for analysis in the field. In this case, it is necessary to be able to use trace information to generate 3D surface roughness data. As discussed in detail in previous sections, this is extremely difficult because rock surfaces tend to be highly anisotropic. It is critical, therefore, to be able to use fracture trace information in conjunction with geological data (e.g., rock type, tectonic history...) to generate estimates of surface morphology with sufficient accuracy to predict shear behavior.

The results presented here suggest the potential to use laboratory techniques to capture the relevant geometrical features of fracture surfaces for specific rock types. More importantly, the results indicate the possibility of defining functional relationships between measurable surface parameters and potential contact area and the minimum apparent dip angle, which, in turn, can be used to predict shear behavior. To get to the point where these kinds of functional relationships can be used with confidence in field applications will require many more laboratory tests to determine how much variability there is in the parameters for each rock type, and how the parameters depend on scale.

In determining how surface parameters vary with rock type, it is important to take into consideration all of the various processes that natural fractures are exposed to over geologic time. The test specimens used here were induced tensile fractures. Thus, an important consideration is how the behavior of these "fresh" joints is different from in situ fractures. The results of experiments in which surface parameters were measured before and after shear tests give some indication of how these parameters change during shearing, and, thus, how they would likely be different for in situ fractures. In general, as would be expected, damage induced by shearing results in a more uniform surface roughness. Additional work is required to analyze the surface parameters of naturally occurring fractures, and to better understand how these parameters are affected by natural processes such as fluid flow and associated chemical alteration, as well as tectonic processes.

Other important issues in using laboratory data to predict field conditions include scale effects, and any differences between naturally occurring fractures and those studied in the laboratory. Although the results presented here point to the possibility of being able to define parameters that capture the relevant geometrical features of fractures, and also to identify ranges for these parameters that are characteristic for specific rock types, it is essential to understand if these parameters are subject to scale effects. A possible laboratory approach is to compare results obtained with relatively large samples and subsets of the samples. However, a particular problem with this approach for studying shear behavior is that the mechanics tends to be governed by extreme values; e.g. the areas of the surface with the steepest inclination, or the strongest asperities. Thus, in studying scale effects it is critical to work with samples of sufficient size to be representative of the full range of geometrical surface parameters that play a role in shear behavior.

In summary, it appears possible to define parameters that describe three-dimensional surface roughness, and to use these parameters to develop improved models for prediction of peak shear strength. To be able to apply these results to field applications will require additional research to determine the variability of surface parameters for specific rock types and naturally occurring joints, and to better understand how to use available geological data and two-dimensional fracture traces to estimate three-dimensional surface parameters.

Bibliography

Amadei, B., Wibowo, J., Sture, S. & Price, R. H. Applicability of existing models to predict the behaviour of replicas of natural fractures of welted tuff under different boundary condition.

Archambault, G., Gentier, S., Riss, J., Flamand, R. & Sirieix, C. 1995. A re-evaluation of irregular joint shear behaviour on the basis of 3D modeling of their morphology : joint mechanical shear behaviour and modeling *Mechanics of Jointed and Faulted Rock :* 163-168.

Armand, G. 2000. Contribution à la caractérisation en laboratoire et à la modélisation constitutive du comportement mécanique des joints rocheux, *Universite Joseph Fourier, Grenoble*: 189-192.

Barton, N. & Choubey, V. 1977. The shear strength of rock joints in theory and practice *Rock Mechanics,* 10: 1-54.

Bell, J. 1998. Simple scanners reveal shape, size and texture *Opto & laser europe,* April 1998: 29-32.

Beraldin, J. A., Blais, F., Cournoyer, L., Rioux, M., Bernier, F. & Harrison, N. 1998. Portable digital 3D imaging system for remote sites *IEEE-ISCAS98.*

Bergmann, D., Galanulis, K. & Winter, D. 1997. Advanced 3D fringe projection system.

Boulon, M. 1995. A 3D direct shear device for testing the mechanical behaviour and the hydraulic conductivity of rock joints *Mechanics of jointed and faulted rock :* 407-413.

Chryssanthakis, P. & Barton, N. 1990. Joint roughness (JRCn) characterisation of a rock joint and joint replica at 1 m scale *Rock joints :* 27-33.

Den Outer, A., Kaashoek, J. F. & Hack, H. R. G. K. 1995. Difficulties with using continuous fractal theory for discontinuity surfaces *International Journal of Rock Mechanics and Mining Sciences and Geomechanics Abstracts,* 32: 3-9.

Dight, P. M. & Chiu, H. K. 1981. Prediction of shear behaviour of joints using profiles *International Journal of Rock Mechanics and Mining Sciences and Geomechanics Abstracts,* 18: 369-386.

Dong, J. J. & Pan, Y. W. 1996. A hierarchical model of rough rock joints based on micromechanics *International Journal of Rock Mechanics and Mining Sciences and Geomechanics Abstracts,* 33: 111-123.

Fairhurst, C. 1964. On the validity of the Brazilian test for brittle materials *International Journal of Rock Mechanics and Mining Sciences and Geomechanics Abstracts,* 1**:** 535-546.

Ferguson, E. S. (1997) In *Engineering and the mind's eye*MIT Press, Cambridge, Massachusset, pp. 1-11.

Ferrero, M., Iabichino, G., Pancotti, G. & Giani, G. P. 1999. Interpretazione con modelli matematici di misure di rugosità di discontinuità naturali in roccia *XX convegno nazionale di geotecnica :* 101-106.

Fishman, Y. A. 1990. Failure mechanism and shear strength of joint wall asperities *Rock joints :* 627-631.

Flamand, R. (1998).

Gentier, S., Riss, J., Archambault, G., Flamand, R. & Hopkins, D. L. 2000. Influence of fracture geometry on sheared behavior *International Journal of Rock Mechanics and Mining Sciences and Geomechanics Abstracts,* 37**:** 161-174.

Gentier, S. S. & Hopkins, D. L. 1997. Mapping fracture aperture as a function of normal stress using a combination of casting, image analysis and modeling techniques *International Journal of Rock Mechanics and Mining Sciences and Geomechanics Abstracts,* 34**:** 359.

Giani, G. P., Ferrero, A. M., Drusa, M. & Pancotti, G. 1995. Modelli statistici per la caretterizzazione geometrica degli ammassi rocciosi *Ingegneria civile:realtá e prospettive di ricerca*.

Grasselli, G. & Egger, P. 2000a. 3D surface characterization for the prediction of the shear strength of rough joint *Eurock 2000* **:** 281-286.

Grasselli, G. & Egger, P. 2000b. Shear strength equatioin for rock joints, based on 3D surface characterization *GeoEng2000*.

Haberfield, C. M. & Johnston, I. W. 1994. A mechanistically-based model for rough rock joint *International Journal of Rock Mechanics and Mining Sciences and Geomechanics Abstracts,* 31**:** 279-292.

Hopkins, D. L. 2000. The implication of joint deformation in analyzing the properties and behavior of fractured rock masses, undegroung excavations, and faults *International Journal of Rock Mechanics and Mining Sciences and Geomechanics Abstracts,* 37**:** 175-202.

Hsiung, S. M., Ghosh, A., Ahola, M. P. & Chowdhury, A. H. 1993. Assessment of conventional methodologies for joint roughness coefficient determination

International Journal of Rock Mechanics and Mining Sciences and Geomechanics Abstracts, 30**:** 825-829.

Huang, S. L., Oelfke, S. M. & Speck, R. C. 1992. Applicability of fractal characterization and modeling to rock joint profiles *International Journal of Rock Mechanics and Mining Sciences and Geomechanics Abstracts,* 29**:** 89-98.

Huang, T. H. & Doong, Y. S. 1990. Anisotropic shear strength of rock joints *Rock joints :* 211-218.

Huang, X., Haimson, B. C., Qui, X. & Plesha, M. E. 1993. An investigation of the mechanics of rock joints - Part I. Laboratory investigation *International Journal of Rock Mechanics and Mining Sciences and Geomechanics Abstracts,* 30**:** 257-269.

ISO3274 (1996),International Organization for Standardization, Geneva.

ISRM 1978. Suggested methods for the quantitative description of discontinuities in rock masses *International Journal of Rock Mechanics and Mining Sciences and Geomechanics Abstracts,* 15**:** 319-368.

Jaeger, J. C. & Cook, N. G. W. (1971) In *Fundamentals of rock mechanics*(Eds, Chapman and Hall) New York, pp. 77-106.

Jeremy, C. A. 1995. A laser scanning device to measure joint surface roughness *Mechanics of Jointed and Faulted Rock :* 169-174.

Jing, L., Nordlund, E. & Stephansson, O. 1992. An experimental study on the anisotropy and stress-dependency of the strength and deformability of rock joints *International Journal of Rock Mechanics and Mining Sciences and Geomechanics Abstracts,* 29**:** 565-542.

Johnston, I. W. & Lam, T. S. K. 1989. Shear behavior of regular triangular concrete/rock joints - Analysis *Journal of geotechnical engineering,* 115**:** 711-727.

Kimura, T. & Esaki, T. 1995. A new model for the shear strength of rock joints with irregular surfaces *Mechanics of Jointed and Faulted Rock :* 133-138.

Kulatilake, P. H. S. W., Shou, G., Huang, T. H. & Morgan, R. M. 1995. New peak shear strength criteria for anisotropic rock joints *International Journal of Rock Mechanics and Mining Sciences and Geomechanics Abstracts,* 32**:** 673-697.

Kulatilake, P. H. S. W., Um, J. & Pan, G. 1997. Requirements for accurate estimation of fractal parameters for self-affine roughness profiles using the line scaling method *Rock mechanics and rock engineering,* 30**:** 181-206.

Ladanyi, B. & Archambault, G. 1970. Simulation of the shear behaviour of a jointed rock mass *Proceedings of the 11th U.S. Symposium on Rock Mechanics,* 7**:** 105-125.

Lanaro, F. 1999. A random field model for aperture and roughness of rock fractures, *Royal Institute of Technology, Stockholm***:** 33.

Lanaro, F. 2000. A random field model for surface roughness and aperture of rock fractures *International Journal of Rock Mechanics and Mining Sciences and Geomechanics Abstracts,* 37**:** 1195-1210.

Lanaro, F., Jing, L. & Stephansson, O. 1998. 3-D-laser measurements and representation of roughness of rock fractures *Mechanics of jointed and faulted rock :* 185-189.

Lee, D. H. & Juang, C. H. 1991. A new technique for measuring the rock roughness profile of rock joints *Geotechnical testing journal,* 14**:** 320-322.

Lee, Y. H., Carr, J. R., Barr, D. J. & Haas, C. J. 1990. The fractal dimension as a measure of the roughness of rock discontinuity profiles *International Journal of Rock Mechanics and Mining Sciences and Geomechanics Abstracts,* 27**:** 453-464.

Maerz, N. H., Franklin, J. A. & Bennett, C. P. 1990. Joint roughness measurement using shadow profilometry *International Journal of Rock Mechanics and Mining Sciences and Geomechanics Abstracts,* 27**:** 329-343.

Maksimovic, M. 1992. New description for shear strength for rock joint *Rock mechanics and rock engineering,* 25**:** 275-284.

Maksimovic, M. 1996. The shear strength components of a rough rock joint *International Journal of Rock Mechanics and Mining Sciences and Geomechanics Abstracts,* 33**:** 769-783.

Mandelbrot, B. B. (1983) *The fractal geometry of nature,* Freeman.

Matheron, G. (1971) In *Cahiers du centre de morphologie mathematique de Fointanebleau*, Vol. 5.

Mohamed, A. M. O. & Antia, H. E. (1998) In *Geoenvironmental engineering*(Ed, Elsevier) Amsterdam, pp. 185-200.

Nakagawa, S., Hopkins, D., Gentier, S. & Riss, J. 1999. Hydromechanical behavior of fractures in shear: implications for seismic imaging *ISRM9,* 2**:** 947-951.

Odling, N. E. 1994. Natural fracture profiles, fractal dimension and joint roughness coefficients *Rock mechanics and rock engineering,* 27**:** 135-153.

Ohnishi, Y., Chan, T. & Jing, L. 1996. Constitutive models for rock joints *Coupled thermo-hydro-mechanical processes of fractured media,* 79**:** 57-92.

Olsson, R. 1998. Mechanical and hydromechanical behaviour of hard rock joints, *Chalmers University of Technology, Goteborg***:** 56-57.

Patton, F. D. 1966. Multiple modes of shear failure in rock *1st Congress of International Society of Rock Mechanics,* 1**:** 509-513.

Peacock, G. R. (1998),http://www.measurementdevices.com/why.html.

Piggott, A. R. & Elsworth, D. 1995. A comparison of methods of characterizing fracture surface roughness *Fractured and Jointed Rock Masses.*

Plesha, M. E. 1987. Constitutive models for rock discontinuities with dilatancy and surface degradation *International Journal for Numerical and Analytical Methods in Geomechanics,* 11**:** 345-362.

Qui, X., Plesha, M. E., Huang, X. & Haimson, B. C. 1993. An investigation of the mechanics of rock joints - Part II. Analytical investigation *International Journal of Rock Mechanics and Mining Sciences and Geomechanics Abstracts,* 30**:** 271-287.

Re, F. & Scavia, C. 1999. Determination of contact areas in rock joint by X-ray computer tomography *International Journal of Rock Mechanics and Mining Sciences and Geomechanics Abstracts,* 36**:** 883-890.

Reeves, M. J. 1985. Rock surface roughness and frictional strength *International Journal of Rock Mechanics and Mining Sciences and Geomechanics Abstracts,* 22**:** 429-442.

Rengers, N. 1970. Influence of surface roughness on the friction properties of rock planes *Congres of the international society of rock mechanics :* 229-234.

Roko, R. O., Daemen, J. J. K. & Myers, D. E. 1997. Variogram characterisation of joint morphology and asperity deformation during shearing *International Journal of Rock Mechanics and Mining Sciences and Geomechanics Abstracts,* 34**:** 71-84.

Sabbadini, S., Hommand-Etienne, F. & Belem, T. 1995. Fractal and geostatistical analysis of rock roughness before and after shear tests *Mechanics of Jointed and Faulted Rock :* 535-541.

Saeb, S. 1990. A variance on the Ladanyi and Archambault's shear strength criterion *Rock joints :* 701-705.

Stimpson, B. 1982. A rapid field method for recording joint roughness profiles *International Journal of Rock Mechanics and Mining Sciences and Geomechanics Abstracts,* 19**:** 345-346.

Swan, G. 1983. Determination of stiffness and other joint properties from roughness measurements *Rock mechanics and rock engineering,* 16**:** 19-38.

Thomas, T. R. (1999a) In *Rough Surface*(Ed, Press, I. C.) London, pp. 95-97.

Thomas, T. R. (1999b) In *Rough Surface*(Ed, Press, I. C.) London, pp. 20-22.

Tse, R. & Cruden, D. M. 1979. Estimating joint roughness coefficients *International Journal of Rock Mechanics and Mining Sciences and Geomechanics Abstracts :* 303-307.

Wakabkykshi, N. & Fukushige, I. 1995. Experimental study on the relation between fractal dimension and shear strength *Fractured and Jointed Rock Masses*.

Xie, H., Wang, J. A. & Kwasniewski, M. A. 1999. Multifractal characterization of rock fracture surfaces *International Journal of Rock Mechanics and Mining Sciences and Geomechanics Abstracts,* 36**:** 19-27.

Xie, H. P., Wang, J. A. & Xie, W. H. 1997. Fractal effects of surface roughness on the mechanical behavior of rock joints *Chaos Solutions and Fractals,* 8**:** 221-252.

Xu, S. & De Freitas, M. H. 1990. The complete shear stress-vs-shear displacement behaviour of clean and infilled rough joints *Rock joints :* 341-348.

Yang, Z. Y. & Huang, Y. M. 1995. Post-peak shear behaviour of artificial joints *Mechanics of Jointed and Faulted Rock :* 139-144.

Zhao, J. 1997a. Joint surface matching and shear strength. Part A: Joint Matching Coefficient (JMC) *International Journal of Rock Mechanics and Mining Sciences and Geomechanics Abstracts,* 34**:** 173-178.

Zhao, J. 1997b. Joint surface matching and shear strength. Part B: JRC-JMC shear strength criterion *International Journal of Rock Mechanics and Mining Sciences and Geomechanics Abstracts,* 34**:** 179-185.

Curriculum Vitae

Name: Giovanni Grasselli
Date of birth: April 2nd, 1972 in Parma (Italy)
Nationality: Italian
E-mail: giovanni.grasselli@epfl.ch

Education:

5.1998 – 5.2001	Doctoral studies at the Laboratory of Rock Mechanics at the Swiss Federal Institute of Technology (EPFL), Lausanne, Switzerland
4.2000 – 12.2000	SNSF fellowship at the Lawrence Berkeley National Laboratory (LBL), USA
3.1996 – 5.1998	Assistant at the Laboratory of Rock Mechanics at the Swiss Federal Institute of Technology (EPFL), Lausanne, Switzerland
5.1998 – 12.1995:	Graduation in Civil Engineering at the University of Parma (Unipr), Italy

Tesi di Laurea (dissertation): *Comportamento meccanico di masse rocciose discontinue rinforzate con bulloni passivi*
Advisors: Prof. G.P.Giani (Unipr) and Prof. P.Egger (EPFL)